VOL.107 NO.HY1. JAN. 1981

JOURNAL OF THE HYDRAULICS DIVISION

PROCEEDINGS OF
THE AMERICAN SOCIETY
OF CIVIL ENGINEERS

VOL.107 NO.HY1. JAN. 1981

JOURNAL OF THE HYDRAULICS DIVISION

PROCEEDINGS OF
THE AMERICAN SOCIETY
OF CIVIL ENGINEERS

ISSN 0044-796X

AMERICAN SOCIETY OF CIVIL ENGINEERS

BOARD OF DIRECTION

President
Irvan F. Mendenhall

Past President
Joseph S. Ward

President Elect
James R. Sims

Vice Presidents
Robert D. Bay
Francis J. Connell
Lyman R. Gillis
Albert A. Grant

Directors
Martin G. Abegg
Floyd A. Bishop
L. Gary Byrd
Larry J. Feeser
John A. Focht, Jr.
Sergio Gonzalez-Karg
James E. Humphrey, Jr.
Richard W. Karn
Leon D. Luck
Arthur R. McDaniel
Paul R. Munger
William R. Neuman
Leonard S. Oberman
John D. Parkhurst
Celestino R. Pennoni
Robert B. Rhode
S. Russell Stearns
William H. Taylor
Stafford E. Thornton
Robert E. Whiteside
Richard S. Woodruff

EXECUTIVE OFFICERS

Eugene Zwoyer, *Executive Director*
Julie E. Gibouleau, *Assistant to the Executive Director*
Louis L. Meier, *Washington Counsel/Assistant Secretary*
William H. Wisely, *Executive Director Emeritus*
Michael N. Salgo, *Treasurer*
Elmer B. Isaak, *Assistant Treasurer*

STAFF DIRECTORS

Donald A. Buzzell, *Managing Director for Education and Professional Affairs*
Robert A. Crist, Jr., *Managing Director for Publications and Technical Affairs*
Alexander Korwek, *Managing Director for Finance and Administrative Services*
Alexandra Bellow, *Director, Human Resources*
David Dresia, *Director, Publications Production and Marketing*
Barker D. Herr, *Director, Membership*
Richard A. Jeffers, *Controller*
Carl E. Nelson, *Director, Field Services*
Don P. Reynolds, *Director, Policy, Planning and Public Affairs*
Bruce Rickerson, *Director, Legislative Services*
James M. Shea, *Director, Public Communications*
Albert W. Turchick, *Director, Technical Services*
George K. Wadlin, *Director, Education Services*
R. Lawrence Whipple, *Director, Engineering Management Services*

COMMITTEE ON PUBLICATIONS

Stafford E. Thornton, *Chairman*
Martin G. Abegg
John A. Focht, Jr.
Richard W. Karn
Paul R. Munger
William R. Neuman

HYDRAULICS DIVISION

Executive Committee
Ronald E. Nece, *Chairman*
Rudolph P. Savage, *Vice Chairman*
George E. Hecker
Ralph M. Weaver
Charles S. Mifkovic, *Secretary*
John J. Cassidy, *Management Group D Contact Member*

Publications Committee
Melvin W. Anderson, ***Chairman***
John A. Hoopes, ***Vice Chairman***
Philip H. Burgi, *Hydraulic Structures*
Richard H. (Pete) Hawkins, *Surface Water Hydrology*
John A. Hoopes, *Hydromechanics, General*
Gerhard H. Jirka, *Hydraulic Transport and Dispersion*
Chintu Lai, *Hydromechanics, Open Channels*
Frederick A. Locher, *Hydromechanics, Open Channels*
Donn G. DeCoursey, *Sedimentation*
Bryan R. Pearce, *Tidal Hydraulics*
John A. Roberson, *Hydromechanics, Closed Conduits*
John L. Wilson, *Groundwater Hydrology*
John J. Cassidy, *Exec. Comm. Contact Member*

PUBLICATION SERVICES DEPARTMENT

David Dresia, *Director, Publications Production and Marketing*

Technical and Professional Publications

Richard R. Torrens, *Manager*
Joseph P. Cerami, *Chief Copy Editor*
Linda Ellington, *Copy Editor*
Thea C. Feldman, *Copy Editor*
Meryl Mandle, *Copy Editor*
Joshua Spieler, *Copy Editor*
Shiela Menaker, *Production Co-ordinator*
Richard C. Scheblein, *Draftsman*

Information Services

Elan Garonzik, *Editor*

CONTENTS

→

This Journal is published monthly by the American Society of Civil Engineers. Publications office is at 345 East 47th Street, New York, N.Y. 10017. Address all ASCE correspondence to the Editorial and General Offices at 345 East 47th Street, New York, N.Y. 10017. Allow six weeks for change of address to become effective. Subscription price to members is $16.50. Nonmember subscriptions available; prices obtainable on request. Second-class postage paid at New York, N.Y. and at additional mailing offices. HY.

TECHNICAL NOTES

Proc. Paper 15957

DISCUSSION

Proc. Paper 15953

INFORMATION RETRIEVAL

The key words, abstract, and reference "cards" for each article in this Journal represent part of the ASCE participation in the EJC information retrieval plan. The retrieval data are placed herein so that each can be cut out, placed on a 3 × 5 card and given an accession number for the user's file. The accession number is then entered on key word cards so that the user can subsequently match key words to choose the articles he wishes. Details of this program were given in an August, 1962 article in CIVIL ENGINEERING, reprints of which are available on request to ASCE headquarters.

*Discussion period closed for this paper. Any other discussion received during this discussion period will be published in subsequent Journals.

15958 SURFACE HYDROLOGY: I-EXPLANATION OF PHENOMENA

KEY WORDS: Conservation; Erosion; Ground water; **Hydrology;** Infiltration; Mapping; Pollution; **Rainfall; Runoff; Seepage;** Soil water; Topography; Unsaturated flow; **Water resources**

ABSTRACT: Nonisotropic sloping soil leads to a horizontal flow component during rain and infiltration. Splashing of raindrops and flow in the transition zone between the soil bulk and the air also lead to lateral flow. The result is concentration of moisture in concave spots to the point of saturation and even seepage out of the soil. The same occurs at steep soil cuts. Such moisture concentration can explain the formation of runoff during rainfall at low rates that do not exceed infiltration capacity, partial area contribution to runoff, net recharge of groundwater by low-rate rainfall, the formation of rills and gullies in a relatively dry area, delay of runoff after a certain total amount of rain irrespective of rain intensity, variations in soil formation in different parts of the landscape, poor distribution of irrigation water in nonplane fields, and leaching of the soil surface by water that was assumed to run only above the surface.

REFERENCE: Zaslavsky, Dan, and Sinai, Gideon, "Surface Hydrology: I—Explanation of Phenomena," *Journal of the Hydraulics Division,* ASCE, Vol. 107, No. HY1, **Proc. Paper 15958,** January, 1981, pp. 1-16

15959 SURFACE HYDROLOGY: II—DISTRIBUTION OF RAINDROPS

KEY WORDS: Erosion; Ground water; **Hydrology;** Infiltration; **Rainfall; Runoff;** Sediments; **Seepage; Topography;** Water resources

ABSTRACT: Nonuniformity of rainwater distribution over a given soil area is due to two mechanisms. Raindrop splashes produce a net horizontal flow that is proportional to the slope and to the rate of the rainfall. A change in slope causes excess concentration of rain splashes in concave spots and reduces the rain over convex points. The concavity can be measured geodetically. The size of the horizontal discharge was deduced theoretically and measured on a sloping plane in a rain simulator. Both indicated the same order of magnitude. The horizontal discharge over short and steep slopes can reach a tenth of the total rain. The local excess rain can be up to half of the average rain. The other mechanism responsible for localized excess rain is the slanting of rain over slope facing it, as distinct from a soil slope in the rain "shadow." This mechanism can lead to local doubling of the rain intensity.

REFERENCE: Zaslavsky, Dan, and Sinai, Gideon, "Surface Hydrology: II—Distribution of Raindrops," *Journal of the Hydraulics Division,* ASCE, Vol. 107, No. HY1, **Proc. Paper 15959,** January, 1981, pp. 17-35

15960 SURFACE HYDROLOGY: III-CAUSES OF LATERAL FLOW

KEY WORDS: Erosion; Ground water; **Hydrology; Infiltration;** Irrigation; **Rainfall; Runoff;** Seepage; Topography

ABSTRACT: Streamlines bend after they enter a nonuniform, sloping soil. On penetrating to a more permeable soil layer they bend downstream. This can occur in unsaturated soil above a sloping water table or in a layer in which water accumulates because of the presence of less permeable underlying layer. We considered the general case of a nonuniform soil with rotational symmetry at an angle to the vertical, i.e., a sloping soil. General proof is provided that the soil generally behaves as a anisotropic medium so that infiltration also invloves a horizontal net flow component. This net flow component is proportional to the slope, the vertical flow, and the coefficient of anisotropy. The existence of such a mechanism can account for the concentration of water in concave spots, possible seepage, and runoff and erosion phenomena at low rates of rainfall. It can also explain how a previous rainfall leads to earlier onset of runoff during the next rain, etc.

REFERENCE: Zaslavsky, Dan, and Sinai, Gideon, "Surface Hydrology: III—Causes of Lateral Flow," *Journal of the Hydraulics Division,* ASCE, Vol. 107, No. HY1, **Proc. Paper 15960,** January, 1981, pp. 37-52

15961 IV-FLOW IN SLOPING, LAYERED SOIL

KEY WORDS: Ground water; **Hydrology;** Infiltration; **Permeability;** Pollution; **Rainfall; Runoff;** Seepage; Water pollution

ABSTRACT: In a nonuniform soil with rotational symmetry the properties change along a coordinate n that forms an angle α with the vertical. During infiltration there will be a flow component in the parallel direction s downstream, which is proportional to the rain itself and the slope. The horizontal flow is proportional to the vertical flow, the slope, and the coefficient of anisotropy. The last has been calculated for a soil made up distinct layers. In the limiting case of very thin layers or near the saturation point, the vertical and horizontal conductivities are, respectively, the expected arithmetic and harmonic means familiar from saturated flow. The coefficient of anisotropy increases with the rate of vertical flow to a power greater than unity. The horizontal flow component can be many times the vertical one. It finds application in pollution problems and in the study of the underground water regime.

REFERENCE: Zaslavsky, Dan, and Sinai, Gideon, "Surface Hydrology: IV—Flow in Sloping, Layered Soil," *Journal of the Hydraulics Division,* ASCE, Vol. 107, No. HY1, **Proc. Paper 15961,** January, 1981, pp. 53-64

15962 SURFACE HYDROLOGY: V—IN-SURFACE TRANSIENT FLOW

KEY WORDS: Erosion; **Hydrology;** Infiltration; Irrigation; Permeability; Rain; **Runoff; Seepage;** Soil physics; Topography

ABSTRACT: Numerical computation of nonsteady flow in the transition layer at the soil surface was carried out with various geometric dimensions and rain regimes. The main conclusions are: (1)Lateral flow in the transition layer is proportional to the rain and the slope; (2)moisture concentration increases with the concavity of the soil surface and continues long after the rain stops occurring mainly in unsaturated soil; (3)saturation initially occurs at the most concave point within the transition layer; and (4)the saturation zone may spread to the soil surface and cause seepage runoff and erosion. Both saturation and seepage occur after a certain amount of rain has fallen and are little dependent on its intensity. At very low rates of rainfall, no seepage will occur if the transition layer is sufficiently thin. Gullies and rills are not merely the result of seepage at concave spot—they themselves produce more and earlier seepage runoff and erosion; seepage of rain and runoff from concave spots will occur when the amount of rain is either greater or less than the infiltration capacity.

REFERENCE: Zaslavsky, Dan, and Sinai, Gideon, "Surface Hydrology: V—In-Surface Transient Flow," *Journal of the Hydraulics Division,* ASCE, Vol. 107, No. HY1, **Proc. Paper 15962,** January, 1981, pp. 65-93

15986 MULTIPORT SLEEVE VALVE DEVELOPMENT AND APPLICATION

KEY WORDS: **Cavitation; Design;** Energy dissipation; **Flow regulators;** Fluid flow; Hydraulics; Jets; **Laboratory tests;** Pipelines; **Sleeve valves;** Velocity

ABSTRACT: The history of the development and use of multiport sleeve valves is reviewed. The concept of using the multiport sleeve valve as an energy dissipator as well as a control valve for water pipelines is explored. It is expected that high-pressure head flows (150 to 300 m) can be controlled with the use of the multiport sleeve valve. Head loss coefficients for two sleeve valve designs are presented based on laboratory tests of 200-mm valve. Physical and mathematical models are described which were used to develop a horizontal multiport sleeve valve for long pipelines. The multiport sleeve valve is quite versatile with respect to hydraulic and mechanical design.

REFERENCE: Burgi, Philip H., Green, Edward O., and Thibault, Raoul E., "Multiport Sleeve Valve Development and Application," *Journal of the Hydraulics Division,* ASCE, Vol. 107, No. HY1, **Proc. Paper 15986,** January, 1981, pp. 95-111

JOURNAL OF THE HYDRAULICS DIVISION

SURFACE HYDROLOGY: I—EXPLANATION OF PHENOMENA

By Dan Zaslavsky[1] and Gideon Sinai[2]

INTRODUCTION

The following is the first of a series of articles devoted to a new approach in the study of surface hydrology. The main premise is that during rain and flow in a nonsaturated soil, a horizontal flow component may exist which leads to a number of phenomena as yet unexplained or, at best, poorly explained.

The senior writer was asked, as long ago as 1964, to review the engineering practice concerning erosion in water channels as well as its rationale. The resulting study indicated that there is very often little correlation between high-water runoffs or surface shear forces and the formation or widening of rills and gullies. The importance of seepage forces and piping mechanisms has been realized and has led to the measurement of piping in cohesive soils (26,40), but no explanation of the origin of seepage forces in semi-arid zones without the presence of ground water could be found. There had to be another process by which rain percolates into the soil and then rises again to form seepage forces.

In 1968, the senior writer was asked by J. Van Schilfgaarde of the Agricultural Research Service in Beltsville to join the Hydrograph Laboratory for the purpose of reexamining the approach to surface hydrology in general and, in particular, rainfall runoff relations, starting with the premises.

Serious doubts have been raised as to the soundness of the elementary physics and mathematics involved in the classical approach. A number of observed phenomena seem clearly to contradict existing theories, while the very definition of the soil surface (42) poses a fundamental is somewhat philosophical question. The main points in the new development can be summarized as follows. The soil is layered, its surface being the interface between the bulk of the soil

[1]Prof. of Soil and Water Engrg., Faculty of Agricultural Engrg., Soils and Fertilizers Div., Technion—Israel Inst. of Tech., Technion City, Haifa, 32000, Israel.

[2]Lect., Faculty of Agricultural Engrg., Soils and Fertilizers Div., Technion—Israel Inst. of Tech., Technion City, Haifa, 32000, Israel.

Note.—Discussion open until June 1, 1981. Separate discussions should be submitted for the individual papers in this symposium. To extend the closing date one month, a written request must be filed with the Manager of Technical and Professional Publications, ASCE. Manuscript was submitted for review for possible publication on March 23, 1979. This paper is part of the Journal of the Hydraulics Division, Proceedings of the American Society of Civil Engineers, © ASCE, Vol. 107, No. HY1, January, 1981. ISSN 0044-796X/81/0001-0001/$01.00.

and the air. These nonuniformities behave on the whole as a nonisotropy. In sloping soil this is the cause of the horizontal flow component which, in turn, may cause local moisture concentration, runoff at low rates of rain, and seepage forces, leading to erosion.

This article, the first in a series, presents some of the basic phenomena that surface hydrology must explain. It establishes the basic concept of lateral flow, at first in the form of a hypotheses. A number of conclusions are drawn which not only purport to reformulate the science of surface hydrology, but have direct practical applications in irrigation and soil and water conservation.

The subsequent articles will elaborate the theory and consider the partial experimental validation of the different parts of the three suggested mechanisms. These mechanisms are: (1) The splashing of raindrops; (2) the flow in the transitional zone at the soil surface; and (3) flow in a layered soil.

Rain and Runoff

The classical model universally used by hydrologists is that runoff can be formed in either of two ways: (1) The rate of rain exceeds the absorptive capacity of the soil at a given point, implying that at a lower rate of rain there will be no runoff; and (2) a groundwater table or a perched water table is built up which eventually produces seepage or outflows from the soil. Such an outflow of groundwater has always been considered strictly as a part of streamflows or baseflows with a large time-lag, and certainly not occurring during one rainstorm. In fact, the time-lag towards the end of a runoff event, or between such events, was the only accepted way to identify such a baseflow.

These concepts are the basis of papers from the early 1920s onwards (such as Refs. 31, 32, 29, 36, 28, 22, 23, 24, 4, and 33) as well as many others that followed. A typical statement, found in a comprehensive textbook (33) reads: "Storm runoff ordinarily is considered to be that portion of the total runoff . . . which reaches the point of measurements within a relatively short period of time . . . The time involved varies from a few minutes . . . The remaining flow of a stream consists of ground water discharge which lags behind the preceding rainfall by an appreciably longer period of time than storm runoff, the period ranging from a matter of days to a number of years." Or, "The maximum rate at which a small plot can absorb rainfall is called its infiltration capacity . . . most of the difference betweeen storm rainfall and storm runoff consists of water that has passed through the surface of the soil into the ground . . ."

No statistical organization of these models, such as in Refs. 34, 13, and 10, departs materially from the basic concept that runoff is constituted principally of rainfall less infiltration. Stochastic models (such as 9, 11, 12, 21, 30, 7, 8, 39), or deterministic models (27,25), can be cited in this connection. Two basic notions underlying all these treatments, whether they are stated explicitly or not, concerning the formation or runoff are:

1. The rate of rain exceeds the infiltration capacity of the soil at a point, implying that at a lower rate of rain there would be no runoff.
2. There is a buildup of a groundwater table or of a perched water table, which eventually flows out of the soil. This outflow of groundwater contributes

only to streamflows and baseflows, after a long delay, but certainly not during one rainstorm.

A physically and mathematically more rigorous treatment of saturated and unsaturated flow in the soil is represented by works such as Refs. 14–20, 2, 3, and 1, but they too do not, in effect, deviate from the two concepts that water will run off either because of its inability to penetrate the soil or after first accumulating in the groundwater. Wherever the groundwater seeps out of the soil, runoff may be formed, but this is dealyed until long after the rain has ceased.

Actual observations of runoff occurring during a rainstorm within a delay as short as a few minutes, or even only a fraction of a minute, indicate that the foregoing concept cannot be general and at best draws but a partial picture. While it appears to be evident that rain which exceeds the infiltration capacity of the ground will run off (on condition that there is no surface detention), it still does not explain why sometimes quick runoffs are caused by relatively light rains much lower than the infiltration capacity. A number of hypotheses have been advanced to account for this fact, yet they often hardly as much as admit the phenomenon itself.

One of the more common explanations is that of a "partial area contribution." It presupposes that there are some parts of the soil surface which have a very low infiltration capacity, but the existence of such insufficiently permeable areas is deduced from runoff measurements rather than based on direct observation. While there is no doubt that less permeable areas may contribute more surface rainfall excess, it is also certain that runoff may occur without such areas and at low-intensity rains.

The infiltration capacity of the soil has been presumed to be a unique figure. This simplistic concept, which has prevailed for so many years, does not allow for the dependence of runoff on antecedent moisture. In more sophisticated treatises (e.g., Refs. 14–20), a more realistic picture of unsaturated flow in the soil is admitted. We shall not refer here to a number of articles that relate the rate of infiltration to the water storage in the soil. The actual nature of the phenomenon can best be understood by consulting Braester (6). According to this work, surface moisture gradually increases during the rain, the infiltration capacity of a uniform soil is simply its hydraulic conductivity, and the soil approaches saturation, after a long time, if the rate of rainfall equals or surpasses the hydraulic conductivity. Even if the rain exceeds the infiltration capacity, a certain amount of time is needed for surface saturation and flooding to commence. This time will depend on the rain intensity, on a number of soil properties in addition to the saturated hydraulic conductivity, and on antecedent moisture. All papers relating the infiltration mechanism to rainfall and runoff assume one dimensional vertical flow. In a nonuniform soil, a different definition of the infiltration capacity is required.

A high antecedent moisture alone cannot account for runoff phenomena. Analysis and observations of unsaturated flow have indicated that a very short time after the cessation of a rainshower the vertical soil column reaches a more or less fixed moisture content known as the field capacity. Intervals between rainstorms as long as a few days are insufficient to evaporate more than a few millimeters of water from the soil, and often not even that. This amount

evaporated can be made good by a few minutes of rain. In many places, therefore, rainstorms during a rainy season fall on soil with a moisture content that varies within very narrow limits. Still, it is common experience that there is a cumulative effect with gradually increasing runoffs. It is equally common experience in many regions that little or no runoff occurs before a few hundred millimeters of rain have fallen. In the hills of Judea and Samaria, Israel, the relevant threshold is around 400 mm of rain, which is hardly affected by the time distribution. The intensity of a given storm has only a subsidiary effect on the runoff, constituting an addition to the accumulated total rain and antecedent moisture. The rise of groundwater, at any rate in Israel, cannot serve as an explanation. These well known observed facts which ran counter to a preconceived physical explanation, have merely spurred investigators to invent statistical tricks and obfuscating factors. The worst part of these exercises has been that these statistical abstractions were given names that pretend to grace true physical entities. The basic dilemmas remain: How does runoff form when the rainfall does not exceed the infiltration capacity over the whole field? Why is there an increase in runoff later in the rainy season?

At least two more ideas should be mentioned that attempt to explain runoff. One is the formation of a surface crust (35) which has been shown to develop in direct correlation with the cumulative rainfall. In experiments run by rain simulators it was found that the infiltration capacity is reduced with increasing rainfall, e.g., some wind-blown loess soils of Israel can strat out with an infiltration capacity of 30 mm/h–40 mm/h and end up with 3 mm/h–5 mm/h after cumulative rain totalling some 200 mm, although there will be some recovery of surface permeability after each drying period. The initial rate of infiltration for any new rain will be at least 10 mm/h–20 mm/h. Only the final rate of infiltration, which is obtained after a few tens of millimeters, will be very low. Observations indicate, however, that runoff starts much earlier. Other soils are much less sensitive to puddling by the rain. The crust formation can explain only part of the problem.

The other concept, which has already been mentioned, is that of a partial contribution or partial area. It states that small parts of the soil surface have a very low infiltration capacity and thus contribute considerably to runoff while the other parts do not at all. This concept cannot either be proved or disproved. It is only another way of saying that there must be some reason for runoff despite the fact that the rainfall does not seem to exceed the infiltration capacity. There can certainly be parts of the area where the rain exceeds the infiltration capacity.

In the following it will be demonstrated how some parts of the landscape contribute more to runoff than others. These parts, however, are not neceessarily less permeable. Rather they are related mainly to the topographic configuration. It would be erroneous to consider infiltration as one dimensional vertical flow.

Further Analysis of Conventional View Concerning Runoff

This analysis follows largely the ideas set out in Refs. 37, 42, 43, and 44.

Scalars and Vectors.—Traditionally, infiltration into the soil has been almost synonymous with vertical flow. In reality, vertical flow is only one of three (but certainly two) flow components. The horizontal-flow component cannot

be added arithmetically to the infiltration as if both were scalars. The commonly used equation

$$R = P - I \quad \text{(1)}$$

in which R = runoff; P = precipitation; and I = infiltration can serve at best as an overall scalar balance over an area in which the infiltration, I, is not actually measured at a point but is the difference between the measured precipitation and the outflow through a well-defined and measurable river or channel (assuming the boundaries of the drainage basin to be determinable by its topography alone). Thus Eq. 1 cannot be considered an equation for a specific point, nor is it capable of predicting runoff, but it is to calculate net recharge over a field, employing the measured values of the rain and the runoff.

Errors in *P* and *I*.—Precipitation can be measured, albeit with limited accuracy (on the order of ±20%). Infiltration capacity can be measured or estimated in a very rough manner. It can change in a storm (35), and it is not constant either in time or in space. A change by as much as half an order of magnitude is not uncommon.

It is therefore unrealistic to expect much by way of accuracy in the prediction of runoff, R, which is most commoly 5%–10% of the P (precipitation). Eq. 1, or any similar equation of differences, sophisticated as it may look, cannot be seriously considered as a tool for prediction based on actual measurements.

Rational Method.—The rational method expresses the runoff as a proportion of the rainfall. Representing a large volume of experience, it has the operational advantage that errors in the runoff are proportional only to the errors in the recorded or estimated rain. So far it has lacked a convincing physical explanation and is based almost exclusively on intuition.

S.C.S. Method.—As described in the National Engineering handbook of the United States Department of Agriculture, the S.C.S. Method improves on the Rational Method by allowing for an initial detention of rain and a nonlinear relationship between runoff and rain. It is interesting to note that on a large proportion of very common soils, runoff does not begin before several inches of rain have penetrated the soil. This is represented by the S.C.S. Method as being a function of the total rainfall irrespective of the rainfall distribution or any short-time intensity.

Is it Possible to Measure Surface Runoff?—The answer to the question of measuring runoff, R, depends on its definition. If by runoff is meant the outflow through a well-defined channel that drains a sizeable area, then such outflow is reasonably meaningful and measurable. However, at any given point in the field or when defined as overland sheet flow or, as it is sometimes more accurately called, runoff supply, it defies unequivocal measurement as well as definition. It is as difficult to define surface runoff as it is to define the soil surface itself. This problem of definition will be treated later in this report. It is reasonably clear that at the soil surface there is a transition between the soil bulk and the air. In the direction from the soil bulk outward, porosity as well as hydraulic conductivity gradually increase. It may be hard to accept this very fundamental argument about the transitive nature of the soil surface, but at least the practical problem of intercepting the runoff for measurement will be appreciated. The result will strongly depend on the depth at which such interception will be performed. A common fallacy is to produce a "deep enough" cutoff and let

"every drop of water" climb above it. This method of measurement definitely affects the quantity to be measured and undoubtedly tends to exaggerate the value of the apparent runoff. The alternative method is to provide a very thin horizontal threshold that is supposed to divide between the runoff and the flow within the soil. The question here is how thin the threshold is and at what elevation is it installed. The soil surface being irregular, it is legitimate to ask what is the size of the irregularities to which the dividers should conform in order to separate the soil bulk from the air.

It would appear to be much more reasonable, and in fact feasible, to measure the horizontal flux component or, still easier, the horizontal discharge (by the vertical integration of the horizontal fluxes). This, in fact, is what is measured near a vertical cutoff. Stagnation near such a wall may cause part of the water to overflow, and part of it to underflow, the cutoff. Horizontal flow can take place within the soil or outside of it. There is no means to distinguish between the two. The problem is not one of a mere technical limitation but is of a fundamental nature.

In summary, the notion of on-surface runoff as point values distributed over the soil area is fundamentally questionable and practically impossible to measure.

Popular as it is (from kindergarten onwards), the model of Eq. 1 still lacks a real demonstration of relevancy to either a physical understanding, a consistent mathematical formulation, or a practical measurement.

Concentration of Water in Concave Areas—Observations

Concentration of moisture in concave areas has been observed (38). This concentration occurs without any runoff in the usual sense of the word. By "concave" it is meant not only the bottom of a slope or of a valley but any transition from a steep to a moderate downward slope. Concentration of moisture without runoff in concave areas is a phenomenon that cannot be explained by any existing hydrological models. Such a concentration has been observed by the writers in a region of sand dunes in the Northern Sinai with 70 mm rain/yr and an infiltration capacity of some 500 mm/h. It occurred both on steep and on moderate slopes. When travelling in the southern part of Israel following the rain, the green sheets of seasonal grass and shrubs can be seen covering concave parts of the landscape. Bedouin are wont to plant their barley only in concave parts of the landscape. The accumulation of moisture has been observed in areas where no surface runoff could possibly have taken place, where no water table was present, and where no highly impermeable layer and perched water were evident.

In the sandy flowerbulb-growing area near Lisse (The Netherlands), it has been observed that in a soil cross section under a concave surface the sand was wetted to a considerably greater depth than under level surfaces (according to a personal communication from van der Valk and Knotterrus). This in turn had its effect on moisture availability to plants and on wind erosion patterns.

Looking at fields under rain or after a rain, water often seems to appear in some very shallow concave parts either in the form of small puddles or just as shining soil surfaces.

Concave parts in fields often suffer from excessive wetness, bad trafficability, and even aeration problems. Shallow waterways accumulate moisture and stay

wet for a long time even where there is no water table.

Any model attempting to explain surface hydrology should be compatible with this phenomenon of moisture accumulation in concave areas. It must be noted that surface runoff will not stop at a concavity caused by a transition from a slope of 12% to a slope of 10%. Every drop of water will either infiltrate vertically or become runoff with no accumulation at the point of concavity. A new mechanism must be postulated to explain this phenomenon.

Main Observation in Beer-Sheba Experiment (37,38)

Field observations were carried out in a commercial field north of Beer-Sheba. The curvature of the soil surface was measured geodetically through the elevation, z, at different points according to the formula

$$\nabla^2 z \cong \frac{(z_{i+1,j} + z_{i-1,j} + z_{i,j+1} + z_{i,j-1} - 4z_{ij})}{h^2} \quad \ldots\ldots\ldots\ldots\ldots\ldots (2)$$

The elevation was measured at grid points i and j as defined in Fig. 1.

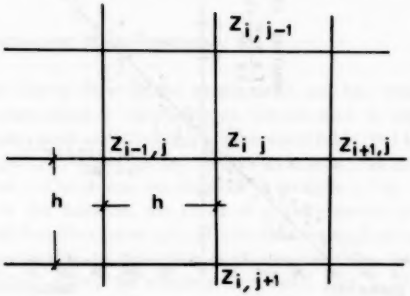

FIG. 1.—Two Dimensional Grid for Geodetically Measured Soil Surface Elevation Z_{ij}

Moisture contents were measured at depths of 20 cm and 40 cm over an area of 70 m × 70 m. The field was planted substantially parallel with the contour lines. The main slope was 12%. Yields were also measured. The results are summarized in Fig. 2, the concavity being estimated by $\nabla^2 z$ as in Eq. 2. The correlation between the moisture concents, C, two weeks after the rain, and the curvature, was found at $r = 90\%$ to be

$$C = 8.67 + 50.4(\nabla^2 z) \quad \ldots\ldots\ldots\ldots\ldots\ldots\ldots\ldots\ldots\ldots (3)$$

For the sake of brevity, detailed measured yields (which were correlated exactly with the moisture) will not be cited here. Overall yields reached more than 2 tons/ha in the concave part (concavity equals 0.08 − 0.1 m^{-1} in Fig. 2) and as little as 0.2–0.3 tons/ha in some convex parts [concavity (−0.09) − (−0.05) in Fig. 2].

No runoff in the usual sense was observed. The soil was a loess-loam which

was plowed and disked in the ordinary commercial manner. No water table, perched water, or impermeable layer was found anywhere near the area dealt with. Rainfall totalled about 250 mm. Diagnostic tests in addition to the moisture content measurements were made (salinity, fertility, clay content, etc.), but no visible trends that could be related to the variations in the moisture content or the yield were discovered.

The observation made in this experiment quantifies the qualitative impression gained from observing many areas. It must be assumed that there were little or no differences in the rainfall distribution. The soil at the surface was uniform, so that there were only small differences in the infiltration rate of the rain. The rain wetted the soil to a limited depth only, so that there was no net recharge of the groundwater. Where, then, did the differences in moisture originate? If surface runoff is excluded, there must be some other mechanism of lateral flow within the soil. This flow would have to be such as to occur

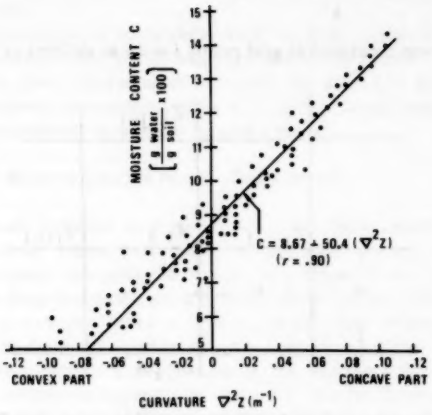

FIG. 2.—Correlation of Moisture Content at 20 cm and 40 cm Depth 10 Days after Rain with Soil Surface Curvature or Concavity

in a nonsaturated soil and to lead towards accumulation in a concave part of the landscape.

Soil Forming Processes (41)

The concentration of water in concave parts of the landscape can explain some soil forming processes. The pedological "genetic" formation of a clay "B" horizon is already very pronounced on flat land, but the layer so formed is found to be thickest in concave parts (excluding hydromorphic alluvial bottom land). On the high-lying convex parts of the slope, the development of B horizon is smallest.

Many theories have related this distinction to overland flow and erosion, but they are, in fact, unable to explain how relatively steep concave slopes

manage to "catch" more water or clay than others to form a thick B horizon. Erosion, adduced by some of the extant theories, cannot account for this, for how can erosion carry away any B horizon from under an A horizon? By what way can it leave a distinct if faintly developed B horizon? Can it really be that some tens or hundreds of years of B horizon development are followed by a few years of erosion?

In the opinion of the present writers, the development of a loamy or clayey B horizon on dune sand parent material can serve as a perfect model capable of unsettling existing theories and of offering some new insights. Observations in Israel have clearly shown that the clay is imported into the sand by rainwater and settling dust. It is equally evident that water is the vehicle by which the clay enters the sand to accumulate in the B horizon. Dune sand has a hydraulic conductivity of some 10^3 cm/day. Only an unusual rain-squall lasting a few minutes may have an intensity exceeding this hydraulic conductivity, the infiltration capacity of such short-term rain spurts actually being several times larger (5,6). It is very unlikely that any runoff and surface flow will occur on sand dunes. How, then, can clay, carried by water, accumulate in concave parts of the landscape without surface runoff, a high water table, or impermeable subsoil layers?

Suggested Explanation and More Phenomena

The concept of lateral flow in the unsaturated soil has been introduced by the writer (42). According to this concept, lateral flow is not caused by the boundary conditions, such as the position of the water table, but by soil anisotropy caused by soil layering. When the layers are horizontal, the main driving force (gravity) is normal to the layers, so the flow is straight down. When the layers are at an angle to the horizon, the force of gravity points downstream from the normal and will therefore cause a horizontal flux component pointing downhill.

It was thus reasonable to postulate (and was, in fact, later proven) that, at least under steady state, the average horizontal flux $\bar{q}_h$ is proportional to the average vertical flux, $\bar{q}_v$, to the slope, $\tan \alpha$, and to a coefficient of anisotropy, U:

$$\bar{q}_h = \bar{q}_v U \tan \alpha \quad \ldots \quad (4)$$

This simple expression for lateral flow can have a number of possible explanations. In a concave landscape, the incoming slope is larger than the outgoing one. Therefore, the incoming horizontal flux is higher than the outgoing one, leading to moisture accumulation in low-lying ("concave") parts. In the mathematical terms for two dimensional problems (z vertical and x horizontal) the slope can be expressed as follows:

$$\tan \alpha = -\frac{\partial z}{\partial x} \quad \ldots \quad (5)$$

Then, assuming as a first approximation that $\bar{q}_v$ and U are not functions of x, the conservation law applied to Eq. 4 yields

$$-\frac{\partial \bar{q}_h}{\partial x} = \frac{\partial C}{\partial t} + q_v^* = \bar{q}_v U \left(\frac{\partial^2 z}{\partial x^2} \right) \quad \ldots \quad (6)$$

in which C = the moisture content; and q_v^* = the additional outgoing water caused by increased vertical flux. In short, any concave part of the landscape, $(\partial^2 z/\partial x^2) > 0$, leads to higher moisture contents and a higher share of vertical infiltration. The more water there is, the greater the development of the B horizon. Furthermore, on convex parts of the landscape there is a shortage of moisture and a smaller vertical flow ($\partial^2 z/\partial x^2 < 0$). In fact, as the B horizon develops, the anisotropy U does likewise, and q_v^* grows progressively more negative. The development of the B horizon in convex parts of the landscape then ceases of its own accord. This new explanation is interesting inasmuch as it also interprets the fainter B horizon on straight and convex slopes in genetically mature soil catenas. This explanation does not have to rely on the questionable crutch of erosion and runoff theories.

The lateral flow component and the moisture accumulation on concave parts of the slope could explain the observations made in the Beer-Sheba experiment. If the lateral flow component and the moisture accumulation can be shown to be of sufficient magnitude, they could explain the occurrence of saturation in parts of the field, leading to seepage out of the soil and the formation of overland flow. The "partial area contribution" would then get a new meaning. Rain falling on areas with surface seepage will not infiltrate into the ground, but not because of the limited infiltration capacity, the value of which is totally irrelevant in this case. In addition, part of the area is waterlogged not because of the ratio of rain to the infiltration capacity. It is, rather, because of some mechanism leading to a local accumulation of water. The new concept, put forward by the present writers, postulates that this accumulation of water leads, in the first place, to locally increased groundwater recharge and may also lead to runoff. This is contrary to the traditional measuring of "partial area contribution," according to which there is less groundwater recharge where runoff originates.

If the rain is able to penetrate into the ground, if only to a shallow depth, before turning into overland flow, it has an altogether different effect on leaching and pollution. In an appreciable number of observations of stormwater composition, the relatively high concentration of some solutes could not be explained unless the rain had entered the soil first.

If localized waterlogged areas can be formed by lateral flow, this would explain why a certain amount of total rain is needed and some time must elapse before significant runoff occurs. Analyzing Eq. 6 indeed shows that the rate of excess accumulation, $(\partial C)/(\partial t) + q_v^*$, depends on the rate of rain, $\bar{q}_v$.

It could be that total excess moisture accumulation depends on the total amount of rain. Waterlogged areas can no longer absorb rain regardless of its intensity so that as rain continues to fall, they contribute to overland flow in rills, gullies, and rivers.

If the rain first penetrates into the ground and then seeps back out again in concave parts, this would explain field erosion by the formation of seepage forces. Depressions in the soil surface are often a starting point of erosion, which can now be accounted for by local high accumulations of moisture and the concentration of streamlines, which in turn produce high seepage forces (cavitation points).

Road cuts, steep river banks, and landslides truncate the soil layers. The lateral flow reaches the cut soil surface but cannot seep out as long as the

soil is unsaturated or the water pressure is negative. The streamlines then bend downward and accumulate until sufficient pressure builds up for seepage to occur usually followed by erosion.

Concentration of rainwater at concave points of the landscape could explain net groundwater recharge in some areas of very limited rain. This is a natural form of "water harvesting" whereby certain parts of the landscape are allotted several times more rainwater than the average. This runs counter to the "partial-area-contribution" theories, which state that the parts that contribute to runoff are excluding most of the rainwater by being impermeable. The lateral flow concept, on the other hand, clearly shows that waterlogged areas can form, exhibiting a greater measure of deep percolation and supplying runoff at one and the same time.

It has been suggested (42) that all soils without exception have a more permeable layer at their surface. This is due to the simple fact that the porosity approaches unity towards the air. This in itself produces a lateral flow component wherever the soil surface slopes. It has also been suggested (37,43,44) that while splashing raindrops produce a real lateral flow component, very much as in Eq. 4, they do not cause water to seep out of the soil. A detailed treatment of the mechanisms leading to lateral flow will be the subject of future parts of this report.

If Eq. 4 is proven to be physically sound, then it will have what may be termed a fringe benefit in the accuracy of predicting runoff. Given errors in measuring the rain, $\bar{q}_r$ will produce only the same relative errors in the horizontal flow component similar to the rational runoff equation. There is no amplification of the relative error because of the smaller value of the runoff compared with the rain and the infiltration as in Eq. 1. In fact, Eq. 4 does not assume the existence of runoff and infiltration in the usual sense. Every drop of rain may be supposed to be at the soil surface and neither above nor below it. Horizontal flow is formed in the transitional zone of the soil surface rather than below or above it. Which part of it will form into a streamflow is a different problem.

Formation of Gullies and Rills by Water Erosion (42)

Gullies and rills often form in areas of little runoff. In fact, they develop mostly by extending their upper end uphill, where the quantity of streamflow is smallest. The most baffling observation is that this upward advance of erosion channels is often caused by undermining, which seems to be due to water coming out of the soil and not pouring over it. Such undermining is followed by caving-in and then by a gradual transport of the debris by overland flow. In many instances the present writers have observed subsoil channels that seemed to start and end where there is neither overland flow nor a water table nor a distinct impermeable layer.

The explanation of this and other erosion phenomena depends on the acceptance of two processes, i.e.: (1) A mechanism by which outcoming water erodes the soil; and (2) a mechanism by which water comes out of the soil.

The first mechanism is undoubtedly that of seepage forces. At sharply concave points, very high hydraulic gradients can arise due to the convergence of streamlines. The drag forces exerted by the outflowing water can then detach soil particles, overcoming even high cohesion (40,26).

The seepage force mechanism is inconceivable without water coming out of

the soil. When it does, it must do so at a positive pressure (at least somewhat higher than atmospheric), while at the same time the soil must be saturated or nearly so.

In common thinking saturated soil is related to either of two cases: (1) A high or perched water table situated above an impermeable layer; and (2) overland flow, which forms whenever the rain exceeds the soil's infiltration capacity.

The questions to be answered by the present writers were how water outflow could occur in the absence of a water table or a perched water table and in the event of the rain's not exceeding the infiltration capacity.

It has here been suggested that there is a lateral flow component that can occur with any amount of rain and in unsaturated soil. This is the horizontal flow within the soil and close to the soil surface, which can cause moisture accumulation in concave parts of the landscape to such an extent that it may even reach saturation. Saturation, of course, can be followed by outflow from the soil, by erosion, and by runoff.

A badly gullied valley around Nahal Bohu in the Israeli Negev was subject to soil conservation and afforestation. In the preparatory stage, two aerial photographs taken 20 yr apart were compared. The tips of some of the gullies were advancing at an average rate of about 1 m/yr, the process invariably being tunnelling followed by a cave-in. The advancing gullies were in nearly every instance in concave parts of the landscape, where the topography is amphitheater-like. The measures proposed for counteracting further erosion were: (1) Underground drainage; (2) flow barriers; and (3) filters. Although there was no obvious water table nor any other zone of saturated soil, the drains would nevertheless draw off water. If this model for the formation of rills and gullies is correct, i.e., by outflowing water, then any increased infiltration of water into the soil augments gullying. Turning an area into irrigated land as well as certain "conservation" measures could thus mean higher ground water recharge and worsened gullying conditions.

More Observations: Surface Hydrology of Straw Roof

After he had presented some of these ideas at an experimental station in Ohio, the first writer was shown an amphitheaterlike drainage basin with a spring at its mouth. There was no evident impermeable layer, nor did measurements indicate saturated flow around or below a very small area where water was seeping out. Yet the seepage continued long after the rain had ceased. Since then, many such places, e.g., agricultural fields and roadcuts, have been observed with evidence of erosion and seepage.

The "straw roof" example is probably the best means to unlodge some of the old-established concepts and point to better ones. The building of straw or reed covered ("thatched") roofs is a practice shared by primitive tribes near the equator with some very well-to-do private houseowners in Northern Europe. An "expert" hydrologist, if asked for his opinion, would first measure the infiltration capacity of the straw and would then pronounce it too high for a roof. But pace the expert's opinion, not a drop of rain gets through the straw into the building's inside. Every drop of rain is shed clear off the roof, not a single drop runs along its surface as "overland flow." There is no "ground water" or "perched water." How confusing!

This case, though extreme, indicates some of the limitations of present-day surface hydrology. No builder in his right mind would make a straw roof flat. The "waterproofing" is related to the slope and apparently to the anisotropic of the medium. The flow within the roof is not saturated except possibly at the lowest rims.

Conclusions

The assertion that most soils are nonisotropic with respect to water flow is hardly in need of proof, since this view has been a commonplace, at any rate, as far as saturated flow is concerned. The present writers extend it, without proof, to nonsaturated soils, and this, in turn, leads to the conclusion that in any soil with sloping layers there will be a flow component parallel with the layers. It is postulated that the horizontal flow component will be proportional to the vertical component and the slope.

If this postulate is correct, even if only approximately, then rainwater must accumulate in concave parts of the landscape and at soil cuts. Another mechanism of rain accumulation in concave parts is probably that involving raindrop splashing.

Many phenomena can be related to the lateral flow mechanism and to the accumulation of water at certain points in an otherwise nonsaturated soil. Among these are:

1. Major portions of the rainfall are absorbed by the soil and only later reemerge by seepage.
2. This mechanism could explain why runoff follows a certain total amount of rain and not necessarily rainfall of a momentarily high intensity.
3. It is possible to conceive of runoff with rain nowhere exceeding the infiltration capacity.
4. "Partial area contribution" to runoff is made not only by less permeable soils but also by soils locally waterlogged due to lateral flow.
5. The same waterlogged areas also contribute to the net recharge of ground water, even though the average rainfall would be unable to do so.
6. Local accumulations of water and water seepage out of the soil could explain a variety of erosion phenomena, especially the formation of rills and gullies.
7. The rain first infiltrates the soil and only later reemerges but with delays that are much shorter than those met with in the case of groundwater. Absorption and reemergence can place within one rainstorm or in practically any other time range.
8. The concepts described can explain various leaching phenomena that were formerly held unaccountable.
9. Also capable of explanation is the formation of a soil catena with 'B' horizon, most highly developed in a concave part and least developed in a convex part of the landscape.

The foregoing statements, if proven correct, should replace at least partly the notions presently current in surface hydrology, i.e., that runoff is produced either by rain that cannot penetrate the soil or by water, from whatever source, the first reaches the ground water table. Further fundamental reservations can

be made concerning the traditional view that runoff is equal to rainfall minus infiltration, reservations that are unconnected with the mechanism of lateral flow.

The practical implications of the new concept could be far reaching. Speaking in general terms, of course, understanding is the first step towards many new or improved applications. The whole subject of watershed hydrology, and erosion mechanisms is due for revision, together with commonly held views about soil and water conservation. The Beer-Sheba experiment not only well illustrates the phenomenon of moisture concentration and its hydraulic significance, but it also points to an immediate practical problem. Obviously, even the most uniform irrigator cannot avoid an eventual nonuniform water distribution, unless high local curvatures are eliminated by grading. This is certainly a surprising criterion for field leveling.

Future work could usefully make a detailed study of the mechanisms causing lateral flow. A part of such a study will be presented in a future installment of this report, but the extremely wide scope of this subject excludes any possibility of a complete coverage of the required theoretical studies, the computational methods for specific problems, experimental support, and the formulation and testing of practical applications. Rather, it is hoped that this series of articles will bring about a more widespread effort with these aims in view. The next article will propose a theory and preliminary experimentation with raindrop splashes. Next, we shall demonstrate in general the formation of lateral flow due to gradual changes in soil properties, whether at or near the surface or deeper in a layered soil. Finally, we shall use numerical solutions to study in detail the process of moisture accumulation in concave parts of the landscape.

Acknowledgment

This work was supported by the United States-Israel Binational Science Foundation and by the Division of Soil Conservation and Drainage at the Israel Ministry of Agriculture. The senior writer was given invaluable help in summarizing and writing these reports by the Institute for Land and Water Reclamation at Wageningen, the Netherlands. Numerous meetings with scientists and engineers preceded the conviction that the problem is universal enough, and the suggested explanation plausible enough, to be presented.

Appendix I.—References

1. Abbott, M. B., Ashamalla, A. F., and Rodenhuis, G. S., "On the Numerical Computation of Stratified Groundwater Flow," *Bulletin of the International Association of Hydrological Scientists*, Vol. 17, No. 17, 1972, pp. 177–182.
2. Amerman, C. R., "Hydrology and Soil Science in Field Soil Water Regime," *SSSA Special Publication No. 5*, 1973, pp. 167–180.
3. Amerman, C. R., Klute, A., Skaggs, R. W., and Smith, R. E., "Soil Water," *Reviews of Geophysics and Space Physics*, Vol. 13, No. 5, 1975, pp. 451–454.
4. Barnes, B. S., "Structure of Discharge Recession Curves," *Transcript American Geophysical Union 20*, 1939, pp. 721–725.
5. Braester, C., Zaslavsky, D., Neuman, S. P., and Dagan, G., "A Survey of the Equations and Solutions of Unsaturated Flow in Porous Media," *First Annual Report, Part I, Project No. A10-SWC-77*, Hydraulic Engineering Laboratory, Technion, Haifa, Israel, 1971.
6. Braester, C., "Moisture Variation of the Soil Surface and the Advance of the Wetting

Front During Infiltration of Constant Flux," *Water Resources Research*, Vol. 9, No. 3, 1973, pp. 687–694.
7. Buras, N., *Syntific Allocation of Water Resources*, American Elsevier Publishing Company, Inc., New York, N.Y., 1972.
8. Chow, Ven Te, *Handbook of Applied Hydrology*, Chow Ven Te, ed., McGraw-Hill Book Co., Inc., New York, N.Y., 1964.
9. Chow, Ven Te, and Rasaseshan, S., "Sequential Generation of Rainfall and Runoff Data," *Journal of the Hydraulics Division*, ASCE, Vol. 91, No. HY4, Proc. Paper 4416, July, 1965, pp. 205–223.
10. Clarke, R. T., "Mathematical Models in Hydrology," *Irrigation and Drainage Paper, No. 19*, FAO, Rome, Italy, 1973.
11. Crawford, N. H., and Linsley, R. K., "The Synthesis of Continuous Streamflow Hydrographs on a Digital Computer," *Technical Report 12*, Department of Civil Engineering, Stanford University, Palo Alto, Calif., 1962.
12. Crawford, N. H., and Linsley, R. K., "Digital Simulation in Hydrology—Stanford Watershed Model IV," *Technical Report 39*, Department of Civil Engineering, Stanford University, Palo Alto, Calif., 1966.
13. Diskin, M. H., "Definition and Uses of the Linear Regression Model," *Water Resources Research*, Vol. 6, 1970, pp. 1668–1673.
14. Freeze, R. A., "The Continuity Between Groundwater Flow Systems and Flow in the Unsaturated Zone," *Proceedings of the Hydrology Symposium: No. 6*, University of Saskatchewan, Nov., 1967, pp. 205–240.
15. Freeze, R. A., "The Mechanism of Natural Groundwater Recharge and Discharge. 1. One-Dimensional, Vertical Unsteady, Unsaturated Flow Above a Recharging or Discharging Groundwater Flow System," *Water Resources Research*, Vol. 5, No. 1, 1969, pp. 153–171.
16. Freeze, R. A., "Three-Dimensional, Translent, Saturated-Unsaturated Flow in a Groundwater Basin," *Water Resources Research*, Vol. 7, No. 2, 1971, pp. 347–366.
17. Freeze, R. A., "Role of Subsurface Flow in Generating Surface Runoff. 1. Base Flow Contributions to Channel Flow," *Water Resources Research*, Vol. 8, No. 3, 1972, pp. 609–623.
18. Freeze, R. A., "Role of Subsurface Flow in Generating Surface Runoff. 2. Upstream Source Areas," *Water Resources Research*, Vol. 8, No. 5, 1972, pp. 1272–1283.
19. Freeze, R. A., "Streamflow Generation," *Reviews of Geophysics and Space Physics*, Vol. 12, No. 4, 1974, pp. 627–647.
20. Freeze, R. A., "Simulation of Subsurface Flow in Watershed Models," *IBM Seminar on Regional Groundwater Hydrology and Modelling*, Venice, Italy.
21. Grace, R. A., and Eagleson, P. S., "A Model for Generating Synthetic Sequences of Short-Time Interval Rainfall Depths," *Proceedings of the International Hydrology Symposium*, Fort Collins, Colo., Vol. 1, 1967, pp. 268–276.
22. Horton, R. E., "Surface Runoff Phenomena, Analysis of the Hydrograph," *Horton Hydrological Laboratory*, Publication 101, 1935, 73 pages.
23. Horton, R. E., "An Approach Toward a Physical Interpretation of Infiltration Capacity," *Proceedings*, Soil Science Society of America, Vol. 5, 1940, pp. 399–417.
24. Izzard, C. S., "Hydraulics of Runoff from Developed Surfaces," *Highway Research Board Proceedings*, Vol. 26, 1946.
25. James, L. D., "An Evaluation of Relationships Between Streamflow Patterns and Watershed Characteristics Through Use of OPSET: A Self-Calibrating Version of the Stanford Watershed Model," *Report No. 36*, Water Resources Institute, University of Kentucky, 1970.
26. Kassiff, G., Zaslavsky, D., and Zeitlen, J. G., "Analysis of Filter Requirements for Compacted Clays," *Proceedings of the 6th ICSMFE Division*, 1965, pp. 495–499.
27. Kisiel, C. C., "Time Series Analysis of Hydrologic Data," *Advances in Hydroscience*, Academic Press, New York, N.Y., 1969.
28. Linsley, R. K., Jr., Kohler, M. A., and Paulhus, J. L. H., *Hydrology for Engineers*, MacGraw-Hill Book Co., Inc., New York, N.Y., 1958.
29. Lowdermilk, U. D., "Forest Destruction and Slope Denudation in the Provice of Shansi," *China Journal*, Vol. 4, 1926, pp. 127–135.
30. Matalas, N. C., "Mathematical Assessment of Synthetic Hydrology," *Water Resources Research*, Vol. 3, 1967, pp. 937–945.

31. Meinzer, O. E., "Outline of Groundwater Hydrology, with Definitions," *Water Supply Paper No. 494*, United States Geological Survey, 1923.
32. Meinzer, O. E., ed., *Hydrology*, Chapt. 11, Dover Publications, New York, N.Y., 1942.
33. Rouse, H., ed., *Engineering Hydraulics*, Chapt. 4, John Wiley and Sons, Inc., New York, N.Y., 1950.
34. Schreiber, H. A., and Kincaid, D. R., "Regression Models for Predicting On-site Runoff from Short Duration Convective Storms," *Water Resources Research*, Vol. 3, 1967, pp. 389–395.
35. Seginer, I., and Morin, J., "A Model of Surface Crusting and Infiltration of Bare Soils," *Water Resources Research*, Vol. 6, No. 2, 1970, pp. 629–633.
36. Sherman, L. K., "Streamflow From Rainfall by Unit-Graph Method," *Engineering News Recorder*, No. 01, 1932, pp. 501–505.
37. Sinai, G., and Zaslavsky, D., "Rainflow in the Soil and Near its Surface-Observation Models and Solutions," *Publication No. 264*, Faculty of Agricultural Engineering, Technion, Haifa, Israel, Sept. 1976.
38. Sinai, G., Zaslavsky, D., and Golany, P., "Influence of Anisotropy in Soil," Permeability on Surface Runoff Publication 232, Faculty of Agricultural Engineering, Technion, Haifa, Israel, 1974.
39. Visser, W. C., "The Aim of Modern Hydrology," *Technical Bulletin 90*, Institute for Land and Water Management Research, Wageningen, Holland, 1974.
40. Zaslavsky, D., and Kassiff, G., "Theoretical Formulation of Piping Mechanism in Cohesive Soils," *Geotechnique*, Vol. XV, No. 3, 1965, pp. 305–316.
41. Zaslavsky, D., and Rogowski, A. S., "Hydrologic and Morphologic Implications of Anisotropy and Infiltration in Soil Profile Development," *Proceedings*, Soil Science Society of America, Vol. 33, No. 4, 1969, pp. 594–599.
42. Zaslavsky, D., "Some Aspects of Watershed Hydrology," Special Report to the United States Department of Agriculture, *Agricultural Research Service*, 1970.
43. Zaslavsky, D., and Sinai, G., "Lateral Flow Due to Rain in Unsaturated Soil," Second Annual Report, *Project No. A-10-SWC-77*, Faculty of Agricultural Engineering, Technion, Haifa, Israel, 1972.
44. Zaslavsky, D., and Sinai, G., "Surface Hydrology," Nota 1017, *Instituut voor Cultuurtechnick en Waterhuishouding*, Wageningen, Holland, Nov., 1977.

Appendix II.—Notation

The following symbols are used in this paper:

C = volume of moisture per unit volume of soil;
q = water flux;
U = coefficient of soil anisotropy;
x = horizontal coordinate;
z = elevation, topographical; and
α = slope of soil surface or soil layers.

Subscripts

h = horizontal (water flux);
i = rows in topographical grid;
j = columns in topographical grid; and
v = vertical water flux.

Superscript

$*$ = excess vertical flow.

JOURNAL OF THE HYDRAULICS DIVISION

SURFACE HYDROLOGY: II—DISTRIBUTION OF RAINDROPS

By Dan Zaslavsky[1] and Gideon Sinai[2]

INTRODUCTION

In a previous report (6) it was postulated that there exist four mechanisms by which a horizontal flow component is associated with rain or with vertical flux in the soil. It was further asserted that that component must increase with the slope of the soil and could even be proportional to the slope. It certainly is proportional to either the vertical flux or the rain. Such a lateral flow had to be postulated in order to explain a number of phenomena.

In the present paper the first of these mechanisms, that involving raindrop splashes, is analyzed. To begin with, a general mechanistic theory is developed while, for the specific case of vertical rain and symmetric outflight of the splashes, an expression is obtained for the horizontal flow. It is indeed seen to be proportional to the slope, the rainfall, and an experimental coefficient which incorporates mass ratios, the kinetic energies of the splashes, and some geometrical parameters.

A preliminary experiment actually showed the downstream horizontal flow of splashes to be proportional to the slope and of an order of magnitude as predicted by the theory.

Slanting rain over a rough soil is another cause for nonuniform rain distribution. Together with the concentration of splashes in concave spots, it causes variations in the effective rain distribution. The variations and their dependence on the roughness of the soil surface will be assessed.

In their turn, the variations in the effective rain distribution may lead to nonlinear and nonhomogeneous relations between the rainfall average and its

[1]Prof. of Soil and Water Engrg., Faculty of Agricultural Engrg., Soils and Fertilizers Div., Technion—Israel Inst. of Tech., Technion City, Haifa, 32000, Israel.

[2]Lect., Faculty of Agricultural Engrg., Soils and Fertilizers Div., Technion—Israel Inst. of Tech., Technion City, Haifa, 32000, Israel.

Note.—Discussion open until June 1, 1981. Separate discussions should be submitted for the individual papers in this symposium. To extend the closing date one month, a written request must be filed with the Manager of Technical and Professional Publications, ASCE. Manuscript was submitted for review for possible publication on March 23, 1979. This paper is part of the Journal of the Hydraulics Division, Proceedings of the American Society of Civil Engineers, © ASCE, Vol. 107, No. HY1, January, 1981. ISSN 0044-796X/81/0001-0017/$01.00.

mean effect, expressed in such events as runoff and groundwater recharge.

The nonuniform distribution of the rain or, in other words, local high concentrations, may explain in part the formation of runoff at low average rates of rain and a number of other phenomena. Newly adopted parameters such as variance of the rain, roughness of the soil surface, the azimuth, and the elevation of the rainfall, stand out as important parameters in surface hydrology.

Why do Raindrop Splashes Produce Real Lateral Flow?

Raindrops that hit the soil break up into smaller droplets ("splashes"), which rebound (2,3,4). If the soil slopes, the splashes will travel farther downhill than uphill. The virtual center of gravity of the array of droplets resulting from

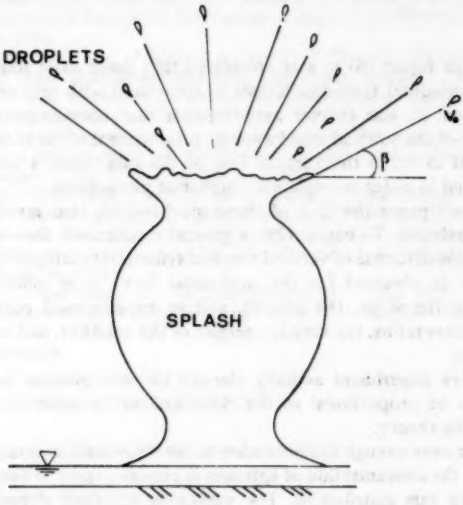

FIG. 1.—Typical Splash Shape Caused by Raindrop Hitting Soil Covered with Water Layer of Depth h [Mutchler (2)]

the original raindrop will be found downhill from the first point of impact. This means that, given a certain distribution of rain intensity at some horizontal surface above the soil, the eventual "effective" rainfall distribution over the surface of the soil will be the result of a downhill translation. The horizontal discharge amounts to the rate of rainfall multiplied by the horizontal shift of the center of gravity of the raindrops. An observer watching the passing splashes will count more going downhill than uphill. The net difference amounts to a very real net lateral flow, which can be demonstrated experimentally. At least for moderate slopes we may state that the downhill translation increases with the slope. Over a long and uniform slope the resultant horizontal flow will not be noticable and the final rain distribution will remain unchanged, whereas

at the top of the slope, at its bottom, and at any point of change in the slope, the effects of the horizontal flow will be felt.

In the following we shall present three more or less independent studies, i.e.: (1) An experimental evaluation of the net downhill flow as a function of the character of the slope; (2) a demonstration of moisture concentration at the bottom of slopes; and (3) a theory attempting to predict the lateral flow due to raindrop splashes.

Model for Raindrop Splashes

A raindrop hitting a water surface will produce a crown of splashes (Fig. 1), a phenomenon that has been investigated by several workers (2,3,4). The splashes arise at a fixed angle, β, with the horizon. The configuration of the splashes and the distances travelled by each splash have been found to be symmetrical around the initial flight path; but the experiments have concerned only vertical flight. Splashes also occur on a nonsaturated soil surface; but we know of no systematic experimentation for this case.

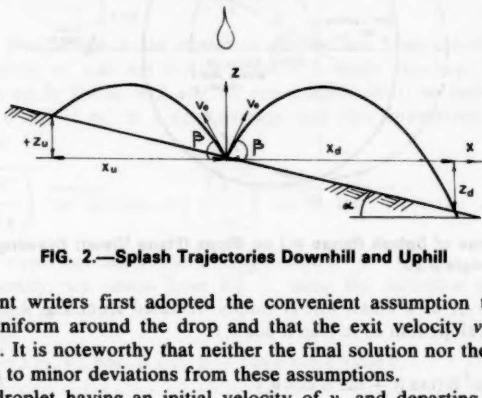

FIG. 2.—Splash Trajectories Downhill and Uphill

The present writers first adopted the convenient assumption that the exit angle β is uniform around the drop and that the exit velocity v_o is more or less uniform. It is noteworthy that neither the final solution nor the conclusions are sensitive to minor deviations from these assumptions.

A single droplet having an initial velocity of v_o and departing at an angle, β, will be assumed to describe a parabolic path (with no air resistance and over a flat gravity field). The components of its velocity are then

$$v_x = v_o \cos\beta \quad (1)$$

$$v_z = v_o \sin\beta \quad (2)$$

and the equation for the flight path is

$$z = x \tan\beta - \frac{g\,x^2}{2\,V_o^2 \cos^2\beta} \quad (3)$$

in which z = the vertical coordinate, positive and upward ($z = 0$ at the initial hitting points); x = horizontal coordinate in the plane of flight of a splash ($x = 0$ at the initial hitting point of the raindrop); g = gravity acceleration;

and x_d, x_u = respectively the downstream and upstream distances from $x = 0$ of the points of impact of droplets (Fig. 2). If the angle of slope is α

$$x_d = \frac{2}{g} V_o^2 \cos^2\beta \, (\tan\beta + \tan\alpha) \quad \ldots\ldots\ldots\ldots\ldots\ldots\ldots\ldots\ldots\ldots (4)$$

$$x_u = \frac{2}{g} V_o^2 \cos^2\beta \, (\tan\beta - \tan\alpha) \quad \ldots\ldots\ldots\ldots\ldots\ldots\ldots\ldots\ldots\ldots (5)$$

Consider now a three-dimensional picture (x, y horizontal coordinates and z upward vertical coordinate with the origin at the point of impact). The mass m of a raindrop becomes the combined mass of splashes, $m = \Sigma m_i$. A single droplet forms an angle θ_i with the vector of slope tan α (Fig. 3). The range

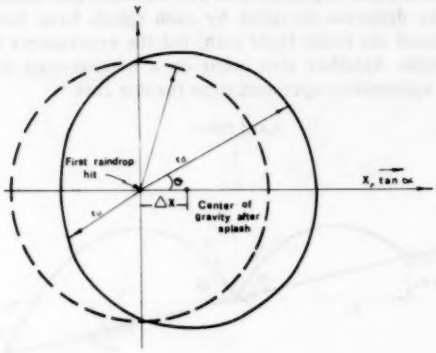

FIG. 3.—Change of Splash Range (r_i) on Slope (Plane View); Drawing is for Slope $\alpha = 20°$ exit angle β 50°

of splashing, r_i, of a mass, m_i, is simply obtained from Eq. 4 and Eq. 5 by adjusting the slope (tan α) to (tan $\alpha \cos\theta_i$)

$$r_i = \frac{2}{g} V_o^2 \cos^2\beta \, (\tan\beta + \tan\alpha \cos\theta_i) \quad \ldots\ldots\ldots\ldots\ldots\ldots\ldots\ldots\ldots\ldots (6)$$

Each droplet at an angle θ_i has, on the average, a conjugate at $\theta_i + \pi$. The difference in range is:

$$\Delta r_i = r_{(\theta_i)} - r_{(\theta_i + \pi)} \quad \ldots\ldots\ldots\ldots\ldots\ldots\ldots\ldots\ldots\ldots\ldots\ldots\ldots\ldots (7)$$

or in full

$$\Delta r_i = \frac{4}{g} V_o^2 \cos^2\beta \tan\alpha \cos\theta_i \quad \ldots\ldots\ldots\ldots\ldots\ldots\ldots\ldots\ldots\ldots\ldots\ldots (8)$$

The distance component in the direction of the slope (x-axis) is:

$$\Delta x_i = r_i \cos\theta_i = \frac{4}{g} V_o^2 \cos^2\beta \cos^2\theta_i \tan\alpha \quad \ldots\ldots\ldots\ldots\ldots\ldots\ldots\ldots (9)$$

The average shift of the center of gravity of the splashes is defined by

$$\overline{\Delta x_i'} = \frac{\overline{\Sigma m_i' \Delta x_i}}{m'} \quad \ldots\ldots\ldots\ldots\ldots\ldots\ldots\ldots\ldots\ldots \quad (10)$$

It should be borne in mind that x_i has been calculated for a pair of masses; that m_i' represents the mass of a drop; while m = the mass of the original raindrop; and m' = the total mass of splinters caused by the raindrop. The full expression for the shift, based on the previous assumption, is obtained by substituting Eq. 9 into Eq. 10, thus:

$$\overline{\Delta x'} = \frac{2}{m'g} V_o^2 \cos^2\beta \tan\alpha \sum_{i=1}^{n} m_i \cos^2\theta_i \quad \ldots\ldots\ldots\ldots\ldots\ldots \quad (11)$$

For many drops (in time and space) we reach the limes, i.e., the integral, assuming equal probability for all angles θ_i, and m_i being independent of θ_i:

$$\lim_{n\to\infty} \frac{1}{n} \sum_{i=1}^{n} \cos^2\theta_i = \frac{1}{\pi} \int_{\theta=0}^{\pi} \cos^2\theta \, d\theta \, \frac{1}{2} \quad \ldots\ldots\ldots\ldots\ldots\ldots \quad (12)$$

Note that the change in the center of gravity has been calculated for the mass of droplets m' and not for the mass of a single raindrop. The solution of Eq. 11 is easily found if β and V_o are considered to be independent, on average, of θ and if m_i' is a time average and also considered independent of θ, for then

$$\overline{\Delta x'} = 2 \overline{\left(\frac{V_o^2}{2g}\right)} \; \overline{\cos^2\beta} \tan\alpha = 2 \overline{\left(\frac{V_o^2}{2g}\right)} \; \overline{\sin^2\beta_i} \; \overline{\tan^{-2}\beta_i} \tan\alpha \quad \ldots\ldots \quad (13)$$

in which the upper bar denotes an average value.

More generally, we obtain from Eq. 6, using the definition of the center of gravity given in Eq. 10

$$\overline{\Delta x'} = \frac{1}{m'} \frac{2}{g} \Sigma m_i V_{oi}^2 \cos^2\beta_i (\tan\beta_i + \tan\alpha \cos\theta_i) \cos\theta_i \quad \ldots\ldots\ldots \quad (14)$$

in which the summation extends over many splashes in time and space. It is divided into two terms. The first $(2/g)\, \Sigma m_i' V_{oi}^2 \cos^2\beta_i \tan\beta_i \cos\theta_i$ would vanish if $V_o m$ and β are independent of θ. If they are not, the probability function relating them must be established. The second term in the summation is

$$\overline{\Delta x'} = \frac{1}{m'} \frac{2}{g} \Sigma m_i' V_{oi}^2 \sin^2\beta_i \tan^{-2}\beta_i \tan\alpha \cos^2\theta_i \quad \ldots\ldots\ldots\ldots \quad (15)$$

The term $\tan\alpha$ can be taken out of the summation sign. The summation result is then

$$\overline{\Delta x'} = \frac{4}{g} \tan\alpha \; \overline{\cos^2\theta_i} \; \overline{\tan^{-2}\beta_i} \; \frac{\overline{V_{oi}^2 \sin^2\beta_i}}{2} \quad \ldots\ldots\ldots\ldots\ldots \quad (16)$$

$$\text{in which} \quad \cos^2\theta_i = \frac{\Sigma m_i' \cos^2\theta_i}{\Sigma m_i'} \qquad (16a)$$

$$\overline{\frac{V_{oi}^2 \sin^2\beta_i}{2}} = \frac{1}{2}\frac{\Sigma m_i' \cos^2\theta_i V_{oi}^2 \sin^2\beta_i}{\Sigma m_i' \cos^2\theta} \qquad (16b)$$

$$\overline{\tan^{-2}\beta_i} = \frac{\Sigma m_i' \cos^2\theta_i V_{oi}^2 \tan^{-2}\beta_i \sin^2\beta_i}{\Sigma m_i' \cos\theta_i V_{oi}^2 \sin^2\beta_i} \qquad (16c)$$

Eq. 16*a* becomes an identity equal to 1/2 when the m_i distribution is independent of θ_i. The term (Eq. 16*b*) is the weighted average of the vertical kinetic energy of the splashes. It expresses the maximum height they reach in their flight. The last term (Eq. 16*c*) is the weighted average of $\tan^{-2}\beta_i$.

Put in words, the shift of the center of gravity of the raindrop due to splashing is proportional to the specific kinetic energy of the splashes $V_o^2/2g$ or, in other words, to the maximum possible height to which these splashes can jump. This kinetic energy is probably related in some manner to that of the original downward velocity less some losses due to friction due to the pick-up of soil particles and to the production of new water surfaces. Consideration of the momentum conservation requires the following two equations to be fulfilled (for a raindrop which falls vertically):

$$\Sigma m_i' V_{xi} \sin\theta_i = \Sigma m_i' V_{oi} \cos\beta_i \sin\theta_i = 0$$

$$\Sigma m_i' V_{xi} \cos\theta = \Sigma m_i' V_{oi} \cos\beta_i \cos\theta = 0 \qquad (17)$$

in which V_{xi} = the horizontal velocity component in direction θ of the droplet i, having a mass m_i'. At the limes of many drops, a symmetry of the horizontal momentum with respect to two orthogonal lines must be maintained. In addition, the probability function of V, m, and β, with respect to any angle, θ, must be continuous. Furthermore, the probability distribution function should be symmetrical around the slope direction. There is a very small number of possibilities for the velocity and the mass distribution of the droplets around the first hitting point of the raindrop that will meet the foregoing conditions. The derivation of the special case, leading to Eq. 13, certainly fulfils these requirements.

Lateral Flow Due to Splashing

A single drop provokes, on average, a mass of splinters or splashes, m, with a translation $\Delta\bar{x}'$. The resultant lateral flow can be found by counting the number of drops passing through a vertical control surface. This is obviously the amount of splinters per unit time, multiplied by the distance upstream ($\Delta\bar{x}'$) over which drops fall and can still pass through the control surface.

The horizontal flow, Q_x, is then simply

$$Q_x = \Delta\bar{x} P = \Delta\bar{x}' P \frac{\Sigma m_i'}{\Sigma m_i} \qquad (18a)$$

$$\Delta\bar{x} = \Delta\bar{x}' \frac{\Sigma m_i'}{\Sigma m_i} = \epsilon \Delta\bar{x}' \qquad (18b)$$

in which $\Delta\bar{x}'$ = the time and area average translation of the splashes; P = the rate of rain; $\Sigma m_i'/\Sigma m_i = \epsilon$ = the ratio between the splashing mass and the original mass of rain; and $\Delta\bar{x}$ = the weighted equivalent translation of rain drops.

Thus, $\Delta\bar{x}$ will be seen to depend on the slope (Eq. 13), on the kinetic energy of the rain, and on the type of soil, but it also depends on the total amount of rain and its intensity, since they determine the wetness conditions at the soil surface. The ratio between the mass of "splinters" and the mass of the rain may change from zero to more than unity. In horizontal soil, $\Delta\bar{x}$ will vanish. It is probably monotonic with the slope, at least on small slopes.

In the expression for Q_x in Eq. 18*a* let us introduce the explicit values of $\Delta\bar{x}'$ as in Eq. 16:

$$Q_x = P \tan\alpha \, \epsilon \, 4 \overline{\cos^2\theta_i} \frac{\overline{V_{oi}^2 \sin^2\beta_i}}{2g} \overline{\tan^{-2}\beta_i} \quad \ldots\ldots\ldots\ldots\ldots\ldots \quad (19)$$

By introducing a new parameter, δ_i, the maximum height of the flight trajectory of a single droplet

$$\delta_i = \frac{1}{2g} V_{oi}^2 \sin^2\beta_i \quad \ldots\ldots\ldots\ldots\ldots\ldots\ldots\ldots\ldots\ldots \quad (20)$$

in which V_{oi} and β_i = respectively the speed and the angle of the exit-velocity vector, Eq. 19 will become, with $\overline{\cos^2\theta_i} = 1/2$

$$Q_x = P \tan\alpha \, 2\epsilon \frac{\bar{\delta}}{\tan^2\beta} \quad \ldots\ldots\ldots\ldots\ldots\ldots\ldots\ldots\ldots\ldots \quad (21)$$

The parameter $\bar{\delta}$ may be estimated on the strength of indirect measurements. By looking at the mud stains on walls, the height $\bar{\delta}$ can be observed qualitatively. A more accurate value may be found by measuring the drop density in the air or with the aid of blotting paper stained with methyl blue. From the area stained blue the mass of the drops at every height can be estimated.

To sum up, the horizontal flow in the direction of the slope is

$$Q_x = P\Delta\bar{x} = P \tan\alpha \, U\bar{\delta} \quad \ldots\ldots\ldots\ldots\ldots\ldots\ldots\ldots\ldots\ldots \quad (22a)$$

$$\Delta\bar{x} = \tan\alpha \cdot U\bar{\delta} \quad \ldots\ldots\ldots\ldots\ldots\ldots\ldots\ldots\ldots\ldots\ldots \quad (22b)$$

$$U = \frac{2\epsilon}{\tan^2\bar{\beta}} \quad \ldots\ldots\ldots\ldots\ldots\ldots\ldots\ldots\ldots\ldots\ldots\ldots \quad (22c)$$

Eq. 22 is similar to the fundamental postulation in the first part of this report (6). Due to the extremely short delay and small storage inherent in the splashing phenomenon, eq. 22 may be considered to represent a quasi-steady state. The parameters $\bar{\delta}$ and U are due to the rain energy and soil condition. Their form recalls a layer thickness and coefficient of anisotropy.

Preliminary Measurements of Lateral Flow

The first quantitative experiment was made with impermeable and relatively smooth surfaces on various slopes. Rain was provided by a raintower 17 m

high, in which the average flight of the drops were vertical. The rain was reasonably uniformly distributed in time and space, and the flight velocity closely approximated the final velocities encountered in the open air. Measurements were made of the actual longitudinal splash distribution beyond the upstream and the downstream edges of a wide slope. Nevertheless, a considerable number of splashes fell beyond the sides of the slope. Thus the absolute values of lateral flow measured are rather low and could in real life be at least 20%–30% higher. From the measurements taken, actual mass moments could be deduced and changes in centers of gravity calculated. However, a simpler estimate of the net lateral flow could be obtained by subtracting the net downstream splash discharge from the net upstream splash discharge. The difference is simply the lateral discharge Q_x. In Fig. 4 the results are given, as a function of the

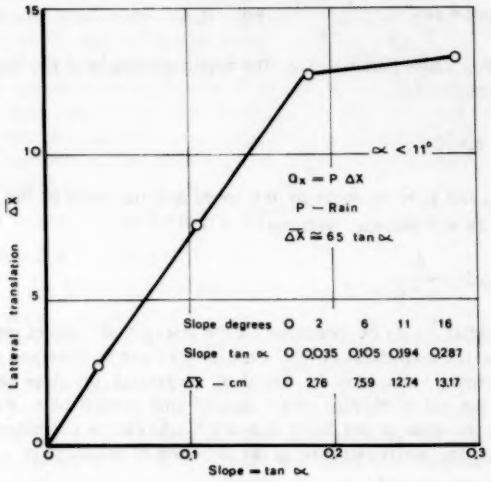

FIG. 4.—Lateral Discharge Q_x due to Splashing Rain of Intensity P over an Impermeable, Smooth Surface of Slope α

slope, in terms of Eq. 22 where $\Delta \bar{x}$ can be calculated from the measured discharge Q_x and the rate of the rainfall, P.

There are two conclusions that can be drawn from the measurements: (1) A considerable lateral flow occurs due to raindrop splashing; and (2) within the range of our experiments, the lateral flow due to raindrop splashing increases monotonically with the slope, while with slopes of up to some 20% it increases linearly with the slope.

An idea of the order of magnitude of $\Delta \bar{x}$ can be gained by observing the height of raindrop splashes on vertical walls. Typically it reaches 30 cm. In Eq. 22 this can be taken to be representative of $\bar{\delta}$. A typical value for β is 45°, so that $\tan^2 \beta = 1 - 1.4$. Let us also assume that $2\epsilon \simeq 2$; we then have $U \simeq 1.4 - 2$, so that

$$\Delta\bar{x} \simeq 40 \tan\alpha \quad \text{to} \quad 60 \tan\alpha, \text{ in centimeters} \qquad (23)$$

The experiment reported in Fig. 4 yields (up to a slope of 20%) a rather higher value, i.e.:

$$\Delta\bar{x} \simeq 66 \tan\alpha, \text{ in centimeters} \qquad (24)$$

so that either the existing angle of the splashes, β, is somewhat smaller or the associated mass thrown up by the splashing raindrops is larger, so that $\epsilon > 1$, or both. The measured and the estimated figures are very similar. The actual figure will probably vary with the roughness, the aggregate strength of the soil, and the soil moisture content. Similarly, it may change with the intensity of the rainfall, not only due to changes in the moisture regime at the soil surface, but also through the increase in the specific kinetic energy of the raindrops associated with increased rain intensity (brought about by an actual increase in the final velocity of the raindrops).

Possible Ratio Between Lateral Flow and Rain

On a long uniform slope the contribution of the lateral flow to the runoff may be negligible, since it is a constant that does not depend on the slope's length. Consider a rain discharge, Q_p, over a slope of unit width and length L:

$$Q_p = P \cdot L \qquad (25)$$

The horizontal splash discharge is Q_x from Eq. 19 or Eq. 22. The ratio between the lateral discharge and the rain discharge is then

$$\frac{Q_x}{Q_p} = \frac{\Delta\bar{x}}{L} = \frac{U\bar{\delta}\tan\alpha}{L} \qquad (26)$$

The parameter $\Delta\bar{x}$ in the preceding experiment was found to be approximately 66 tan α (in centimeters). The ratio thus depends on the steepness and the length of the slope. Assuming rills, gullies, and depressions to occur every 2 m, with a ridge in between, a typical value of the slope length from a ridge to the nearest gully would then be $L \simeq 1$ m. Further, assuming an inclination not exceeding 10%, $\Delta\bar{x}/L$ can reach 6.6%, i.e., 6.6% of the rain flows towards the depression due to splashes alone. This is a considerable amount of lateral flow.

The term $(\tan\alpha)/L$ has an important physical meaning, the concentration of rain in concave places being obviously proportional to this ratio. It is the *slope times the drainage density* of the landscape. Geometrically, it is the *curvature* of the landscape. In order to simplify understanding, it is useful to consider a model of a soil surface sinusoidal in shape, the elevation, z, of which is

$$z = \bar{z} + \frac{A}{2}\sin\left(\pi\frac{x}{L}\right) \qquad (27)$$

The parameter $A/2$ = the amplitude of the sine wave; and L = half-cycle length. The first derivative of z is the slope. Its maximum value is $(\pi A/2L)$, its average value, $\bar{s} = A/L$. The curvature is arrived at with the aid of the

second derivative, its maximum value being ($\pi^2 A/2L^2$) while, expressed in terms of the average slope $\bar{s}$, it is ($\pi^2 \bar{s}/2L$).

Excess Rain in Concave Locations

In the foregoing it has been shown that the lateral flow due to raindrop splashing may be responsible for the accumulation of rainwater in concave locations. A more rigorous expression for excess rain may be obtained from Eq. 22. Consider the slope, tan α, to be a vector resulting from two components in the x and y directions, with z = the elevation. Then

$$-\tan \alpha = 1_x \frac{\partial z}{\partial x} + 1_y \frac{\partial y}{\partial y} \quad \ldots \ldots \ldots \ldots \ldots \ldots \ldots \ldots \quad (28)$$

$\mathbf{Q}_h$, the horizontal flow in the x, y plane, is also a vector parallel with tan α (if the soil surface behaves isotropically and the rain falls vertically):

$$-\mathbf{Q}_h = (P \cdot U\bar{\delta})\left(1_x \frac{\partial z}{\partial x} + 1_y \frac{\partial z}{\partial y}\right) \quad \ldots \ldots \ldots \ldots \ldots \ldots \quad (29)$$

The excess rainwater at a given point can be obtained through the conservation equation

$$p^* = -\text{div}\, \mathbf{Q}_h = (PU\bar{\delta})\left(\frac{\partial^2 z}{\partial_x 2} + \frac{\partial^2 z}{\partial_y 2}\right) \quad \ldots \ldots \ldots \ldots \ldots \quad (30)$$

on the assumption, of course, that the rainfall P and the coefficients, U and $\bar{\delta}$ (Eq. 22), are independent of the coordinates x and y. If they are not, a term should be added to Eq. 30, i.e., **grad** (z) · **grad** ($U\bar{\delta}$). The total amount of rainwater landing on a soil would, according to Eq. 30, be

$$P_t = P + P^* = P(1 + U\bar{\delta}\, \nabla^2 z) \quad \ldots \ldots \ldots \ldots \ldots \ldots \quad (31)$$

in which $\nabla^2 z$ = the curvature which can be measured geodetically [see first article (6)].

The orders of magnitude of the components of the term in brackets of Eq. 31 are of some interest. It has been shown that the term, $U \cdot \bar{\delta}$, can reach a value of 66 cm (at least in the aforementioned experiment). For slopes of 1-m length and elevation differences of only 0.1 m, the curvature is the order of 5×10^{-3} cm^{-1}. Thus the excess rain at such concave points can be 33/100. The effective total can then be nearly 1.5 times the original rain.

A precipitation higher in certain locations than the average rainfall constitutes an extremely significant topographic effect from both the hydrological and the agrotechnical points of view.

The curvature at some points in the field can be very high. Theoretically, the curvature at the intersection of two plane slopes (second derivative of elevation) tends to infinity. This would appear to mean that an infinitely large effective amount of rainwater should be expected there; a problem that has yet to be studied in detail. What is certain is that there is a scale effect, which depends on the typical distances of splash flight and on the minimum wavelength to be taken into account in describing the shape of the soil, assuming that the soil surface can be described as a Fourier series. Infinite excess rain at

a place of infinite curvature does not in any way contradict the physical reality, since it is confined to an infinitestimal area. The writers have conducted experiments with a V-shaped, symmetrical slope, and runoff and erosion appeared almost immediately at the bottom edge. However, this phenomenon may also be explained by secondary splashing and by the flow in the surface transition layer.

Note about Erosion by Raindrop Splashes

The problem of raindrop action on the soil structure will not be fully treated here. For the present analysis it is sufficient to note that the raindrop splashes carry with them soil material the amounts of which are measurable. Typical figures obtained by the writers showed that, in a Loess soil, there was 1%–10% by weight of splashed soil in the rainwater. Typically, treatment of the soil surface by a soil conditioner designed to stabilize soil aggregates in most cases

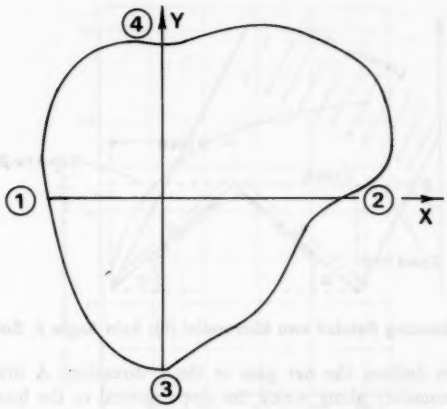

FIG. 5.—Boundaries of Surface Drainage Basin

reduced this figure to 0.25%–0.5%, in some cases it at least reduced the flight distance of splashes. Each millimeter of rain in the previously calculated example, of 1 m slope with fluctuations in elevation of 10 cm, produced 70 g of raindrops flowing towards the depression. The 1%–10% splashed soil means 0.7 g–7 g of soil/m^2 splashed towards the depression which is a considerable amount. It can explain the accumulation of splashed material in soil depressions. One can see such splashed material on almost every soil after any rain. It can explain the appreciable erosion caused once there is an actual runoff coming out of a depression and capable of carrying away the splashed soil.

A typical annual rainfall of 500 mm can move 0.3 mm–3.5 mm of soil downhill in the preceding example and rework more than 10 times this amount.

Summation over Field

Eq. 31 may be integrated over an entire field. For rainwater to be conserved, the following condition must be fulfilled:

$$\int\int P_t\,dxdy = \int\int P\,dxdy + W \quad \ldots\ldots\ldots\ldots\ldots\ldots\ldots\ldots \quad (32)$$

in which W = some finite contribution from, or loss of, rain splashes across the boundaries that becomes relatively negligible for large enough areas.

From equations 31 and 32

$$PU \cdot \bar{\delta} \int\int \nabla^2 z\,dxdy = W \quad \ldots\ldots\ldots\ldots\ldots\ldots\ldots\ldots \quad (33)$$

After the first integration, Eq. 33 reads (Fig. 5)

$$P \cdot U\bar{\delta} \int\left[\left(\frac{\partial z}{\partial x}\right)_2 - \left(\frac{\partial z}{\partial x}\right)_1\right] dy + \int\left[\left(\frac{\partial z}{\partial y}\right)_4 - \left(\frac{\partial z}{\partial y}\right)_3\right] dx = W \quad (34)$$

in which the term $P \cdot U\bar{\delta}\,[(\partial z/\partial x)_2 - (\partial z/\partial x)_1]$ = the net addition of rainwater to a strip of unit width in the y direction due to splashing in the x direction.

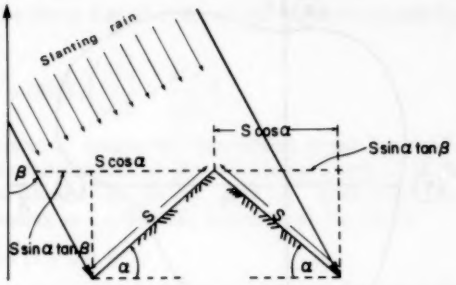

FIG. 6.—Slanting Rainfall into Microrelief (5); Rain Angle β, Soil Slope α

The order term defines the net gain in the y direction. A drainage basin is defined by a boundary along which the slope normal to the boundary is zero. Therefore, over the entire surface of a drainage basin, $W = 0$. There must be a way other than Eq. 33 to express the curved nature of the field and its overall or average impact on hydrological phenomena.

Other Forms of Rain Nonuniformity

The accumulation of rainwater in concave places is an important cause in the nonuniformity of the final distribution of the precipitation. There is another form which has been published in a report before (5). Consider a slanting rain (Fig. 6) falling at an angle β to the vertical over soil sloping at an angle α, the azimuth of the slope veing γ and that of the rain, ω. The effective rain (based on simple geometrical considerations) is then

$$P\,\text{effective} = P(1 + \eta \tan\alpha) \quad \ldots\ldots\ldots\ldots\ldots\ldots\ldots\ldots \quad (35)$$

$$\text{in which} \quad \eta = \tan\beta(\cos\gamma\cos\omega + \sin\gamma\sin\omega)\,1 \quad \ldots\ldots\ldots\ldots\ldots \quad (36)$$

It can be shown that $\eta \tan \alpha$ can easily be ± 1, leading to a virtual doubling of the effective rain on one slope and its reduction to zero on the other. The physical meaning of Eq. 35 is easily verified at its extreme when, e.g., γ and ω have the same value, i.e., the two-dimensional case where the slope and the rainflight have the same aspect. Eq. 35 then becomes

$$P_{\text{effective}} = P(1 \pm \tan \alpha \tan \beta) \quad \ldots \ldots \ldots \ldots \ldots \ldots \ldots \ldots \quad (37)$$

When $\alpha = \beta = 45°$, $P_{\text{effective}}$ is either $2P$ or zero. For a vertical wall a finite rate of rain accumulates on an infinitesimal point ($\tan \alpha \to \infty$). It would be interesting to combine the two mechanisms of concentration in concave areas (Eq. 31) and slanting rain (Eq. 35).

A further complication of the rain behavior at ground level may be expected as a result of variations in the intensity of the rain, P, high up in the air.

Changes in $\bar{\delta}$ and U to be Expected Due to Changes in Rain Data

Formulating a law for the lateral flow due to splashing would be simple enough if the anisotropy U and the jump height $\bar{\delta}$ were independant of the rain. However,

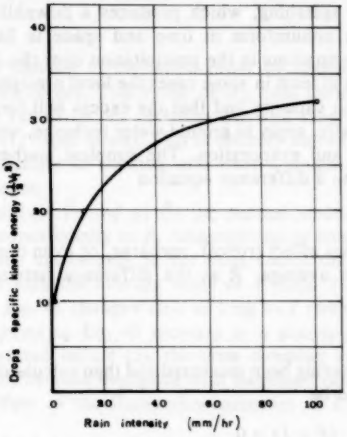

FIG. 7.—Dependence Similar to that in $U \cdot \bar{\delta}$

it is probable that the ratio of the mass splashes to that of the total rainfall as well as the recoverable kinetic energy both change with the rate of the rainfall. Investigations (1,2) indicate that larger raindrops are formed as the intensity of the storm increases. Such larger drops certainly attain higher final velocities. It has been observed (2) that, with a given soil, the specific kinetic energy of the splashes is proportional to the original kinetic energy of the rain drops. The product $U \cdot \bar{\delta}$ is likely to be proportional to the recoverable kinetic energy of the splashes, and it can therefore be expected that the dependence in $U \cdot \bar{\delta}(P)$, is similar to that shown in Fig. 7. The horizontal discharge, Q_h, will therefore be related to the rain intensity, P, by an expression containing the positive power k:

$$\underset{\sim}{Q}_h \sim (p^{1+K}); \quad U\bar{\delta}(P) \sim p^K; \quad 0 < K < 1 \quad \ldots\ldots\ldots\ldots\ldots\ldots \quad (38)$$

This corrects Eq. 22 in which $U \cdot \bar{\delta}$ was considered to be a constant. No experimental proof of Eq. 38 has been attempted, but it is reasonable to assume its correctness.

This in turn indicates that the average, $U\bar{\delta}$, would be the sum of their values at average rain intensity, $\bar{P}$, and a correction term proportional to the variance of the rain over the area. This means that fluctuations in rain intensity lead to an additional contribution of the lateral flow proportional to the rain's variance. It also means that short and strong bursts of rain, even localized ones, can produce heavy lateral flows out of proportion to the rainfall. Higher intensities will be associated with more extreme concentrations in concave places.

Rain Concentration, Runoff, and Ground Water Recharge

The main conclusion to be drawn from the foregoing analysis is that even under rain uniform in the air, the effective rain can at some points on the soil surface and at certain times be higher than the average. This is due to slanting rain and to splashing, which produces a downhill flow of raindrops. Furthermore, a rain nonuniform in time and space is liable to increase the amplitudes of the fluctuations in the precipitation over the field.

Let us assume that at least in some cases the local precipitation can eventually exceed the infiltration capacity and that the excess will form runoff. The same model may, incidentally, apply to ground water recharge, which is the difference between infiltration and evaporation. The simplest mathematical form of the model will conform to a difference equation

$$R = P - I \quad \ldots\ldots\ldots\ldots\ldots\ldots\ldots\ldots\ldots\ldots\ldots\ldots\ldots\ldots\ldots\ldots \quad (39)$$

in which R = some net effect (runoff, recharge, or even crop yield). A common error is to write the average, $\bar{R}$ as the difference between the averages of $\bar{P}$ and $\bar{I}$, thus

$$\bar{R} = \bar{P} - \bar{I} \quad \ldots\ldots\ldots\ldots\ldots\ldots\ldots\ldots\ldots\ldots\ldots\ldots\ldots\ldots\ldots\ldots \quad (40)$$

the averages $\bar{P}$ and $\bar{I}$ having been measured and then calculating $\bar{R}$. More correctly the calculation should be

$$\bar{R}_{\text{eff}} = \overline{P_{\text{eff}} - I} \quad \text{for} \quad (P - I) > 0 \quad \ldots\ldots\ldots\ldots\ldots\ldots\ldots\ldots \quad (41)$$

Earlier on it was demonstrated that P_{eff} can fluctuate widely between zero and a value several times P. If P has an expected value, $\bar{P}$, and a variance σ_p^2, and I, respectively, $\bar{I}$ and σ_I^2, then as a first approximation (neglecting higher statistical moments)

$$\bar{R}_{\text{eff}} = \bar{R} + f(\bar{R}\sigma_p^2, \sigma_I^2, \sigma_{pI}) \quad \ldots\ldots\ldots\ldots\ldots\ldots\ldots\ldots\ldots\ldots \quad (42)$$

in which σ_{pI} = the correlation between fluctuations in P and I. In most cases such a correlation exists, e.g., when I is surface retention and R is either runoff or water recharge, the correlation is positive. Surface crust causes rain to accumulate, especially in concave places. Thus, when I is infiltration, a negative correlation exists with P as far as runoff is concerned.

It may happen that $\bar{R} = 0$, i.e., that the average rain equals the average

infiltration (plus retention, etc.). Runoff may nevertheless occur due to a local concentration of rain as expressed by the statistical terms of Eq. 42. Similarly, very slight rains may effect a net water recharge in some concave places of the landscape due to lateral flow. Eq. 42 has been calculated (5) assuming a normal distribution for both P and I. It can be shown that the result is

$$\bar{R}_{\text{eff}} = \bar{R} + \frac{\sigma_R}{(2\pi)^{1/2}} \exp\left(\frac{-\bar{R}^2}{2\sigma_R^2}\right) - \frac{\bar{R}}{2} erfc\left(\frac{\bar{R}}{\sigma_R\sqrt{2}}\right) \quad (43a)$$

$$\sigma_R^2 = \sigma_P^2 + \sigma_I^2 - 2\sigma_{PI}\sigma_P\sigma_I \quad (43b)$$

$$\bar{R} = \bar{P} - \bar{I} \quad (43c)$$

P and I must not necessarily have a normal distribution, nor, for that matter, can they, if only because $P \geq 0$, $I \geq 0$. However, other distributions, while mathematically more complicated, will at any rate qualitatively lead to similar conclusions. It is interesting to study the shape of Eq. 43 with different values of $\bar{P}$ and σ_R^2. For $\bar{R} = 0$ Eq. 43a reduces to

$$\bar{R}_{\text{eff}} = \frac{\sigma_R}{(2\pi)^{1/2}} \quad (44)$$

Fluctuations of P can be of the same order of magnitude as the average value of P, and even larger. The value of σ_R can, therefore, be about $\bar{P}/2$ or larger, while the runoff or net recharge can still take up a significant part of the total rainfall (1/4 and more). This is entirely due to local concentrations of rainwater thanks either to slanting rain over a rough surface or to lateral flow caused by splashes.

At very high values of $\bar{P}$ (and of $\bar{R}$) the second term in Eq. 43a vanishes and $\bar{R}_{\text{eff}}$ increases proportionally to R. Although this is true only if the standard deviation, σ_R remains unchanged, it has been found that the fluctuations in effective P increase with the average value of P (Eqs. 31 and 35). Therefore, the ratio $(\bar{R}/\sigma_R)$ in Eq. 43 changes only as long as I remains a constant. Thus probably all three terms in Eq. 43 increase in a similar manner. Contrary to what has been suggested before (5), the term denoting local concentration of precipitation does not become negligible with increased rain intensity. It is even possible that the effect of the fluctuation increases as a result, e.g., in view of Eq. 38.

A most interesting conclusion presents itself here. The simplest linear equation (Eq. 29) has led, upon averaging, to a nonlinear relation, i.e., Eq. 43. This is due to a combination of fluctuations and a threshold I. Eq. 43 recalls experimental relations between rain and runoff that are far from linear with $\bar{R}$ (5).

Field Slope and Roughness

In most hydrological models the slope of a field is considered to be an important feature. In the foregoing it has been proved that the local curvature is just as important a feature, at least as far as raindrop splashing is concerned.

The specific mode of averaging depends on the explicit formulation of the end function. As an example, the oldest and most common hydrological model

is exemplified in Eq. 40 and somewhat corrected in Eq. 42. In Eq. 43, a specific statistical distribution is assumed. The variance of P has been related to variations in slope (Eq. 35) or in curvature (Eq. 31).

Let us calculate the variance of P, taking σ_P^2 from Eq. 31, and assuming U and $\bar{\delta}$ to be constant (concentration only in concave spots)

$$\sigma_{P_1}^2 = P^2 U^2 \bar{\delta}^2 \frac{\int\int (\nabla^2 z)^2 \, dxdy}{\int\int dxdy} \quad \ldots\ldots\ldots\ldots\ldots\ldots\ldots\ldots \quad (45)$$

The roughness in this case is obviously the average of the squared curvature. Another variance is due to slanting rain (Eq. 35).

$$\sigma_{P_2}^2 = P^2 \frac{\int\int \eta^2 \tan^2 \alpha \, dxdy}{\int\int dxdy} \quad \ldots\ldots\ldots\ldots\ldots\ldots\ldots\ldots \quad (46)$$

Note that η changes from one point to the other as the aspect of the slope changes. This means that the roughness of the field, as defined in Eq. 46, is not a contant topographical parameter but may vary with changes in the aspect of the rain. Still more complicated cases can be constructed by combining the two mechanisms of slanting rain and concentration in concave spots. So far, only integration over space, as in Eqs. 45 and 46, has been carried out. Fluctuations of the rain intensity P in space and time and the dependence of $U \cdot \bar{\delta}$ on P would require the calculation of yet another variance.

It becomes important at this point to consider the need for measuring different topographic and rain parameters that have always been neglected in the past. These parameters are bound to have a decisive effect on both the local and the temporal concentrations of rain, which can cause ground water recharge, runoff, or at least different degrees of wetness of different parts of the soil.

As an illustration let us imagine a two-dimensional sinusoidal landscape. With the elevation z fluctuating around the average $\bar{z}$ at an amplitude $A_i/2$ and half cycle $x = L_i$ (i indicating a given soil surface wave), we have

$$z = \bar{z} + \frac{A_i}{2} \sin\left(\pi \frac{x}{L_i}\right) \quad \ldots\ldots\ldots\ldots\ldots\ldots\ldots\ldots \quad (47)$$

The slope is

$$-\tan \alpha = \frac{\partial z}{\partial x} = \frac{A_i \pi}{2 L_i} \cos\left(\pi \frac{x}{L_i}\right) \quad \ldots\ldots\ldots\ldots\ldots\ldots\ldots\ldots \quad (48)$$

and the curvature (dispensing with the index as one cycle only is being considered) is

$$\frac{\partial^2 z}{\partial_x 2} = -\frac{A}{2}\left(\frac{\pi}{L}\right)^2 \sin\left(\pi \frac{x}{L}\right) \quad \ldots\ldots\ldots\ldots\ldots\ldots\ldots\ldots \quad (49)$$

The roughness or variance according to Eq. 45 is found from

$$\sigma_P^2 = \frac{1}{L} P^2 U^2 \bar{\delta}^2 \left(\frac{A}{2}\right)^2 \left(\frac{\pi}{L}\right)^4 \int_o^L \sin^2\left(\pi \frac{x}{L}\right) dx$$

$$= \frac{\pi}{2}\left(\frac{\pi}{L}\right)^4\left(\frac{A}{2}\right)^2 P^2 U^2 \bar{\delta}^{-2} \quad \ldots\ldots\ldots\ldots\ldots\ldots\ldots\ldots\ldots\ldots \quad (50)$$

while the standard deviation of the precipitation at the soil surface is

$$\sigma_{P1} = PU\bar{\delta}\frac{A}{L^2}\left(\frac{\pi}{2}\right)^{5/2} \quad \ldots\ldots\ldots\ldots\ldots\ldots\ldots\ldots\ldots\ldots \quad (51)$$

As mentioned earlier, the term $A\pi^2/L^2 2$ denotes the maximum curvature of the soil surface. The parameter (A/L) is the average local slope and $1/L$ is the drainage density. For $L \sim 1$ m and A only 0.1 m, $U\bar{\delta}$ can be 0.50 m (as measured). The standard deviation will be around $0.2P$.

A second example is that of slanting rain (Eq. 46). Assuming $\eta = 1$ and rain to fall at an angle of 45°

$$\sigma_{P2} = P\frac{A}{L}\left(\frac{\pi}{2}\right)^{3/2} \quad \ldots\ldots\ldots\ldots\ldots\ldots\ldots\ldots\ldots\ldots \quad (52)$$

with $(A/L) = 0.1$ the value is about $0.18\,P$. Much higher values are obtained when the relief of the soil is steeper and the angle of the slanting rain shallower.

A rough estimate of the final variance of the precipitation on the soil surface may be gained by adding up the separate variances. The total standard deviation can thus easily amount to 30% of the average rain intensity even if the rain is originally perfectly uniform in time and space at some height above the soil.

Summary and Conclusions

A theory has been suggested relating the horizontal flow to rain splashes. Relying on certain assumptions, that flow was found to be proportional to the slope and to the rainfall itself as well as to a given fraction of the kinetic energy of the splashes. A rough estimate of the incalculable parameters showed them to be of the same order as the measured ones. Measuring the horizontal shift of the center of gravity due to splashing is relatively simple, and the results validate the proportionality to the slope up to an inclination of 20%. The horizontal flow due to rain splashes can reach in magnitude several percent of the rate of rain over a given area. It becomes quite important in steep and short slopes.

Local concentrations of rain splashes occur in concave parts of the landscape, concentrations of rainwater of up to 50% of the average precipitation over the entire area having been shown to be possible. The measure of the concentrations is proportional to the curvature of the soil surface, but the behavior at very high curvatures, i.e., a sharp change in slope, has still to be investigated. Rain concentration there is probably moderate.

Another cause for higher local effective rain is the interaction between rain slanting (the angle at which the rain falls) and surface roughness. This interaction can easily cause a doubling of the rain over some parts of the surface. The combination of concentration in concave spots and over some slopes facing the slanting rain produces on the whole a rain variance of a very high value, and even if the most traditional view, i.e., that runoff is rain minus infiltration, is adopted, it is seen that the rain can, locally and temporarily, be much higher

than the average. The rain can thus produce waterlogging and runoff even if its average does not exceed the soil's infiltration capacity. In a similar way local ground water recharge can occur even if, on the average, the rate of infiltration does not exceed evaporation. A suitable way to average these parameters has been described. It is very interesting to note that, taken on average, a basically linear relationship produces a strongly nonlinear one much like the relations found between rain and runoff.

The conclusions based on the foregoing analyses do not only make for a better understanding of effective rain distribution. They clearly point to the necessity to measure hitherto neglected parameters that affect surface hydrology. They are the variances of the rain, infiltration, and whatever other parameters enter into the equation. Furthermore, the character and the slant of the rain must be related to one type of soil roughness parameter which involves the square of the slope and its aspect to the rain. The other type of roughness parameter is independent of direction and is found to be the square of the local soil surface curvature. Both types of roughness depend on the details in which the surveying of a soil surface and the calculation are performed. They are not unique. Just how the roughness is to be calculated and how it affects the hydrology of a watershed should be the subject of future studies. It may be relevant to future agrotechnical practices, to the characterization of watersheds, and to the choice of prototype watersheds to be studied.

The calculation of horizontal flow with the aid of rain splashes enables the discharge of soil eroded by splashes to be estimated.

Appendix I.—References

1. Chow, Ven Te, ed., *Handbook of Applied Hydrology*, McGraw-Hill Book Co., Inc., New York, N.Y., 1964.
2. Mutchler, C. K., "Parameters for Describing Raindrop Splash," *Soil and Water Conservation*, Vol. 22, No. 3, 1967.
3. Mutchler, C. K., "Splash of Water Drop at Terminal Velocity," *Soil Science*, Vol. 169, 1970, pp. 1311–1312.
4. Mutchler, C. K., "Splash Amounts from Water Drop Impact on a Smooth Surface," *Water Resources Research*, Vol. V, No. 1, 1971.
5. Zaslavsky, D., "Some Aspects of Watershed Hydrology," *Special Report U.S.D.A. ARS 41157*, United States Department of Agriculture, 1970.
6. Zaslavsky, D., and Sinai, G., "Surface Hydrology: I—Explanation of Phenomena," *Journal of the Hydraulics Division*, ASCE, Vol. 107, No. HY11, Proc. Paper 15958, Jan., 1980, pp. 1–16.

Appendix II.—Notation

The following symbols are used in this paper:

A = twice amplitude of soil surface elevation;
g = gravitational acceleration;
i = infiltration, surface retention or any entity subtractable from original water input;
L = length of slope;
m = mass;
n = number of raindrops;

p = rate of precipitation;
Q = discharge;
R = net effect—rain minus infiltration, infiltration minus evaporation;
r = radial distance;
U = coefficient of nonisotropy;
V = velocity of raindrops, of rain splashes;
W = volume of rain splashing across border;
x = horizontal coordinate, distance of point of impact (with subscript);
y = horizontal coordinate (normal to x and to z);
z = elevation or vertical coordinate, positive upward;
α = soil surface slope angle (inclination);
β = angle between flight of outgoing splash and horizon, or angle between raindrop flight and vertical;
γ = azimuth angle of slope;
δ = maximum height of flight of rain splashes;
ϵ = the ratio between mass of splashes and mass of original raindrop;
η = trigonometric function of slanting rain;
θ = angle between splash flight and slope vector;
π = radians of semicircular arc;
σ = standard deviation or correlation; and
ω = azimuth of rain flight.

Subscripts

x = in x component;
o = exit velocity of splash;
u = upward or upstream;
d = downward or downstream;
i = of single splash;
1 = of infiltration;
p = of rain;
h = horizontal component;
eff = effective; and
R = of R.

Superscripts

$( )'$ = of total splashes belonging to one raindrop; and
$( )^*$ = excess (of rain or moisture).

JOURNAL OF THE HYDRAULICS DIVISION

SURFACE HYDROLOGY: III—CAUSES OF LATERAL FLOW

By Dan Zaslavsky[1] and Gideon Sinai[2]

INTRODUCTION

In the first part of this report (15) we stipulated the existence of certain mechanisms by which rain and vertical infiltration do not penetrate straight down into the soil. They induce a horizontal flow component which is proportional to the slope, the rainfall, and some coefficient of anisotropy. Such mechanisms could explain a number of phenomena in hydrology, erosion, and soil-formation processes.

It should be further amplified that many observations of such phenomenon have been made in the past and recorded fatefully by some investigators. The investigations by J. D. Hewlett and his coworkers (8,9) should be mentioned in particular. They reported two fundamental observations. One is: "There is little doubt that the largest component of stormflow from forests and most wildlands begins as subsurface flow. Sometimes the term *interflow* is used synonymously with subsurface stormflow, but other times it is used to refer to any nonvertical subsurface flow above the water table." The second observation is that: "Channel precipitation is augmented first by expansion of the surface and subsurface areas contributing water either by flow through the soil pores into the channel or by displacement of stored water from further upslope . . ." The area adjacent to the stream channel is the main source of stormflow because the lower slope continually receives soils and ground water from upslope; thus the soil near the stream is wetter at the beginning of a storm, causing the source area to expand from the channel upward and outward" (see Ref. 8,

[1]Prof. of Soil and Water Engrg., Faculty of Agricultural Engrg., Soils and Fertilizers Div., Technion—Israel Inst. of Tech., Technion City, Haifa, 32000, Israel.

[2]Lect., Faculty of Agricultural Engrg., Soils and Fertilizers Div., Technion—Israel Inst. of Tech., Technion City, Haifa, 32000, Israel.

Note.—Discussion open until June 1, 1981. Separate discussions should be submitted for the individual papers in this symposium. To extend the closing date one month, a written request must be filed with the Manager of Technical and Professional Publications, ASCE. Manuscript was submitted for review for possible publication on March 23, 1979. This paper is part of the Journal of the Hydraulics Division, Proceedings of the American Society of Civil Engineers, © ASCE, Vol. 107, No. HY1, January, 1981. ISSN 0044-796X/81/0001-0037/$01.00.

pp. 92–95). They named this phenomenon the "Variable Source Area."

It is the purpose of the present report to explain these undeniable phenomena, and to formulate them in a rigorous manner.

In the second part of the report (16) the mechanism of raindrop splashes was shown to be in good accord with the aforementioned stipulation. It produces a real horizontal flow component which is proportional to the rainfall, the slope, a simulated thickness of the splashings layer, and a certain coefficient. The thickness and the coefficient appear to increase with the rainfall intensity. The mechanism of raindrop splashes can explain how rain accumulates in concave spots. Slanting rainfall hitting slopes that face it is another mechanism that can explain local rain excess. These local rain concentrations can explain why flow in soil depressions can commence long before the average rainfall exceeds the average infiltration capacity. However, this mechanism of rain redistribution fails to explain several phenomena that call for horizontal flow within the soil. The splashing of raindrops cannot account for soil moisture accumulation over greater distances, such as encountered in the Beer-Sheba experiment (15) or mentioned by Hewlett et al. (8,9). It is also a very brief phenomenon that ceases a fraction of a second after the rain stops. In contrast, some processes of accumulation take days or weeks. Erosion due to seepage forces must involve rain that first enters the soil and eventually seeps out.

In the present part of the report we shall consider in principle the mechanism that can produce a downstream flow component more or less parallel to the soil surface and within the soil. In most general terms, the arguments supporting such a mechanism are very simple. Let us consider a soil which is not uniform, its nonuniformity taking the form of parallel layers. It may be said that this soil's properties have a rotational symmetry designated by some vector λ_l, and the soil is on the whole anisotropic, one of the principal axes being λ_l. If the force motivating the flow is directed away from λ_l, the flux will also be directed away, but not at the same angle. Consider the soil layers as being in a slope forming an angle α with the horizon; λ_l is therefore at an angle of α to the vertical. The force of gravity thus forms an angle α with λ_l and points downstream. Infiltration will therefore not proceed vertically downwards but will have a horizontal component downstream.

In the following we shall deal in greater detail with the mechanism of horizontal flow within the soil. Its order of magnitude will be assessed and in some cases derived quantitatively.

First, we shall follow the phenomenon through the bending of streamlines and cite an example of horizontal flow near a water table. Next we shall consider the more general case and prove the existence of a horizontal flow component.

Two very important specific types of nonuniformities in the soil are analyzed: (1) Cyclic layered soil; and (2) soil surface air transition layer. Here they are considered only qualitatively. They will be the subject of a detailed quantitative treatment in later parts of this report.

Bending of Streamlines

When a streamline moves from one medium of conductivity K_1 to another of conductivity K_2, it will form different angles, γ_1 and γ_2, with the line normal to the interface (1) so that (Fig. 1)

$$\frac{\tan \gamma_1}{\tan \gamma_2} = \frac{K_1}{K_2} \quad \text{(1)}$$

Fig. 1 can be considered an example representing two soil layers whose interface forms an angle α with the horizon. On passing from a less permeable to a more permeable layer, the streamline will be diverted from a normal direction toward a diagonal direction, thus producing a parallel component. If, as in

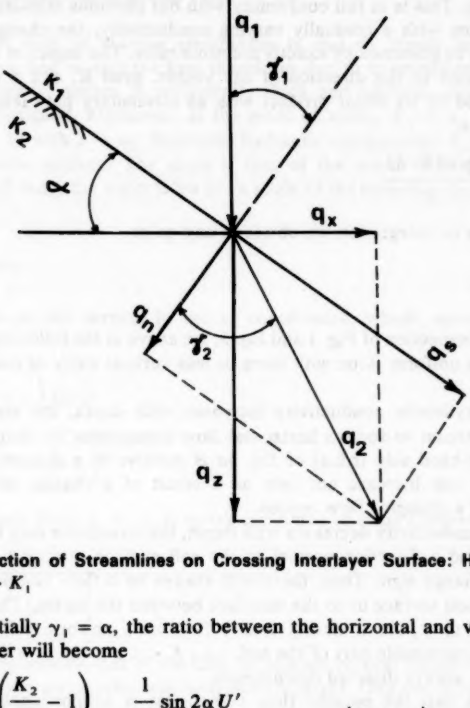

FIG. 1.—Deflection of Streamlines on Crossing Interlayer Surface: Hydraulic Conductivity $K_2 > K_1$

this case, initially $\gamma_1 = \alpha$, the ratio between the horizontal and vertical fluxes in the sublayer will become

$$\frac{q_x}{q_z} = \frac{\tan \alpha \left(\dfrac{K_2}{K_1} - 1\right)}{1 + \dfrac{K_2}{K_1} \tan^2 \alpha} = \frac{\dfrac{1}{2} \sin 2\alpha\, U'}{1 + \sin^2 \alpha\, U'}; \quad U' = \left(\frac{K_2}{K_1} - 1\right) \quad \text{(2)}$$

as can be shown by simple trigonometric considerations.

At small slopes (angles α), $(\tan^2 \alpha)\, K_2/K_1 << 1$, so that

$$\frac{q_x}{q_z} \sim U' \tan \alpha \quad \text{(3)}$$

or $1/2 \sin 2\alpha \sim \sin \alpha$ and $\sin^2 << 1$, so that

$$\frac{q_x}{q_z} \sim \sin(\alpha)\, U' \quad \ldots\ldots\ldots\ldots\ldots\ldots\ldots\ldots\ldots\ldots\ldots\ldots\ldots\ldots\ldots\ldots (4)$$

In more general cases of unsaturated flow, U' takes the same form, K_2 and K_1 being the weighted averages of the horizontal and vertical conductivities, respectively.

If q_z happens to be the rate of infiltration I, which is equal to some steady rainfall, then $K_1 = I$. By substituting I in Eq. 2 or 3, we obtain the horizontal flow component as a function of the steady rainfall or the steady rate of infiltration and the slope. This is in full conformity with our previous stipulation (15).

In a medium with a gradually varying conductivity, the change in the flow direction will be governed by exactly the same rules. The angles of the streamline are then related to the direction of the vector, **grad K**, and a change in tan γ is expressed by its scalar product with an elementary path length, **ds**, along the streamline:

$$\frac{d(\tan\gamma)}{\tan\gamma} = \frac{\mathbf{grad\ K}\cdot\mathbf{ds}}{K} \quad \ldots\ldots\ldots\ldots\ldots\ldots\ldots\ldots\ldots\ldots\ldots\ldots\ldots\ldots (5a)$$

and therefore on integration we obtain at any point

$$\frac{\tan\gamma}{\tan\gamma_1} = \frac{K}{q_1} \quad \ldots\ldots\ldots\ldots\ldots\ldots\ldots\ldots\ldots\ldots\ldots\ldots\ldots\ldots\ldots\ldots (5b)$$

By simple inspection of Fig. 1 and Eq. 5, we arrive at the following conclusions in regard to a uniform slope with more or less vertical entry of the water:

1. If the hydraulic conductivity increases with depth, the streamlines will curve downstream to form a horizontal flow component by virtue of the fact that the right-hand side (r.h.s) of Eq. 5*a* is positive in a downward direction. Note that K can increase not only as a result of a change in soil but also as a result of a changing flow regime.
2. If this conductivity decreases with depth, the streamline may turn upstream but not beyond a direction normal to the soil surface, i.e., tan γ can vanish but cannot change sign. Thus, there will always be a flow component parallel either to the soil surface or to the interface between the layers. This component can decrease to $q_1 \sin\alpha$ during steady flow in a uniform soil and to zero in a highly impermeable part of the soil, i.e., $K << q_1$; $\tan\gamma \to 0$. The parallel component is always directed downstream.
3. The fact that the parallel flow component is proportional to the slope can explain the concentration of moisture in concave spots.

It seems mathematically simpler to use the components q_s and q_n in Fig. 1, respectively parallel and normal to the interfaces. From Eq. 1 and some simple geometrical considerations we obtain:

$$\frac{q_s}{q_n} = \tan\gamma = \frac{K}{K_1}\tan\gamma_1 \quad \ldots\ldots\ldots\ldots\ldots\ldots\ldots\ldots\ldots\ldots\ldots\ldots\ldots\ldots\ldots\ldots (6)$$

In the case where q_1 is vertical at the point of entry and $\gamma_1 = \alpha$ is the slope, $q_{s_1} = q_1 \sin\alpha$; $q_{n_1} = q_1 \cos\alpha$ (assuming only for this derivation that

q_n is positive downward), and the simple result is

$$\frac{q_s}{q_n} = \frac{K}{q_1} \tan \alpha \quad \ldots \quad (7)$$

From Eqs. 6 and 7 one can review the foregoing conclusions more simply. The parameter $q_s \to 0$ only when $K \to 0$ or $\alpha \to 0$. The parallel flow component is exactly proportional to the slope.

Bending of Streamlines above Water Table

The simplest case of curving streamlines is that of steady accretion at a phreatic surface due to rain (or loss therefrom due to evaporation). If the soil above the phreatic surface is sufficiently thick and uniform, the streamlines will enter it vertically. Moreover, at the point of entry, $K_1 = q_1$ (Fig. 1) (for proof see Eq. 14 with $z \to \infty$). Saturated hydraulic conductivity K_{sa} is observed near the phreatic surface. The slope is that of the water table $\alpha \equiv \gamma_1$. The streamlines will enter the water table at an angle to the normal, which, according to Eq. 7, is

$$\frac{q_s}{q_n} = \frac{K_{sa}}{q_1} \tan \alpha \quad \ldots \quad (8)$$

or at an angle to the vertical in the xz coordinates, which, according to Eq. 2, is

$$\frac{q_x}{q_z} = \frac{\left(\frac{K_{sa}}{q_1} - 1\right) \tan \alpha}{\left(1 + \frac{K_{sa}}{K_1} \tan^2 \alpha\right)} \quad \ldots \quad (9)$$

If, during steady flow, $q_z = q_1$ at every depth due to mass conservation:

$$q_x = \frac{(K_{sa} - q_1) \tan \alpha}{\left(1 + \frac{K_{sa}}{K_1} \tan^2 \alpha\right)} \quad \ldots \quad (10)$$

It is interesting to note that in the case of smaller vertical fluxes the horizontal component at the water table will be relatively larger. One can actually calculate the horizontal projection of a streamline as it descends from the soil surface. If one assumes a saturation surface at elevation zero, one can derive the equation for the pressure head ψ from Darcy's equation

$$dz = -\frac{d\psi}{1 - \frac{q_1}{K}} \quad \ldots \quad (11)$$

bearing in mind that q_1 is in the negative z direction. Assuming an empirical relationship between the conductivity K and the pressure head ψ, we integrate Eq. 11, e.g., from Eqs. 10 and 11 we assume

$$K = K_{sa} \exp a(\psi + \psi_0); \quad \psi + \psi_0 < 0 \quad \ldots\ldots\ldots\ldots\ldots\ldots \quad (12)$$

in which a and ψ_0 = empirical coefficients; and K_{sa} = the saturated hydraulic conductivity.

Introducing this expression into Eq. 11 and integrating, we obtain the distribution $K(z)$ implicitly

$$z - z_0 = -\frac{1}{a} \ln \frac{\dfrac{K}{K_{sa}} - \dfrac{q_1}{K_{sa}}}{1 - \dfrac{q_1}{K_{sa}}} \quad \ldots\ldots\ldots\ldots\ldots\ldots\ldots\ldots \quad (13)$$

Solving for K we arrive at

$$K = q_1 + (K_{sa} - q_1) \exp\,[-a(z - z_0)] \quad \ldots\ldots\ldots\ldots\ldots\ldots \quad (14)$$

in which z_0 = the elevation of saturation face at $\psi = \psi_0$. With the aid of Eq. 6 in which K_{sa} is replaced by any K from Eq. 14, we can calculate the parallel translation of a streamline (which is indentical to a path line under steady flow) using the identities $(ds/dn) \equiv (q_s/q_n)$ and $(dz = dn \cos_\alpha)$:

$$ds = \frac{K}{K_{sa}} \tan\alpha \; dn = \left\{1 + \left(\frac{K_{sa}}{q_1} - 1\right) \exp\,[-a(n\cos\alpha - z_0)]\right\} \tan\alpha \; dn \quad (15)$$

and on integration:

$$\Delta s = n \tan\alpha + \left\{1 - \exp\left[-a(n\cos\alpha - z_0)\right]\left(\frac{K_{sa}}{q_1} - 1\right)\right\} \frac{\tan\alpha}{a\cos\alpha} \ldots \quad (16)$$

In the case of a large term $n \cos\alpha - z_0$, Eq. 16 is approximated by

$$\Delta s \cong n \tan\alpha + \left(\frac{K_{sa}}{q_1} - 1\right) \frac{\tan\alpha}{a\cos\alpha} \quad \ldots\ldots\ldots\ldots\ldots\ldots \quad (17a)$$

The first term is simply the deviation of the vertical from the normal. The second term is the deviation of the streamline from the vertical. Thus the horizontal component of the streamline over a sufficiently great depth is

$$\Delta x \cong \left(\frac{K_{sa}}{q_1} - 1\right) \frac{\tan\alpha}{a} \quad \ldots\ldots\ldots\ldots\ldots\ldots\ldots\ldots \quad (17b)$$

It is independent of the depth. In many drainage problems the slope is between 0.01 and 0.1, and the hydraulic conductivity changes from 10 mm/day–100 mm/day. The drainage rate may attain 2 mm/day–3 mm/day. The coefficient a can have a typical value of 0.01 cm^{-1}. It is evident that the horizontal projection Δx can range from a few centimeters to many meters as the water moves from the soil surface to the water table. This result is particularly striking when one considers certain shallow water tables of waterways and drains. Even in the case of relatively flat land, the groundwater slope increases towards the drain and the lateral flow component within the unsaturated soil becomes significant.

This special case of nonuniform conductivity and lateral flow is due to the

specific boundary conditions of the case and has already gained recognition (Refs. 2–7). However, instead of applying the numerical technique and thereby losing the insight, we prefer the simple analytic derivation that provides a better demonstration of the essence of the phenomenon and its order of magnitude.

Flow in Nonuniform Soil—General Considerations

Consider a nonuniform soil where properties change in a direction n normal to the direction s (Fig. 2); n and s form an angle α with the z and x coordinates, respectively. The flux q_0 is taken to be known somewhere in the medium. Of special interest is q_0 which is vertical in the positive z direction (as evaporation) or in the negative z direction (as infiltration).

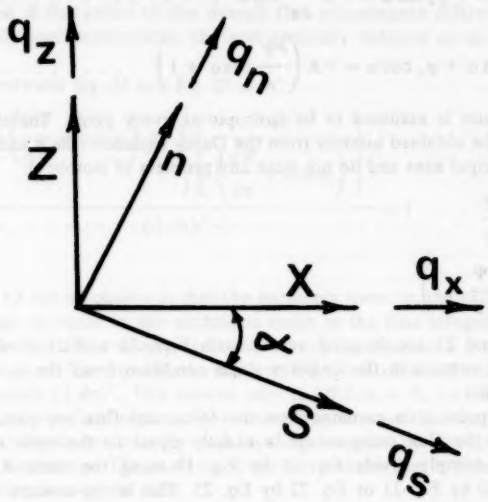

FIG. 2.—Upright and Sloping Coordinate Systems and Related Flow Components

In order to solve an actual problem, we require information on the hydraulic properties of the medium and certain boundary conditions. The most general case is of very little interest if its solution is too complicated. Here we are interested mainly in two cases: (1) With uniformity along s, e.g., $\partial\Psi/\partial S = 0$, $\partial K/\partial S = 0$, etc.; and (2) with a uniform slope as in item 1 and a steady-state flow.

While these are not the most general cases, they are sufficient to lead us to some of the more important conclusions or at least provide us with a good starting point, lending an insight into hydrologic processes.

Nonuniform Soil—Basic Equations of Flow and General Derivation of Anisotropy

According to Darcy's law and assumption about uniformity along s, the fluxes

in the n, s directions are

$$q_s = K \sin \alpha \quad \ldots \quad (18)$$

$$q_n = -K\left(\frac{\partial \Psi}{n} + \cos \alpha\right) \quad \ldots \quad (19)$$

in which $K(n, \Psi)$ is the hydraulic conductivity that can vary with the pressure head, Ψ, and the location along n, explicitly, but not in the s direction.

The fluxes expressed in terms of the x, z system are derived from Eqs. 18 and 19 by simple geometric transformation

$$q_x = q_s \cos \alpha + q_n \sin \alpha = -K \frac{\partial \Psi}{\partial n} \sin \alpha \quad \ldots \quad (20)$$

$$q_z = -q_s \sin \alpha + q_n \cos \alpha = -K\left(\frac{\partial \Psi}{\partial n} \cos \alpha + 1\right) \quad \ldots \quad (21)$$

The medium is assumed to be isotropic at every point. Therefore, q_x and q_z can also be obtained directly from the Darcy equation (the n and s directions are the principal axes and do not raise any problem of isotropy):

$$q_x = -K \frac{\partial \Psi}{\partial x} \quad \ldots \quad (22)$$

$$q_z = -K\left(\frac{\partial \Psi}{\partial z} + 1\right) \quad \ldots \quad (23)$$

Eqs. 22 and 23 are in good accord with Eqs. 20 and 21 if we transform the gradient vectors in the uniform slope condition from the n, s system to the x, z system.

At every point it is assumed that the force and flux are parallel, so that the ratio of the flux components is exactly equal to the ratio of the force components (simply divide Eq. 18 by Eq. 19 using the same K in both or divide Eq. 20 by Eq. 21 or Eq. 22 by Eq. 23. This is the essence of assuming isotropy at a point.

The first question to be answered is whether or not the medium as a whole behaves isotropically or not. In order to reach a general conclusion, let us consider path lines (that are identical to the streamlines only under steady flow). The ratios of path components in the s and n directions are found by dividing Eq. 18 by Eq. 19, and integrating over n and dividing by $\int dn$ for averaging:

$$\frac{\int \frac{q_s}{q_n} dn}{\int dn} = \frac{\int \frac{\sin \alpha \, dn}{\frac{\partial \Psi}{\partial n} + \cos \alpha}}{\int dn} \quad \ldots \quad (24)$$

Note that $(q_s/q_n) = (ds/dn)$, along a path line so that the numerator in Eq. 24 is simply $\int ds$. The entire fraction expresses the ratio of parallel to normal paths of flow. The fraction (q_s/q_n) is the angle of the flux vector at a point, while the r.h.s. of Eq. 24 gives the angle of the overall flux vector.

The r.h.s. is obtained by finding expressions for q_s and q_n from Eqs. 18 and 19. It is clear that if $\partial\Psi/\partial n$ varies with n, the overall slope of the water path also varies with n. The overall ratio of the parallel force $\bar{F}_s$ to the normal force $\bar{F}_n$ is found by integrating the parallel gradient components separately over n and dividing them by the normal component integrated over n:

$$\frac{\bar{F}_s}{\bar{F}_n} = \frac{\sin\alpha \int dn}{\int \left(\frac{\partial\Psi}{\partial n} + \cos\alpha\right) dn} \quad \ldots\ldots\ldots\ldots\ldots\ldots\ldots\ldots \quad (25)$$

Clearly the ratios in Eqs. 24 and 25 become identical only in the following two cases: If $\partial\Psi/\partial n = 0$; or if $\sin\alpha = 0$, i.e., horizontal soil layering. It is evident that if the ratios of the overall flux components differ from those of the overall force components, the soil generally behaves as an anisotropic medium.

The ratio between Eq. 24 and Eq. 25 is

$$\frac{\left(\frac{\bar{q}_s}{\bar{q}_n}\right)}{\left(\frac{\bar{F}_s}{\bar{F}_n}\right)} = \frac{\int \left(\frac{\partial\Psi}{\partial n} + \cos\alpha\right) dn \int \left[\left[\frac{dn}{\left(\frac{\partial\Psi}{\partial n} + \cos\alpha\right)}\right]\right]}{(\int dn)^2} > 1 \quad \ldots\ldots\ldots \quad (26)$$

The proof of the inequality is that the harmonic mean in the second integral is smaller than or equal to the arithmetic mean in the first integral. In effect, this means that on the average, the conductivity in direction s is greater than that in direction n. The equality to unity in Eq. 26 is obtained only when the numerator equals $(\int dn)^2$. This occurs only if $\partial\Psi/\partial n = 0$, i.e., in a uniform soil with a uniform flow regime. It is interesting to note that such anisotropy is generally induced not only by soil layering but also by changes in Ψ due to boundary conditions. The analysis of the streamlines near a phreatic surface in the preceding is a special case.

In a cyclic medium and in steady flow, Ψ fluctuates around an average value and $\partial\Psi/\partial n$ fluctuates around zero. Thus, over a complete cycle, the first integral in Eq. 26 reduces to $\cos\alpha \int dn$ and Eq. 26 reduces to

$$\frac{\left(\frac{\bar{q}_s}{\bar{q}_n}\right)}{\left(\frac{\bar{F}_s}{\bar{F}_n}\right)_{\text{cyclic}}} = \frac{\int \frac{dn}{\frac{1}{\cos\alpha}\left(\frac{\partial\Psi}{\partial n}\right) + 1}}{\int dn} > 1 \quad \ldots\ldots\ldots\ldots\ldots\ldots \quad (27)$$

Care must be taken in the case of a horizontal soil since Eqs. 26 and 27 were obtained by division of Eqs. 24 and 25, both of which vanish under such conditions.

In summary, in cases where $\partial\Psi/\partial n \neq 0$ and $\alpha \neq 0$, there is always a flux away from the force. If the force is on the average vertical, like gravity, there is always a net horizontal component downstream.

Examples of Soil Anisotropy

We have demonstrated that streamlines curve downstream on passing from a less permeable layer to a more permeable one. Alternatively, within a uniform soil, the streamlines bend downstream when the pressure increases with depth. We have also proved that in any nonuniform sloping soil there will be a net horizontal flow component. Furthermore, we have furnished evidence supporting our stipulation (15) that under conditions of vertical infiltration the horizontal flux is proportional to the vertical flux and to the slope. The total horizontal flow is therefore also dependent on the overall thickness of the anisotropic medium in which the vertical flow takes place.

The simplest case is that of a saturated, layered soil. We have also dealt with another simple case, i.e., a uniform unsaturated soil with a water table. Hydraulic conductivity increases towards the water table and there will be a lateral, downstream flow component.

In otherwise uniform soil, another change in K can come about at the wetting front. There, the pressure head and K drop to almost zero with depth. Therefore, streamlines that enter the soil vertically by infiltration will tend towards a direction normal to the wetting front. If the front is at a slope, there will be a net horizontal component upstream, e.g., if $\partial\Psi/\partial n$ is very high in Eq. 24 as at a wetting front, $(q_s/q_n) \rightarrow 0$.

Unsaturated flow in a layered soil can show irregular behavior. In an unsaturated layer overlying a less permeable layer, the pressure head and K will increase with depth. The opposite will occur in the underlying layer. Thus the streamlines may describe a zigzag course moving downstream within the more permeable layer and upstream within the less permeable one. However, the net effect is movement downstream, as has been proved in Eqs. 26 or 27.

During evaporation of moisture from the soil there will also be a gradual increase in the pressure head with depth and the net effect in both uniform and layered soils will be of a downstream, horizontal flow component.

In the following we shall consider qualitatively a two-layer problem and a surface transition problem. In forthcoming parts of this report they will be treated quantitatively.

Two-Layer Problem—Qualitative Considerations

Let us consider a permeable layer of saturated conductivity K_{sa_1} and thickness D_1 overlying a less permeable layer (K_{sa_2}, D_2) (Fig. 3). The rain is of intensity q_1, which is smaller than the hydraulic conductivity, K_{sa_1} of the top layer. Thus the flow in this layer will be unsaturated and under negative pressure. If D_1 is sufficiently large, the flow regime at the top will asymptotically approach $K_1 = q_1$ and the hydraulic gradient will approach unity (see Eq. 14 with $z \rightarrow \infty$). As the flow approaches the interface between the layers, the pressure will increase gradually. The hydraulic conductivity within the top layer will gradually increase towards saturation, $K_1 \rightarrow K_{sa_1}$. In Fig. 2 two adjacent vertical sections are shown. Compare the pressure head curve in the upper one with that in the lower one. At two points along a horizontal line C-D the elevation is the same. The pressure head Ψ is higher in the upper section (curve 1) than in the lower one (curve 2). Therefore there must be a flow component

in the horizontal direction, i.e., downstream.

Let us study this problem in the light of the streamline equations 3 and 4. At the top of layer 1 (Fig. 2), $K_1 \rightarrow q_1 < K_{sa}$. At the bottom of this layer $K_1 = K_1''$, i.e., it increases and may approach K_{sa1}. Owing to the presence of the less permeable layer and as a result of the unsaturated flow, there is a build-up of moisture, pressure, and conductivity above the interface. The flow direction in the top layer will then change from vertical ($q_x = 0$) to

$$q_x \cong \left(\frac{K_1''}{q_1} - 1\right) \tan(\alpha)\, q_1 \quad \ldots\ldots\ldots\ldots\ldots\ldots\ldots\ldots\ldots\ldots\ldots\ldots \quad (28)$$

(from Eq. 3, identifying K_1'' with K_2, and q_1 with K_1). It thus becomes evident that if there is a more permeable layer at the soil surface and if the flow is unsaturated, the streamlines will bend downstream. It can be claimed that

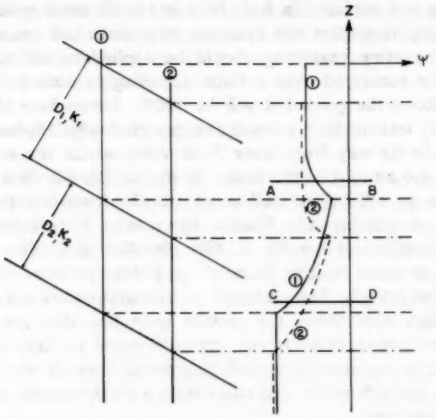

FIG. 3.—Pressure Head (ψ) Distribution for Vertical Flow through Sloping, Two-Layered Soil System

every soil, without exception, has a more permeable layer at its surface. Therefore, in every sloping soil subjected to prolonged rainfall, the streamlines will bend downstream. In other words, at the surface of every sloping soil there will be a horizontal flow component downstream. This is true both under completely unsaturated conditions and in the presence of a water table. Furthermore, one is led to the following conclusions:

1. The horizontal flow component is proportional to the vertical flow at all depths. The same also holds for the total horizontal discharge. Implicitly, the horizontal flux also increases due to the coefficient of anisotropy $[(K_1''/q_1) - 1]$ which in turn increases with the rate of vertical flow. Thus, the horizontal flow is proportional to the steady rainfall intensity with a power higher than a unity.

2. If there is a change in the slope, the landscape becoming concave, there

is also a concentration of moisture. This is due to the fact that horizontal inflow exceeds the horizontal outflow. A very high saturated hydraulic conductivity (K_{sa}) usually implies a rapid reduction of conductivity due to suction, i.e., a higher value of the coefficient a in Eq. 12. This means that a relatively small soil depth ($z - z_0$ in Eq. 14) is sufficient to make the conductivity equal to the rate of infiltration and to cause the flow to become vertically downward. Thus the very high conductivity at every soil surface validates our assumption that the rain initially penetrates the soil in a vertical direction. The two-layer problem will be treated quantitatively in a later part of this report.

Transition Layer at Soil Surface

In the first part of this report (15) we expressed reservations about the possibility of measuring surface flow because there is no explicit definition of what actually constitutes the soil surface. In Ref. 14 it is argued more generally that in soil physics meaningful entities are averages over time and space and produce a continuum. The same reasoning should be applied to the soil surface, e.g., porosity can be measured over a finite sampling volume or over an area. In the air well above the ground it will be 100%. Somewhere in the soil it may be 50%. At any intermediate point it changes gradually. Hydraulic conductivity changes in a similar way from some finite value within the soil bulk to a very high value in the air, e.g., the change in K_{sa} in Eq. 12. In a similar way the air entry value ψ_0 will be reduced to zero at the transition from the soil bulk to the air ($\psi_0 \rightarrow 0$ in Eq. 12). Finally, the rate of K reduction under suction will increase [coefficient a in Eq. 12 (See also Ref. 10)]. The air can therefore be considered as some limiting form of the porous medium itself (very similar to a very coarse gravel). The pressure of the raindrops is always atmospheric. The rate of flow well above the surface is in fact the rate of rainfall, and the unsaturated conductivity is conveniently equal to this rate. The surface transition layer is not merely a mathematical artifact. It may be very thin in some uniform, smooth sands, but can obtain a thickness of several decimeters in most cultivated soils.

The soil surface is defined by a transition of properties. Its direction is defined by a surface normal to the property gradient. One of the many such surfaces could be chosen in accordance with some convenient conservation requirement, e.g., that the total porosity remains unchanged (14). The said property may change abruptly at this representative surface. We may conclude that a clear-cut soil surface can replace the transition only as a mathematical artifact.

An important consequence of the aforementioned is that every rainfall, irrespective of its intensity, penetrates completely into the soil (at least into its surface transition zone). If we are consistent in our views, there is no such thing as surface runoff over a large surface because the rain can never exceed the hydraulic conductivity of the uppermost part of the soil surface, i.e., the air itself. Saturation due to rain of high intensity, when such occurs, will always be manifest initially within the surface transition zone.

The splashing of raindrops has been proved (16) to cause a horizontal flow component proportional to the slope, explicitly proportional to the rate of rainfall, and implicitly proportional to some fractional power of the rain. Evidently, a steady flow through the surface transition layer is related in exactly the same

way to the rain. The response time of the splashing raindrops is measured in fractions of a second. It can therefore be considered quasi-steady (behaving identically to the rain itself). Flow in the transition layer can be delayed, depending on its thickness. It is anticipated that thin transition layers will react more rapidly.

At the wetting front the flow-motivating force is mainly the pressure gradient, which is expected to be normal to the surface. Therefore, the flow will tend to be normal to the soil surface ($q_x \to 0$) (Fig. 1) and even to have a slight upstream flow component ($q_x < 0$) (Fig. 1). Well behind the wetting front the main force will be gravity and a horizontal downstream flow ($q_x > 0$) (Fig. 1) will be formed.

The flow in the surface transition layer can sometimes be observed as tiny trickles of water or shiny soil surfaces. Very small concave spots where water concentrates can be considered in detail as such or be averaged out as parts of a thicker transition layer. The exact limit depends on the arbitrarily selected scale of observation. Calculation of a steady flow through a transition layer is possible if the hydraulic parameters are known. Nonsteady flow will be treated in detail in the last part of this report.

Significance of Flows in Surface Transition Layer

Let us first consider a well-cultivated, heavy soil, with a good stable structure. The hydraulic conductivity at the top (not necessarily near the air) can reach 10^{-1} cm/s or even 1 cm/s. Such values have actually been measured by the senior writer in a drainage research field at Hazorea, Israel. In the subsoil the hydraulic conductivity may drop to 10^{-6} cm/s or less. This means that the anisotropy coefficient ($\bar{K}_n/\bar{K}_v$) − 1 can range from almost zero at an extremely low rate of rainfall up to the order of 10^6. One can actually observe lateral flows of a few meters or tens of meters over a vertical infiltration of a few decimeters. After rain or irrigation water puddles form in slightly concave spots. This example is obviously extreme and almost trivial. The observations reported earlier north of Beer-Sheva (15) are far less trivial and fit the foregoing analysis. Even a change of two orders of magnitude in the hydraulic conductivity within the surface transition layer and a slope of 1% can produce a horizontal flow equal to the vertical one. The slopes in the region north of Beer-Sheva were steeper (closer to 10%).

We have no direct measurements of field anisotropy. The assemblage of such data and treatment of certain other aspects should be the subject of future research efforts.

The two processes, raindrop splashing and flow in the surface transition layer, can combine to produce lateral flow and moisture concentration. Under laboratory conditions one can test the flow within the transition layer separately by applying moisture lacking the high kinetic energy of the raindrops. In nature it will be difficult to distinguish between the two. In an earlier part of this report (16) we mentioned an experiment involving a V-shaped soil slope. Runoff started almost immediately at the sharp bottom edge. Raindrop splashing alone cannot account for this. Since in this case there was no impermeable layer or pervasive saturation of the soil directly by the average rain, the phenomenon may be related to flow in the surface transition layer. This deduction is also supported

by the fact that the runoff at the sharp 'V' edge involved liquefaction of the soil and erosive flow. Such a flow can occur only if water seeps out of the soil. Raindrop splashes may be considered to remain outside the soil. However, the rain enters the transition zone and can then seep out.

Apparently, the water flow in the surface transition zone can be quite significant in cases where raindrop splashing is unpronounced. It can respond to more extreme curvatures of the soil surface (greater than 1 m^{-1}) where it can produce runoff and erosion with very small amounts of rain and within a relatively short time. At the other extreme, it can lead to the accumulation of moisture at relatively moderate curvatures (smaller than 0.1 m^{-1}), as in the Beer-Sheva experiment where the effect of raindrop splashing was negligible.

The thickness of the transition zone is dependent not only on geometry but also on effects such as the transfer of momentum in liquid flow (12). Most soils have a looser structure at their surface with some aggregates, root holes, and other irregularities. Freshly exposed soil cuts will develop such thicker transition zones in the course of time. Surface lateral flow and erosive mechanisms will follow accordingly.

Some surface transition layers may be very similar to a straw roof. Examples are litter-covered forest soils and possibly even certain grass-covered areas where the old growth may have a marked orientation parallel to the soil surface.

The concept of surface transition may find interesting application in the solution of certain other water flow problems such as the discharge of water at a seepage face. Accordingly, the flow medium will be described as consisting of highly permeable layers at the surface. The concept of a seepage face thus becomes redundant. The streamlines simply bend downstream in the transition zone, diverging from the normal on entering more permeable layers. In what has been termed the seepage face, the flow is more or less parallel to the surface but occurs within the soil. Such a comprehension of seepage is significant not only in contributing to the physical consistency of our flow analysis. It can explain how certain small, geometrical, surface irregularities can cause local outflows and erosion due to extreme seepage forces.

Conclusions

It is significant that a downstream horizontal flow component occurs whenever the pressure head and K decrease with elevation. This is certainly the case during drainage and the drying of the soil surface by evaporation. The presence of a surface transition layer heightens this effect. Thus lateral flow and moisture concentration in concave parts of the landscape will continue long after the rain has stopped. This process will keep the concave parts wetter for long periods and shorten the time interval preceding the onset of runoff when the next rain falls. It appears that lateral flow takes on universal importance during saturated and unsaturated flow, prolonged rainfall, and the drainage and frying of the surface. It occurs at seepage faces, in natural, exposed soil, and possibly in litter-covered soil.

The derivations were made for a soil which is isotropic at any point. The nonisotropic behavior is only on the average. This derivation does not exclude cases where the soil is intrinsically nonisotropic. The mathematics is only more tedious, and the phenomena more extreme.

Irrigation of cultivated soils must be effected by the lateral flow of water. Farmers have been emphasizing the importance of leveling fields. The term leveling appears to be a semantic error bound up with a misinterpretation of the mechanism. In practice, the leveling of fields entails the provision of plane surfaces (also having gentler slopes). It is possible that leveling is not as important as "planing." Very small scale, sharp, local curvatures, such as furrows cause nonuniformities in the moisture distribution that are averaged out by the soil itself and by the plants. Nevertheless, sharp-edged furrows invariably lead to erosion and the rapid development of runoff. In the light of the previous analysis, some thought should be given to the shape of furrows. Nonuniformities in the moisture distribution can also be caused by more moderate curvatures. Moreover, they can occur on such a scale that cannot be evened out by the root volume of a single plant or by lateral redistribution of water at greater soil depth. Thus a plane surface configuration of a field is a prerequisite for even distribution of rain or irrigation water.

We have completed the description of the four mechanisms leading to lateral flow components: (1) Splashing of raindrops; (2) flow within a surface transition layer; (3) flow in a layered soil; and (4) bending of streamlines near a water table. The last three are merely different forms of soil nonuniformity. However, they are here arranged according to depth and time lag.

In all four phenomena the horizontal flow is found to be proportional to the vertical flow. All four have been shown to possess possible significance. They could thus explain most of the phenomena mentioned in the first part of this report (15).

Appendix I.—References

1. Bear, J., Zaslavsky, D., and Irmay, S., *Physical Principles of Water Percolation and Seepage*, UNESCO, Paris, France, 1968.
2. Freeze, R. A., "The Continuity Between Groundwater Flow Systems and Flow in the Unsaturated Zone," *Proceedings of the Hydrological Symposium*, No. 6, University of Saskatchewan, Nov., 1967, pp. 204–240.
3. Freeze, R. A., "The Mechanism of Natural Groundwater Recharge and Discharge. 1. One-Dimensional, Vertical, Unsteady, Unsaturated Flow Above a Recharging or Discharging Groundwater Flow System," *Water Resources Research*, Vol. 5, No. 1, 1969, pp. 153–171.
4. Freeze, R. A., "Three-Dimensional, Transient, Saturated-Unsaturated Flow in a Groundwater Basin," *Water Resources Research*, Vol. 7, No. 2, 1971, pp. 347–366.
5. Freeze, R. A., "Role of Subsurface Flow in Generating Surface Runoff, 1, Base Flow Contributions to Channel Flow," *Water Resources Research*, Vol. 8, No. 3, 1972, pp. 609–623.
6. Freeze, R. A., "Role of Subsurface Flow in Generating Surface Runoff, 2, Upstream Source Areas," *Water Resources Research*, Vol. 8, No. 5, 1972, pp. 1272–1283.
7. Freeze, R. A., "Streamflow Generation," *Reviews of Geophysics and Space Physics*, Vol. 12, No. 4, 1974, pp. 627–647.
8. Hewlett, J. D., and Nutter, W. L., *An Outline of Forest Hydrology*, University of Georgia Press, Athens, Ga., 1969.
9. Hewlett, J. D., and Hibbert, A. R., "Fact Affecting the Response of Small Watersheds to Precipitation in Humid Areas," *International Symposium on Forest Hydrology*, Pergamon Press, Oxford, England, 1967.
10. Mualem, Y., "Hydraulic Properties of Unsaturated Porous Media," *P.M. 38/74*

Research No. 012-295, Technion, Haifa, Israel, 1974.
11. Mualem, Y., and Dagan, G., "Methods of Predicting the Hydraulic Conductivity of Unsaturated Soils," *USA-Israel (BSF) Research Project No. 442*, Hydraulic Laboratory, Technion, Haifa, Israel, 1976.
12. Suffman, P. G., "On the Boundary Condition at the Surface of the Porous Medium," *Studies in Applied Mathematics*, Vol. L, No. 2, 1971, pp. 93–101.
13. Zaslavsky, D., "Some Aspects of Watershed Hydrology," *Special Report No. ARS 41-157*, ARS, United States Department of Agriculture.
14. Zaslavsky, D., "The Average Entities in Kinematics and Thermodynamics of Porous Materials," *Soil Science*, Vol. 106, 1968, pp. 358–362.
15. Zaslavsky, D., and Sinai, G., "Surface Hydrology: I—Explanation of Phenomena," *Journal of the Hydraulic Division*, ASCE, Vol. 107, No. HY1, Proc. Paper 15958, Jan., 1981, pp. 1–16.
16. Zaslavsky, D., and Sinai, G., "Surface Hydrology: II—Distribution of Raindrops," *Journal of the Hydraulic Division*, ASCE, Vol. 107, No. HY1, Proc. Paper 15959, Jan., 1981, pp. 17–35.

Appendix II.—Notation

The following symbols are used in this paper:

a = experimental constant;
D = thickness of soil layers;
i = rate of infiltration into soil;
K = hydraulic conductivity;
q = water flux in velocity dimensions;
U = coefficient of anisotropy or ratio $(K_2/K_1) - 1$;
x = horizontal coordinate;
z = vertical coordinate;
α = slope of soil surface or soil layers;
γ = angle between incoming streamline and normal to interface;
λ_i = symmetry vector;
Ψ = pressure head; and
ψ_0 = air entry value.

Subscripts

1, 2 = two successive layers;
x = in x direction;
z = in z direction;
s = parallel to layers or soil surface;
n = normal to layers or soil surface;
sa = saturated; and
0 = initial, fixed value.

JOURNAL OF THE HYDRAULICS DIVISION

SURFACE HYDROLOGY: IV—FLOW IN SLOPING, LAYERED SOIL

By Dan Zaslavsky[1] and Gideon Sinai[2]

INTRODUCTION

In the three previous parts of this report soil layering has been mentioned as one of the causes of a lateral flow component induced by infiltration. It has been generally proved that as soon as the soil is not uniform and it is sloping, there must be a downstream flow component parallel to the slope. In the following we shall treat specifically a soil consisting of distinct layers. If the hydraulic characteristics of each layer are known, it is possible to determine the flow and calculate the total horizontal discharge. In fact, the description of the soil as being made up of distinct layers also enables us to simulate transition layers.

For the specific case of a cyclic two-layered soil and steady-state flow, the soil actually behaves as an anisotropic medium. The average parallel and normal conductivities can be calculated. The following is based to a large extent on an earlier special report by the same writers (4).

BASIC FLOW EQUATIONS

Consider a nonuniform soil with properties changing in a direction n. The parallel direction is s (Fig. 1); n and s form an angle α with the elevation z and the horizontal coordinate x.

We assume first: (1) Uniformity along s, e.g., $\partial\Psi/\partial S = 0$, $\partial K/\partial S = 0$, etc., Ψ being the pressure head and K the hydraulic conductivity; (2) a uniform slope as just mentioned and a steady-state flow; and (3) the medium is isotropic at any point. Any anisotropy is, on the average, induced.

[1]Prof. of Soil and Water Engrg., Faculty of Agricultural Engrg., Soils and Fertilizers Div., Technion—Israel Inst. of Tech., Technion City, Haifa, 32000, Israel.

[2]Lect., Faculty of Agricultural Engrg., Soils and Fertilizers Div., Technion—Israel Inst. of Tech., Technion City, Haifa, 32000, Israel.

Note.—Discussion open until June 1, 1981. Separate discussions should be submitted for the individual papers in this symposium. To extend the closing date one month, a written request must be filed with the Manager of Technical and Professional Publications, ASCE. Manuscript was submitted for review for possible publication on March 23, 1979. This paper is part of the Journal of the Hydraulics Division, Proceedings of the American Society of Civil Engineers, © ASCE, Vol. 107, No. HY1, January, 1981. ISSN 0044-796X/81/0001-0053/$01.00.

According to Darcy's law (Fig. 1), the fluxes in the n and s directions are:

$$q_s = K \sin \alpha \quad (1)$$

$$q_n = -K\left(\frac{\partial \Psi}{\partial n} + \cos \alpha\right) \quad (2)$$

in which $K(n, \Psi)$ = the hydraulic conductivity that can vary explicitly with the pressure head, Ψ, and the location along n.

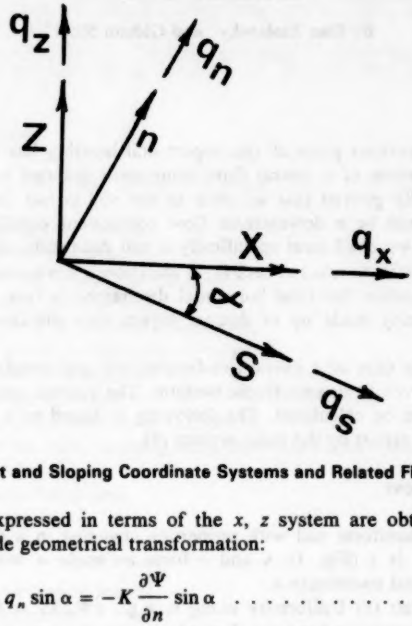

FIG. 1.—Upright and Sloping Coordinate Systems and Related Flux Components

The fluxes expressed in terms of the x, z system are obtained from Eqs. 1 and 2 by simple geometrical transformation:

$$q_x = q_s \cos \alpha + q_n \sin \alpha = -K \frac{\partial \Psi}{\partial n} \sin \alpha \quad (3)$$

$$q_z = -q_s \sin \alpha + q_n \cos \alpha = -K\left(\frac{\partial \Psi}{\partial n} \cos \alpha + 1\right) \quad (4)$$

Owing to point isotropy, q_x and q_z can also be derived directly and simply from the Darcy equation (the n and s directions are the principal axes and do not raise any problem of isotropy):

$$q_x = -K \frac{\partial \Psi}{\partial x} \quad (5)$$

$$q_z = -K\left(\frac{\partial \Psi}{\partial z} + 1\right) \quad (6)$$

Eqs. 5 and 6 correspond to Eqs. 3 and 4 if we transform the gradient vectors

from the n, s system to the x, z system as in Eqs. 12 and 13.

In accordance with the conditions of steady flow and uniform slope, the same fluxes cross the soil surface and any other surface parallel to it. On a control surface of Fig. 2

$$-P\cos\alpha\, dA = q_n\, dA \quad \ldots\ldots\ldots\ldots\ldots\ldots\ldots\ldots\ldots\ldots\ldots\ldots\ldots\ldots (7)$$

P being the intensity of the rainfall on a horizontal surface above the soil. Introducing Eq. 7 into Eqs. 1 and 2 after factoring out dA we obtain

$$q_n = -P\cos\alpha = -K\left(\frac{\partial\Psi}{\partial n} + \cos\alpha\right) \quad \ldots\ldots\ldots\ldots\ldots\ldots\ldots\ldots\ldots\ldots (8)$$

$$q_s = K\sin\alpha \quad \ldots\ldots\ldots\ldots\ldots\ldots\ldots\ldots\ldots\ldots\ldots\ldots\ldots\ldots\ldots\ldots (9)$$

These three equations (two in Eq. 8 and one in Eq. 9) provide the basis for our further calculation.

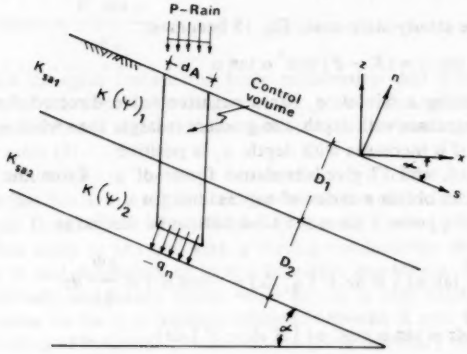

FIG. 2.—Control Element in Two-Layer Flow Problem

According to Eqs. 8, 9, 3, and 4, the flux components in the x, z directions are

$$q_x = -K\left(\frac{\partial\Psi}{\partial x} + 1\right) = \frac{1}{2}(K - P)\sin 2\alpha \quad \ldots\ldots\ldots\ldots\ldots\ldots\ldots (10)$$

$$q_z = -K\left(\frac{\partial\Psi}{\partial z} + 1\right) = -(P\cos^2\alpha + K\sin^2\alpha) \quad \ldots\ldots\ldots\ldots\ldots\ldots\ldots (11)$$

Using simple geometrical relations and recalling that $\partial\Psi/\partial s = 0$, we obtain

$$\frac{\partial\Psi}{\partial x} = \frac{\partial\Psi}{\partial n}\sin\alpha \quad \ldots\ldots\ldots\ldots\ldots\ldots\ldots\ldots\ldots\ldots\ldots\ldots\ldots\ldots\ldots (12)$$

$$\frac{\partial\Psi}{\partial z} = \frac{\partial\Psi}{\partial n}\cos\alpha \quad \ldots\ldots\ldots\ldots\ldots\ldots\ldots\ldots\ldots\ldots\ldots\ldots\ldots\ldots\ldots (13)$$

On eliminating $\partial\Psi/\partial\eta$ from the foregoing we obtain the following rather trivial result:

$$\frac{\partial\Psi}{\partial x} = \frac{\partial\Psi}{\partial z}\tan\alpha = -\left(\frac{\partial\Psi}{\partial z}\right)\frac{\partial z_o}{\partial x} \quad \ldots\ldots\ldots\ldots\ldots\ldots\ldots\ldots \quad (14)$$

in which $z_o(x)$ = the elevation of some surface n = constant.

By substituting the left-hand side of Eq. 14 into Eq. 10 we obtain yet another expression for q_x:

$$q_x = -K\frac{\partial\Psi}{\partial z}\tan\alpha \quad \ldots\ldots\ldots\ldots\ldots\ldots\ldots\ldots\ldots\ldots \quad (15)$$

Now $\partial\Psi/\partial z$ can be derived from Eq. 11 in one of two forms

$$\frac{\partial\Psi}{\partial z} = -\left(\frac{q_z}{K} + 1\right) = -\left(1 - \frac{P}{K}\cos^2\alpha - \sin^2\alpha\right) \quad \ldots\ldots\ldots\ldots \quad (16)$$

Thus, for the steady-state case, Eq. 15 becomes:

$$q_x = (q_z + K)\tan\alpha = (K - P)\cos^2\alpha\tan\alpha \quad \ldots\ldots\ldots\ldots\ldots\ldots \quad (17)$$

Note that during a rainfall q_z has a negative value directed downwards. If the pressure decreases with depth, the gradient is larger than when q_x is negative upstream, and if it increases with depth, q_x is positive.

Eqs. 3, 10, 15, and 17 give alternative forms of q_x. From the relationship in Eq. 17 one can obtain a series of expressions for q_z.

Integration of q_x over z gives the total horizontal discharge

$$Q_x = \int q_x\,dz = \tan\alpha\left(\int K\,dz + \int q_z\,dz\right) = -\tan\alpha\int K\frac{\partial\Psi}{\partial z}\,dz \quad \ldots\ldots\ldots \quad (18)$$

$$\text{or} \quad Q_x = \int q_x\,dz = \tan\alpha\cos^2\alpha\left(\int K\,dz - P\int dz\right) \quad \ldots\ldots\ldots\ldots\ldots \quad (19)$$

For convenience we define the averages:

$$\bar{K}_x = \frac{1}{D}\int K(\Psi)\,dz; \quad -\bar{q}_z = \frac{1}{D}\int q_z\,dz; \quad \bar{q}_x = \frac{1}{D}\int q_x\,dz \quad \ldots\ldots\ldots\ldots \quad (20)$$

Then from Eq. 18

$$\bar{q}_z D = D\,\bar{q}_z\left(\frac{\bar{K}_x}{\bar{q}_z} - 1\right)\tan\alpha = \bar{q}_z\,U\tan\alpha\,D; \quad U = \left(\frac{\bar{K}_x}{\bar{q}_z} - 1\right) \quad \ldots\ldots\ldots \quad (21)$$

in which $\bar{q}_z$ = the average downward vertical flow. From Eq. 19 one obtains an alternative expression for the average horizontal flow with steady rainfall

$$\bar{q}_x D = P\,U^*\tan\alpha; \quad U = \left(\frac{\bar{K}_x}{P} - 1\right)\cos^2\alpha \quad \ldots\ldots\ldots\ldots\ldots\ldots \quad (22)$$

Eq. 21 gives the basic ratio between the horizontal and vertical components of flow, which applies both in steady and nonsteady flow. Eq. 22 provides a similar ratio between the rain and the average horizontal flux, which applies only in the case of steady flow. Note that the magnitude of $\bar{q}_z$ is not necessarily

equal to P, and that q_z is nonuniform on the x- or z-axes. When angles α are sufficiently small, $\cos^2 \alpha \rightarrow 1$ and Eq. 22 is simplified.

The horizontal flow component is the value we actually need. It is related to a unique coordinate system and can be integrated over a map. We shall therefore have to continue using it although the employment of n, s coordinates is more elegant.

The total discharge in the s direction is Q_s. By integrating Eq. 9 we obtain:

$$Q_s = \sin \alpha \int K \, dn \quad \ldots \ldots \ldots \ldots \ldots \ldots \ldots \ldots \ldots \ldots \quad (23)$$

both in steady and nonsteady flow.

The average parallel flux component $\bar{q}_s$ is

$$\bar{q}_s = \bar{K}_s \sin \alpha; \quad \bar{K}_s = \frac{\int K dn}{\int dn} \quad \ldots \ldots \ldots \ldots \ldots \ldots \ldots \quad (24)$$

In steady-state flow we obtain from Eq. 8 the very simple expression

$$\frac{\bar{q}_s}{q_n} = -\frac{\bar{K}_s}{P} \tan \alpha = \frac{\bar{K}_s \sin \alpha}{q_n} \quad \ldots \ldots \ldots \ldots \ldots \ldots \ldots \quad (25)$$

Eqs. 21 and 22 again feature the basic relationship that was stipulated in the first part of this report (1) and was later proved for splashing raindrops (2). This relationship has also been demonstrated for the bending of streamlines near a water table (3).

So far the uniformity of the slope has been limited to the requirement that $\partial \Psi / \partial s = 0$ or that this term is negligible in the calculation of the first approximation of the vertical flow regime. Eqs. 21 and 22 are not limited to a two-layered cyclic soil, but apply to any soil with a varying conductivity along the n-axis, whether due to soil properties or to the boundary conditions. Eq. 21 is valid for both nonsteady and steady flows, while Eq. 22 is only valid for the latter. In specific cases we have to assume relations between K and Ψ and find the actual distribution of hydraulic parameters for given boundary conditions.

Examples and Orders of Magnitude

Net Recharge of Deep Groundwater.—The net recharge is introduced into the soil in the form of seasonal pulses. However, these seasonal pulses are damped and the flow becomes virtually steady after several wavelengths. In the various equations P must now be considered not as a rain but as the net groundwater recharge. If the net recharge is P mm/yr and the moisture content is C, then the wavelength is about P/C, e.g., if the moisture content is 0.3 and the net recharge is about 0.3 meter, the wavelength is about 1 m. A net recharge of 300 mm/yr is equivalent to about 10^{-6} cm/s.

Let us now consider a series of soil layers changing from clay or rock with a conductivity approximating the rate of net recharge, i.e., 10^{-6} cm/s to highly permeable ones in which moisture accumulates.

The average ratio between components parallel and normal to the layers is given by Eq. 25. The parameter $\bar{K}_s$ will be affected by the layers with high conductivity. The highest conductivity values will be obtained for coarse-grained soil in the presence of perched water. Clearly the ratio can attain several orders

of magnitude. The same can be estimated from Eqs. 21 or 22. The coefficient of anisotropy is obviously not a constant. It varies from zero at low flow rates to possibly very high values.

Flow Behind Wetting Front.—Sufficiently far behind the wetting front the flow can be almost steady. Such flow is established within a relatively short time, especially if there is an impeding layer at the soil surface. In such a case the formulas incorporating rain P can be used as a first approximation for averaging over the wetted profile.

Two-Layer Problem

Consider two parallel soil layers (Fig. 3) forming an angle α with the horizon. Their thicknesses are D_1 and D_2, respectively, and their saturated conductivities

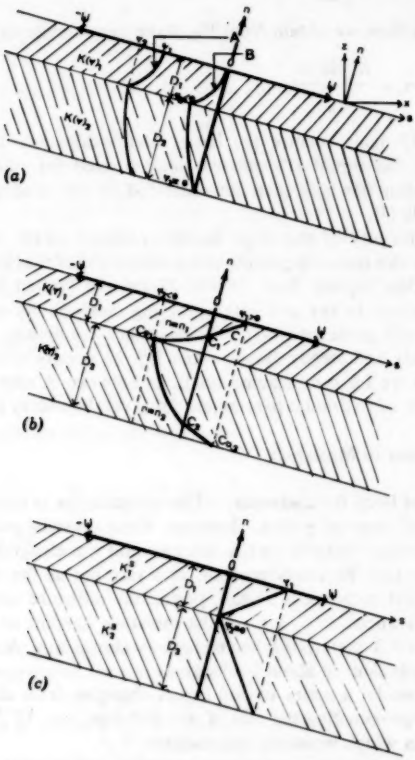

FIG. 3.—Two-Layer Pressure Head Distribution: (*a*) State A—No Saturation, State B—Initial Saturation; (*b*) State C—Partial Saturation; (*c*) State D—Complete Saturation

are K_{sa1} and K_{sa2}, respectively. Each layer is isotropic and uniform. The soil consists of a cyclic arrangement of these two layers repeating itself many times.

From Eq. 8, by solving for dn and integrating (steady state), we obtain

$$\cos \alpha \int dn = \int \frac{K(\Psi)\, d}{P - K(\Psi)} \quad \ldots\ldots\ldots\ldots\ldots\ldots\ldots\ldots\ldots\ldots \quad (26)$$

From Eq. 11 we similarly obtain along the z coordinate

$$\cos^2 \alpha \int dz = \int \frac{K(\Psi)\, d}{P - K(\Psi)} \quad \ldots\ldots\ldots\ldots\ldots\ldots\ldots\ldots\ldots\ldots \quad (27)$$

The boundaries of integration are shown in Fig. 3 which describe two layers at four flow stages. The conditions are presented in Table 1.

The actual values of Ψ_1 and Ψ_2 can be found from an implicit equation as a function of the rain P.

TABLE 1.—Conditions of Boundaries of Integration

Stage of flow (1)	First Layer		Second Layer		Figure (4)
	n-boundary (2)	Ψ-value	n-boundary (3)	Ψ-value	
Top and bottom layers unsaturated throughout	0	Ψ_1	$-D_1$	Ψ_2	3
	$-D_1$	Ψ_2	$-(D_1 + D_2)$	Ψ_1	
Saturation appears in the top layer so that $\Psi_1 = 0$	0	0	$-D_1$	Ψ_2	3
	$-D_1$	Ψ_2	$-(D_1 + D_2)$	0	
Partial saturation so that $\Psi_2 < 0$; $\Psi_1 > 0$; 0-n_1 is saturated	0	$\Psi_1 > 0$	$-D_1$	Ψ_2	4
	$-n_1$	0	$-(D_1 + n_2)$	0	
	$-D_1$	$\Psi_2 < 0$	$-(D_1 + D_2)$	Ψ_1	
Both layers are completely saturated $K_{1s} < P < K_{2s}$	0	Ψ_1	$-D_1$	0	5
	$-D_1$	0	$-(D_1 + D_2)$	Ψ_1	

The solution is readily obtained by introducing a relation $K(\Psi)$ for the two layers. Then $\Psi(n)$ or $\Psi(z)$ is found as well as $K(n)$ or $K(z)$. From these, in turn, one can calculate $\bar{Q}_n$ from Eq. 19 or $\bar{Q}_z$ from Eq. 23.

As an example, let us consider the experimental relation for the ith layers with K_{sa} as the saturated conductivity, and a_i and Ψ_{oi} as the experimental coefficients:

$$K_i = K_{sai} \exp a_i(\Psi + \Psi)_{oi}, \quad \text{for} \quad \Psi + \Psi_o < 0;$$

$$K_i = K_{sai}, \quad \text{for} \quad \Psi + \Psi_o > 0 \quad \ldots\ldots\ldots\ldots\ldots\ldots\ldots\ldots\ldots\ldots \quad (28)$$

Introducing Eq. 28 into Eq. 26 one obtains

$$\cos \alpha(n - n_o) = -\frac{1}{a_i} \ln \frac{P - K_i(\Psi)}{P - K_{io}(\Psi)} \quad \ldots\ldots\ldots\ldots\ldots\ldots\ldots\ldots \quad (29)$$

in which n_o = an initial point on n within a given layer (1); and $K_i(\Psi) = K_{io}(\Psi)$.

Eq. 29, when written for two layers of thickness, D_1 and D_2, gives

$$\exp(-a_1 D_1 \cos\alpha) = \frac{P - K_{sa1} \exp a_1(\Psi_1 - \Psi_{o1})}{P - K_{sa2} \exp a_1(\Psi_2 - \Psi_{o2})} \quad \ldots\ldots\ldots\ldots \quad (30)$$

$$\exp(-a_2 D_2 \cos\alpha) = \frac{P - K_{sa2} \exp a_2(\Psi_2 - \Psi_{o2})}{P - K_{sa2} \exp a_2(\Psi_1 - \Psi_{o2})} \quad \ldots\ldots\ldots\ldots \quad (31)$$

We cannot express Ψ_1 and Ψ_2 explicitly in an analytic manner, although these are the two unknowns in Eqs. 30 and 31.

Note that the boundary conditions in the foregoing table assume transition to saturation at $\psi = 0$. In reality this transaction occurs when $\Psi - \Psi_o = 0$.

Pressure Distribution Streamlines and Average Anisotropy

In the case of a cyclic repetition of the two layers, certain interesting general deductions can be made.

Let us consider Eq. 26 and calculate $\bar{K}_s$ according to its definition in Eq. 24. Eq. 29 is most convenient for this purpose. If we consider K_t as a variable and K_{to} as a fixed value:

$$\frac{\bar{K}_s}{P} = \frac{1}{P}\frac{\int K dn}{\int dn} = 1 - \left\{ \frac{1}{a_1 \cos\alpha} [\exp(-a_1 \cos\alpha\ D_1) - 1] \right.$$

$$- \frac{K_{1o}}{P a_1 \cos\alpha} [\exp(-a_1 \cos\alpha\ D_1) - 1] + \frac{1}{a_2 \cos\alpha} [\exp(-a_2 \cos\alpha\ D_2) - 1]$$

$$\left. - \frac{K_{2o}}{P a_2 \cos\alpha} [\exp(-a_2 \cos\alpha\ D_2) - 1] \right\} \Big/ (D_1 + D_2) \quad \ldots\ldots\ldots\ldots \quad (32)$$

We now prefer to have K_{1o} and K_{2o} adjacent to each other on either side of a single interface between the two layers. The condition at the interface is that Ψ is the same on both sides, e.g., Ψ_2.

Consider first a case in which $K_{10} = K_{2o}$. Under this unique condition the $K(\Psi)$ curves of the separate layers intersect each other. In this special case the layers seem to disappear and anisotropy is reduced to zero. Then:

$$K_{1o} = K_{2o} = P_t = K_{sa1} \exp a_1(\Psi_2 + \Psi_{o1}) \quad \ldots\ldots\ldots\ldots\ldots\ldots \quad (33)$$

such that $$\Psi_2 = \frac{\left[\ln \frac{K_{sa2}}{K_{sa1}} - (a_1 \Psi_{o1} - a_2 \Psi_{o2}) \right]}{(a_2 - a_1)} \quad \ldots\ldots\ldots\ldots \quad (34)$$

For any rain other than P_t there will be positive anisotropy. If the rainfall exceeds this value, the layer which has the higher saturated conductivity will be more permeable. If it is less than P_t, the layer which has the lower saturated conductivity will be the more permeable one. The transition value of rain P_t is very small. On the whole, the aforementioned phenomenon disappears if there are more than two layers in the profile. Note that when Eq. 32 is written with the conditions of Eq. 33, all the terms in the brackets vanish, the integral

reduces to 1, and the anisotropy becomes zero.

The streamlines zigzag from layer to layer. In the more permeable layer the K build-up with depth and the streamlines diverge from the normal in a downstream direction. In the less permeable layer the streamlines converge toward the normal. At the interface the streamlines undergo abrupt changes in direction.

At a high rate of rainfall when $K_{1o} = K_{sa1}$ and $K_{2o} = K_{sa2}$, Eq. 32 becomes irrelevant. In fact, it is equivalent to the case where $a_1 = a_2 = 0$, i.e., any change in Ψ causes no change in K. In this case the expression reduces to an indeterminate term. For this case, and for decreasing D_1 and D_2 values, it is suggested that the exponentials be expanded by a series as follows:

$$\exp(na_1 \cos\alpha\, D_1) - 1 = -a_1 \cos\alpha\, D_1 + \frac{1}{2} a^2 \cos^2\alpha\, D_1^2 \quad \ldots\ldots\ldots \quad (35)$$

At sufficiently small values of $a_1 D_1$ or $a_2 D_2 \cos\alpha$, we obtain

$$\frac{\bar{K}_s}{P} = \frac{\bar{q}_s}{\bar{q}_n \tan\alpha} = \frac{1}{P}\frac{\int K dn}{\int dn} \cong \frac{1}{P}\frac{D_1 K_1 + D_2 K_2}{D_1 + D_2} \quad \ldots\ldots\ldots\ldots\ldots \quad (36)$$

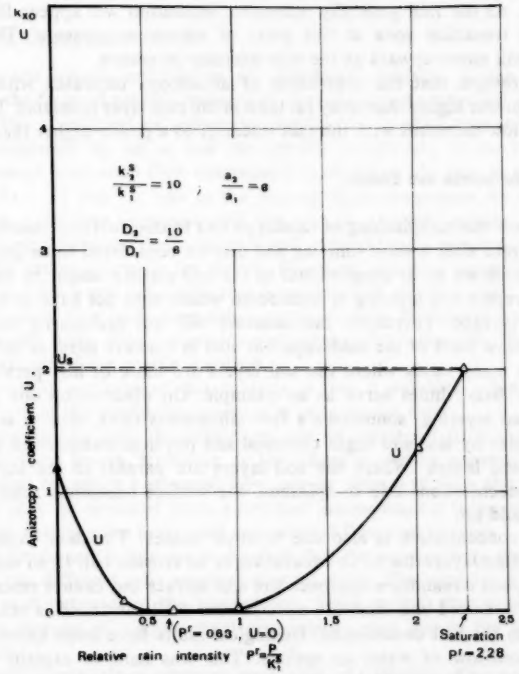

FIG. 4.—Anisotropy Coefficient U as Function of Rain Intensity P in Cyclic Two-Layer Problem

It is interesting to note that the right-hand-side (r.h.s) of Eq. 36 is the arithmetic mean of K. It is the exact mean in saturated flow and the approximate one for unsaturated flow when the layers' thicknesses D_1 and D_2 approach zero.

The coefficient of anisotropy $(\bar{K}_x/\bar{q}_z) - 1$ has been calculated as an example for two layers in which

$$\frac{D_2}{D_1} = \frac{10}{6}; \quad \frac{K_{1sa2}}{K_{1sa1}} = 10; \quad \frac{a_2}{a_1} = 6 \quad \ldots\ldots\ldots\ldots\ldots\ldots\ldots\ldots \quad (37)$$

with $\Psi_o = 0$. The abcissa in Fig. 4 gives the rate of rainfall P in terms relative to K_{sa1}. Two specific points are given: $P/K_{sa1} = 2.28$ where saturation appears at the surface; and $P/K_{sa1} = 0.63$ where $P = P_t$ and there is no lateral flow.

The method used for a two-layer problem can also be employed for a transition zone at the soil surface if the latter is represented by a sequence of layers, each uniform and isotropic and varying slightly from its neighbors. Some of the details of such a study are interesting, e.g., if the saturated hydraulic conductivity decreases monotonically with depth, there must be a maximum in the pressure head distribution within the surface transition zone and above this maximum the streamlines bend downstream; below it they bend back towards the normal. As the rain gradually increases, saturation will appear first within the surface transition zone at this point of maximum pressure. The site of saturation will move upward as the rain intensity increases.

It is instructive that the coefficient of anisotropy increases with the rate of rain to a power higher than unity (at least in the two-layer problem). Therefore, the lateral flow increases with the rain intensity to a power higher than two.

Water Concentration and Efflux

Lateral flow due to splashing of raindrops and to thin surface transition layers follows the rain after a short time lag and may be considered to be quasisteady. Its rate was shown to be proportional to the soil surface slope. In the present part of the report any layering is considered which does not have to be parallel to the soil surface. Therefore, the moisture will not necessarily concentrate only in concave parts of the landscape but also in concave parts of the layers.

There are many cases where the soil layers are more or less parallel to the soil surface. Sand dunes serve as an example. On observation one discovers such repeated layering, sometimes a few millimeters thick, due to segregation of the particles by size and slight chemical and physical stabilization of freshly deposited sand layers. Where the soil layers are parallel to the surface, the moisture concentrations due to splashes, the surface transition zone, and the layering all add up.

Moisture concentration is also due to other causes. The most common one is the truncation layers due to an excavation or an erosion cut. In an unsaturated soil the diagonal streamlines approach the soil surface but cannot emerge. They then bend downward and moisture accumulates until saturation is reached and seepage from the soil commences. Geological faults have been known to give rise to the outflow of water as springs. This was hard to explain when no saturated water table could be observed in the vicinity of such faults. The aforementioned unsaturated lateral flow offers an explanation.

In pollution studies one wishes to follow the actual flow path of the water.

It can be predicted that infiltrating polluting water can move laterally over large distances before reaching the groundwater table. At one observation site, more than 100 m of interbedded clay lenses and sands were sampled above the groundwater table. It was estimated that the spreading diameter of a point source of polluting water would continue to increase as long as some impounded water remained within the sandy layers. In this case the coefficient of anisotropy is of the order of the ratio between the conductivity of the sand and that of the clay conductivity. The slope was recorded as a percentage and the anisotropy in thousands. Thus, the pollutant was expected to travel a horizontal distance of several hundred meters to several kilometers before reaching the water table. Observations tended to confirm the qualitative predictions. Surface pollutants may readily move near the surface in depressions and rills and gullies where the onset of salinization is early and water seeps out rather than in.

The following may be considered an interesting application of lateral flow in regard to pollution. A convex cover of soil layers, if properly constructed, can act as a "straw roof." Though highly permeable, it can prevent the penetrating water from leaching through a source of pollution. Very often engineers restrict their search to impermeable materials when attempting to prevent flow through a structural element. Here, we suggest another possible way of obtaining such protection.

Analysis and Conclusions

Layered soil usually behaves as an anisotropic medium. If the layers are at a slope, the force of gravity operates at an angle α to the principal coordinates n and s. The coefficient of anisotropy relates the parallel component to the normal component by sin α, and the parallel component to the rain by tan α. The average horizontal flow component is related to the rain at steady flow by $[(\bar{K}_s/P) - 1] \cos^2 \alpha$, and to the vertical flow component by $(\bar{K}_s/\bar{q}_z) - 1$. The last parameter increases with the rain to a power greater than unity. The relationship between the horizontal and vertical flow components is reminiscent of the rational formula for runoff. However, runoff is generally replaced by horizontal flow, and the coefficient increases with the rain itself.

The horizontal flow leads to moisture concentration. However, the latter does not necessarily bring about saturation and seepage from the soil. These depend on the thickness of the profile involved.

An interesting outcome of this analysis is that it provides a hint about the possible form of the conductivity tensor in unsaturated flow.

In certain special cases the anisotropy can be calculated from the properties of the individual layers. However, in the future it will be necessary to adopt some method by which horizontal flow can be estimated from the anisotropy. The latter may be obtained from watershed measurements using some overall relationship between the horizontal and vertical flow components.

Also of fundamental interest is the fact that the conductivity pressure head curves of two different soils intersect at some point. This crossing has an effect on the overall behavior of the layered soil. Some models that assume parallel curves for reasons of mathematical convenience may distort the phenomenon in principle.

Interesting applications relate to problems of pollution. The pollutant may spread over a significant distance horizontally while penetrating into the ground.

The prospect of waterproofing an underground volume by layering is also of interest in solving engineering problems.

The next part of this report will deal with the computation of nonsteady flow in the surface transition layer.

Appendix I.—References

1. Zaslavsky, D., and Sinai, G., "Surface Hydrology: I—Explanation of Phenomena," *Journal of the Hydraulics Division*, ASCE, Vol. 107, No. HY1, Proc. Paper 15958, Jan., 1981, pp. 1–16.
2. Zaslavsky, D., and Sinai, G., "Surface Hydrology: II—Distribution of Raindrops," *Journal of the Hydraulics Division*, ASCE, Vol. 107, No. HY1, Proc. Paper 15959, Jan., 1981, pp. 17–35.
3. Zaslavsky, D., and Sinai, G., "Surface Hydrology: III—Causes of Lateral Flow," *Journal of the Hydraulics Division*, ASCE, Vol. 107, No. HY1, Proc. Paper 15960, Jan., 1981, pp. 37–52.
4. Zaslavsky, D., and Sinai, G., "Lateral Flow Due to Rain in Unsaturated Soils," *Second Annual Report, Project A10-SWC-77*, Soil Sciences Laboratory, Agricultural Engineering, Technion, Haifa, Israel, 1972.

Appendix II.—Notation

The following symbols are used in this paper:

a = experimental coefficient (L^{-1});
D = thickness of individual layer;
K = hydraulic conductivity;
n = coordinate normal to soil layers;
P = rate of rain (LT^{-1}) or rate of net recharge;
Q = discharge;
q = flux vector or flux component (LT^{-1});
s = coordinate parallel to layers;
U, U^* = coefficient of anisotropy;
x = horizontal coordinate;
z = vertical coordinate, positive in upward direction;
α = angle between soil layers and horizon; and
Ψ = pressure head for $\Psi > 0$, suction for $\Psi < 0$.

Subscripts

s = s component;
n = n component;
x = x component;
z = z component;
o = Z_o, relating to interface between layers;
Ψ_o = air entry value (L);
i = ith layer;
1 = first layer;
2 = second layer;
sa = saturated;
t = relating to point where unsaturated conductivities of two layers become equal;
$(\bar{\ })$ = average; and
* = different definition of coefficient of anisotropy.

JOURNAL OF THE HYDRAULICS DIVISION

SURFACE HYDROLOGY: V—IN-SURFACE TRANSIENT FLOW

By Dan Zaslavsky[1] and Gideon Sinai[2]

INTRODUCTION

The final part of the report on Surface Hydrology deals with a more problematic aspect, i.e., the numerical computation of the nonsteady flow through the surface transition layer. We have previously established that this transition layer has properties grading from those in the soil bulk to those in the air. Sometimes it can be fairly thick, as in a plough layer. In some well cultivated, heavy, clay soils, the hydraulic conductivity can change by six orders of magnitude over a soil thickness of 2 dm–4 dm. In smooth, fine-grained soil, the transition layer is greatly reduced, its thickness being of the order of the grain diameter.

It should be noted that a change in porosity alone, e.g., from 30%–100%, can alter the hydraulic conductivity by one order of magnitude or more.

In an earlier part of this report (8) we presented a general proof that whenever there exists a sloping transition layer the streamlines of the rain will enter the soil and then bend downstream. During steady rainfall the horizontal flow will be proportional to the rain and the slope. Does this also apply in the case of nonsteady rain?

To date, the hydraulic properties of the transition layer have never been actually measured. We regard it as being made up of a discrete number of layers changing stepwise. Some of the parameters assigned to these layers are taken from actual soils; others are our proposals based on certain rules. We are still at the stage where we required knowledge of the nature of flow phenomena in principle. The exact numerical result is of minor significance. The numerical solutions have been used as a method of experimentation to study the influence of the slope, the curvature, the rain regime, and the thickness of the transition

[1]Prof. of Soil and Water Engrg., Faculty of Agricultural Engrg., Soils and Fertilizers Div., Technion—Israel Inst. of Tech., Technion City, Haifa, 32000, Israel.

[2]Lect., Faculty of Agricultural Engrg., Soils and Fertilizers Div., Technion—Israel Inst. of Tech., Technion City, Haifa, 32000, Israel.

Note.—Discussion open until June 1, 1981. Separate discussions should be submitted for the individual papers in this symposium. To extend the closing date one month, a written request must be filed with the Manager of Technical and Professional Publications, ASCE. Manuscript was submitted for review for possible publication on March 23, 1979. This paper is part of the Journal of the Hydraulics Division, Proceedings of the American Society of Civil Engineers, © ASCE, Vol. 107, No. HY1, January, 1981. ISSN 0044-796X/81/0001-0065/$01.00.

layer on the flow regime. Some major results and conclusions from the numerical solutions are given here. Detailed solutions and some more results can be found in the original work by the writers (5).

Description of Simulation Model

A sinusoidal soil surface is depicted as in Fig. 1. The transition layer is underlain by a thick, uniform soil (H). The shape of the soil surface is given by its elevation z:

$$z = (H + A) + A \cos\left(\frac{x}{L}\pi\right) \quad \ldots\ldots\ldots\ldots\ldots\ldots\ldots\ldots\ldots\ldots\ldots\ldots (1)$$

Here H = the sublayer depth which is 10 m in all cases. The amplitude A varies in the different cases from 2×10^{-4} m–2 m. However, in most cases, A = 2 m. These extreme values were chosen to produce a given range of slopes. The half-cycle L has the values 40 m, 20 m, 2 m, and 0.2 m (see Table 1).

The boundary conditions are as follows (Fig. 1): (1) The vertical line below the hilltop is a symmetry line and thus a streamline; (2) the vertical line below the valley bottom is a symmetry line and thus a streamline; (3) the initial condition is a hydrostatic state throughout the profile, with the phreatic surface ψ =

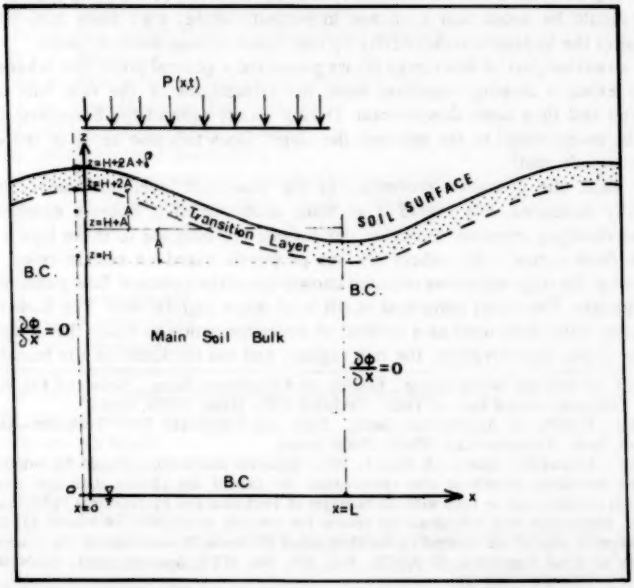

FIG. 1.—Geometry and Boundary Conditions of Flow Problem

0 at $z = 0$; and (4) ψ is the pressure head and z is the elevation.

It can be argued that a state of field capacity could be substituted for the true state of hydrostatic equilibrium. However, the former depends on the history

TABLE 1.—List of Solved Cases and Main Results

Problem number (1)	Main Geometric Data, in meters: L (2)	A_m (3)	δ (4)	Rain, P, in centimeters per hour (5)	Geometric Ratios: A/L (6)	A/L^2 (7)	MAIN RESULTS: Saturation: Total rain, D_{sat}, in centimeters (8)	Time, T_{sat}, in hours (9)	Time steps, TS_{sat} (10)	Seepage: Total rain, D_{seep}, in centimeters (11)	Time, T_{seep}, in hours (12)	Time steps, TS_{seep} (13)
388	20	2	0.45	1.0	0.1	0.005	14.9	14.9	107	21.3	21.3	153
538	20	2	0.45	1.0	0.1	0.005	13.8	13.8	85	19.1	19.1	102
539	20	2	0.45	1.0	0.1	0.005	13.8	13.8	85	18.75	18.75	100
522	20	2	0.45	0.01	0.1	0.005	15.5	1550	163	60	6000	15.5
815	20	2	0.45	4.0	0.1	0.005	17.2	5.8	60	23.2	7.3	109
460	20	2	0.45	(a)*	0.1	0.005	15.0	31.5	142	—	—	—
752 A	20	2	0.15	1.0	0.1	0.005	7.1	7.1	22	7.7	7.7	24
752 F	20	2	0.15	0.01	0.1	0.005	8.0	800	45	12	1200	50
536	20	2	0.05	1.0	0.1	0.005	2.6	5.4	22	3.4	6.2	24
438	20	2	0	0.01	0.1	0.005	—	—	—	—	—	—
533	20	2	0	1.0	0.1	0.005	0.97	6.7	80	0.97	6.7	80
535	40	12	0.45	1.0	0.3	0.0075	14.3	14.3	101	19	19	195
535 L	40	12	0.45	0.01	0.3	0.0075	—	—	—	—	—	—
521	2	0.2	0.45	1.0	0.1	0.05	10.4	10.4	33	24.4	24.4	88
521 K	2	0.2	0.45	0.01	0.1	0.05	—	—	—	—	—	—
379	2	0.02	0.45	1.0	0.01	0.005	16	16	65	38	38	155
379 I	2	0.02	0.45	0.01	0.01	0.005	—	—	—	—	—	—
378 A	2	0.02	0.15	1.0	0.01	0.005	7.5	7.5	13	14	14	26
378 H	2	0.02	0.15	0.01	0.01	0.005	—	—	—	—	—	—
520 A	2	0.2	0.15	1.0	0.1	0.05	5.6	5.6	12	8.4	8.4	15
520 J	2	0.2	0.15	0.01	0.1	0.05	—	—	—	—	—	—
523	2	0.2	0.05	1.0	0.1	0.05	2.4	4.4	49	2.9	4.9	54
537	2	0.02	0.05	1.0	0.01	0.005	3.2	6	24	5.2	8	29
537 B	2	0.02	0.05	0.01	0.01	0.005	—	—	—	—	—	—
524	2	0.02	0.005	0.5	0.01	0.005	2	8.2	40	2.3	8.8	46
525	0.2	0.02	0.15	1.0	0.1	0.5	7	7	25	15	15	45
525 P	0.2	0.02	0.15	0.01	0.1	0.5	—	—	—	—	—	—
526	0.2	2×10^{-4}	0.15	1.0	10^{-3}	5×10^{-3}	7.6	8.8	25	—	—	—
527	0.2	0.1	0.025	1.0	0.5	2.5	4.2	4.2	19	4.6	4.6	21
528	0.2	0.02	0.025	1.0	0.1	0.5	2.5	6.3	30	3.8	7.1	34
529	0.2	2×10^{-4}	0.025	0.5	10^{-3}	5×10^{-3}	8.1	19.6	53	9.35	22.11	85
530	0.2	0.1	0.005	0.5	0.5	2.5	2	8.6	42	2	8.6	42
531	0.2	0.02	0.005	0.5	0.1	0.5	2	8.6	42	2.3	9.2	45
531 U	0.2	0.02	0.005	0.01	0.1	0.5	—	—	—	—	—	—
532	0.2	2×10^{-4}	0.005	0.5	10^{-3}	5×10^{-3}	2.3	7.8	46	2.3	7.8	46
532 W	0.2	2×10^{-4}	0.005	0.01	10^{-3}	5×10^{-3}	—	—	—	—	—	—
534	0.2	0.1	0	0.2	0.5	2.5	0.62	4.1	19	—	—	—

*Intermittent rain.

of its attainment. This substitution should therefore be postponed until such time as computers are able to digest a long-term regime.

The transition zone at the soil surface is represented by eight layers more or less parallel to the soil surface and of equal thickness. In more precise terms, the grid points representing the separate layers were chosen in such

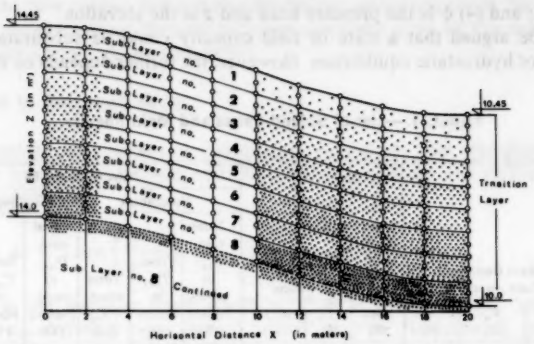

FIG. 2.—Setup of Sublayers to Simulate Surface Transition Layer

a way that they assure uniform thickness of each in a direction normal to the soil surface. Thus the successive sublayers do not exactly follow Eq. 1 less a fixed depth (Fig. 2).

Each layer is considered to be uniform and isotropic. There is a stepwise change in the hydraulic properties of the various layers. The detailed values of the porosity, the retention curves, and the saturated hydraulic conductivities are presented in Figs. 3 and 4.

The parameters for layers 4–8 were taken from actual soil data reported earlier (5). Those for layers 1, 2, and 3 were selected artificially in conformance with the following trends:

1. The saturated hydraulic conductivity (K^s) increases exponentially with elevation:

layer number	1	2	3	4	5	6	7	8
K^s, in centimeters per second	100	10	1	10^{-1}	10^{-2}	10^{-3}	10^{-4}	10^{-5}

2. The rate of conductivity decrease due to moisture depletion, as expressed by the slope in Fig. 4, increases as the saturated conductivity increases.

3. The intersection of the conductivity curves for the layer pairs 1–2, 2–3, 3–4, etc., follows a monotonic order.

4. The moisture content at saturation is the same as the porosity and therefore it approaches 100% in the air above the top layer, and it decreases with depth:

layer number	1	2	3	4	5	6	7	8
porosity	0.9	0.85	0.8	0.75	0.7	0.6	0.5	0.4

5. The rate of moisture decrease due to suction, as expressed by the slope in Fig. 3, increases with porosity.

6. The intersection of the moisture curves for the layer pairs 1–2, 2–3, 3–4, etc., follows a monotonic order.

Differential Equation

The differential equation is

$$\operatorname{div} q_i = \frac{\partial \Theta}{\partial t} \quad (2)$$

in which q_i = the ith flux component; Θ = the volumetric moisture content; and t = the time.

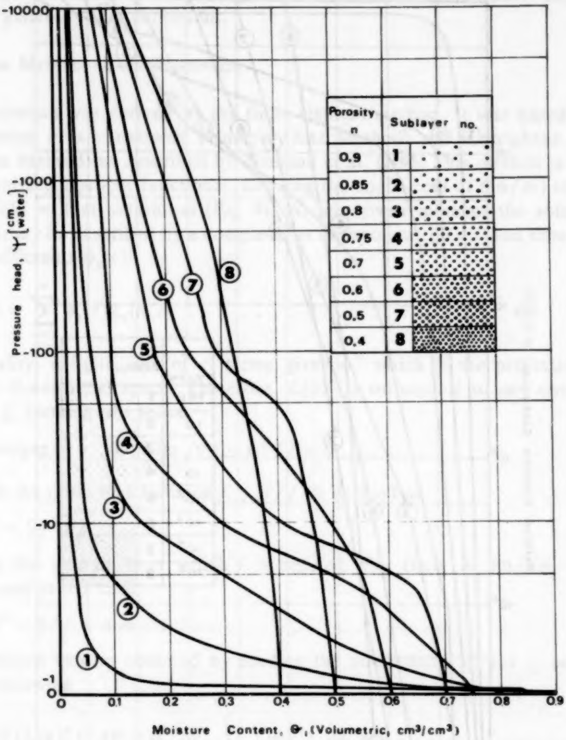

FIG. 3.—Moisture Retention Curves of Eight Sublayers Constituting Surface Transition Layer

The flow equation is

$$q_i = K_{ij} \nabla \phi_j \quad (3)$$

in which K_{ij} = the hydraulic conductivity capable of being an anisotropic tensor; ϕ = the hydraulic head ($\phi = z + \psi$); z = the elevation; and ψ = the pressure head.

Inserting Eq. 3 in Eq. 2, one explicitly obtains

$$L(\psi) = \frac{\partial}{\partial x_i}\left[K^R(\psi)\,K^s_{ij}\frac{\partial \psi}{\partial x_j} + K^R(\psi)\,K^s_{ij}\,1z - \frac{\partial \theta}{\partial \psi}\frac{\partial \psi}{\partial t}\right] = 0 \quad \ldots\ldots\ldots (4)$$

in which the hydraulic conductivity K_{ij} = a product of two terms; $K^R(\psi)$ = an isotropic term varying with ψ; and K^s_{ij} is fixed but anisotropic.

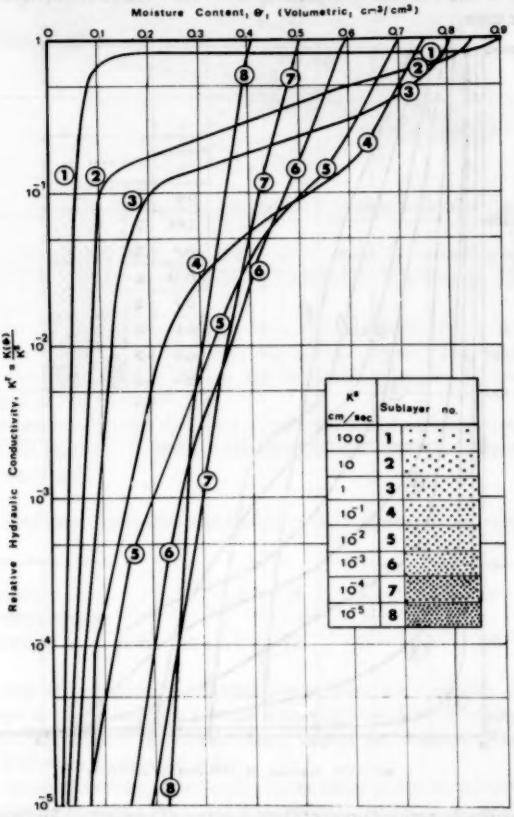

FIG. 4.—Hydraulic Conductivity as Function of Moisture Content $K(\theta)$ in Eight Sublayers Constituting Surface Transition Layer

In reality, although the numerical algorithm used here is capable of solving flow problems for anisotropic media, the problems run here all involved isotropic layers. In the problem under consideration, the anisotropic behavior is merely the result of the overall average behavior of the layered soil. Models proposed earlier dealt with anisotropic media but did not provide computations. In the

following computation, the anisotropy is not assumed to be a fixed value at a point but is rather obtained as an overall behavior. The anisotropy changes with the moisture regime itself. This is contrary to the inference from Eq. 4, where the entire change with moisture is linked to the isotropic term $K^R(\psi)$. Therefore we suspect that the assertion in Eq. 4 that was never really measured is simply incorrect.

The duality between a layered soil and an anisotropic one, established in the previous parts of this report (6–9), leads us to believe that any anisotropy in the soil's hydraulic conductivity will be found to be moisture dependent or more generally flux dependent.

Numerical Method—Brief Description

The solution was derived by the finite-element method. It was based on the combination of a variational principle (Ritz Method) and a weighted residue (Galerkin Method) as described by Neuman et al. (2–4). This method is applied by minimizing a proper functional, allowing the coefficient of $(\partial\psi/\partial t)$ to vanish and $K^R(\psi) = 1$ at saturation (Eq. 4). At any given moment the solution of $\psi(x, z, t)$ may be described by a complete set of functions $\zeta_n(x, z)$ and time-dependent coefficients $\psi_n(t)$:

$$\psi(x, z, t) = \sum_{n=i}^{\infty} \psi_n(t)\,\zeta_n(x, z) \quad \ldots\ldots\ldots\ldots\ldots\ldots\ldots\ldots\ldots\ldots (5)$$

In reality, a finite sum of N terms gives ψ^N which is the projection of ψ in an N-dimensional space. Therefore, $L(\psi)^N$ is orthogonal to any one of the vectors ζ_n forming this space:

$$\psi^N \text{ converges to } \psi \quad \text{if} \quad \lim_{N\to\infty} //\psi - \psi^N// = 0 \quad \ldots\ldots\ldots\ldots\ldots\ldots (6)$$

in which the norm of a function f, $//f//$, is defined as

$$//f//^2 = \int f^2\, dV \quad \ldots\ldots\ldots\ldots\ldots\ldots\ldots\ldots\ldots\ldots\ldots\ldots (7)$$

V being the column over which f is defined. For finite N $\lim //\psi - \psi^N// = \min$, and in our case

$$//L(\psi)^N - 0// = \min \quad \ldots\ldots\ldots\ldots\ldots\ldots\ldots\ldots\ldots\ldots\ldots\ldots (8)$$

The solution can be obtained by feeding the coefficients F_n for ζ_n according to the following

$$\frac{\partial}{\partial F_i}\int_V f[L(\psi)^N]^2\, dV = 0 \quad \text{or} \quad \int_V L(\psi)^N \zeta_n\, dV = 0 \quad \ldots\ldots\ldots\ldots\ldots (9)$$

This Galerkin method provides a solution $\psi(x, z)$ at any given moment t. The derivative $\partial\psi/\partial$tt must therefore be determined independently. For more details the interested reader is referred to the original articles (2,3).

The grid points for solution are presented in Fig. 5, the upper part of which shows the details of the transition layer. The calculation involved the following three stages:

1. Preparatory program calculating the grid coordinates for each problem,

the boundary conditions, and the soil properties at any node.

2. The main multilayer calculation in terms of the pressure head, moisture content, total head, influx, and outflow. It was based on a previously written

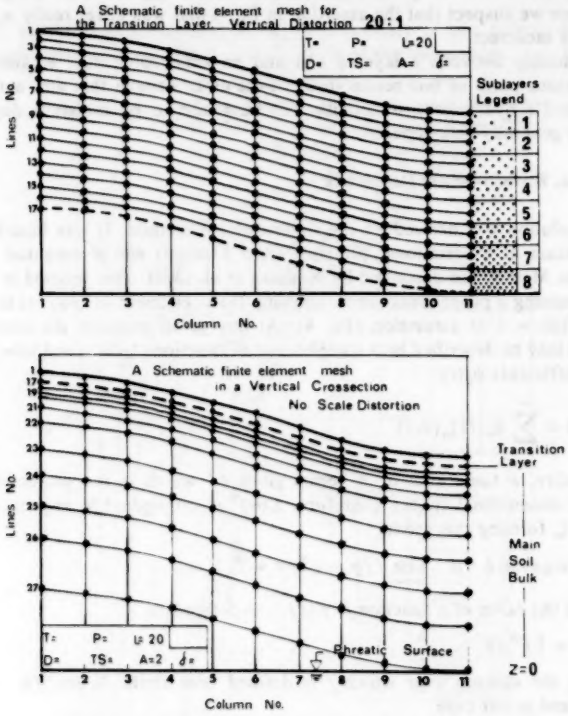

FIG. 5.—Details of Numerical Calculation Mesh Nodes

program (3) that was modified and adopted to the present problems.

3. Data processing and plotting as explained in the following.

Estimate of Solution Quality

The semi-implicit method of calculation with a system of linear equations makes possible convergence of the solution. The choice of the time step Δt affects the manner of convergence. A stepwise change in the influx of rain or outflow of water is expected to introduce a gradual, monotonic change within the flow domain. Excessively large Δt steps cause fluctuations that gradually decay toward the true value. A gradual, stepwise change in the rain over a small number of time steps can eliminate this problem. We shall not go into details of the analysis. The time step was finally obtained by a trial-and-error

method choosing a time step. First

$$\Delta t_1 = t_2 - t_1 \quad \ldots \ldots \ldots \ldots \ldots \ldots \ldots \ldots \ldots \ldots \ldots \ldots \ldots \ldots \ldots \quad (10)$$

and after the first iteration, a corrected time step is selected. This correction takes into account the dynamics of the flow at that time:

$$\Delta t_{11} = \frac{\psi_2 - \psi_1}{K_2 - K_1} \quad \ldots \ldots \ldots \ldots \ldots \ldots \ldots \ldots \ldots \ldots \ldots \ldots \ldots \ldots \ldots \quad (11)$$

in which Δt_{11} is then compared with Δt_1 until $\Delta t_1 < \Delta \tau_{11}$. Obviously, there were sensitive points in the field that determined the necessary time steps.

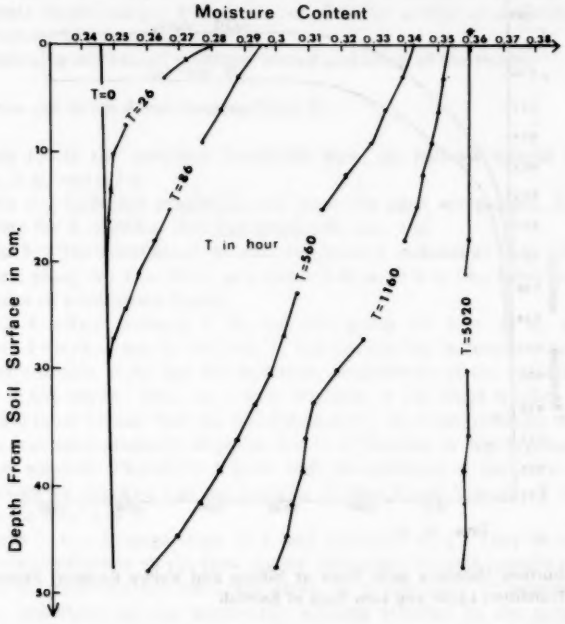

FIG. 6.—Moisture-Depth Distribution at Different Times: Problem 438 with No Transition Layer and Low Rate of Rainfall

The density of grid points must also be related to the rates of change, the typical time constant being $(\Delta x/K) \sim \Delta t$. The density actually employed was much lower than that dictated by the foregoing criterion. A series of tests was carried out to determine the influence of the location of the grid points on the solution. The greatest numerical error was found near the wetting front. Typical errors in head were of about 4 cm, being equivalent to a relative error of 0.5%.

Where the rain flux q locally exceeds the hydraulic conductivity K, the time step is determined by the flux $(\Delta x/q) < (\Delta x/K)$. Difficult cases to solve were

therefore those involving a thin transition layer (small Δz) and high rain intensity. In fact, they called for a relatively greater number of time steps in order to reach the same total rainfall.

The part of the problem that presented the greatest difficulties in computation was the appearance of seepage at the soil surface.

In order to estimate the sensitivity of the solution to the grid density it was increased horizontally from 11 columns–21 columns, with a numerical error of only 0.25% at the wetting front (not more than 3 cm of water). The entire calculation was accurate to within 1 cm of water. Potentially, the accuracy

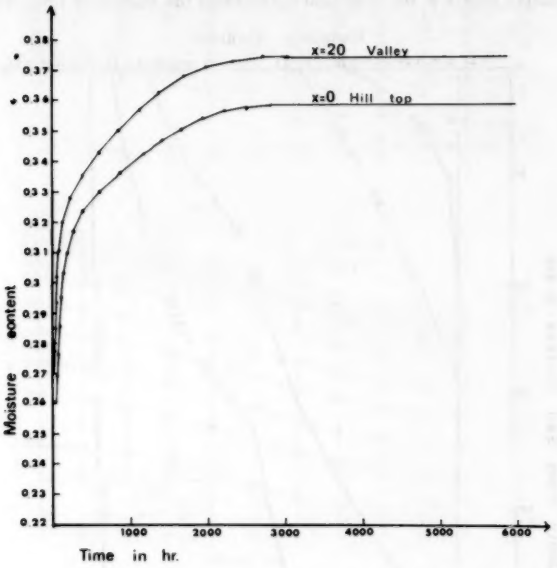

FIG. 7.—Surface Moisture with Time at Hilltop and Valley Bottom: Problem 438 with No Transition Layer and Low Rate of Rainfall

can be increased by doubling the number of grid nodes, involving an approximately 4-fold increase in the cost for executing the program in an IBM 370/168 computer. Therefore a grid of 297 nodes was only used.

The accuracy tests were run on several problems involving different geometric scales and rates of rainfall.

Finally, the moisture content profile at different times (Fig. 6) and the surface moisture at different times (Fig. 7) were plotted and found to be in good accord with classical one-dimensional solutions of infiltration. The run presented in Figs. 6 and 7 is from problem 438 with no transition layer and a very low rate of rainfall (0.01 cm/h). This value can be related to the conductivity of the soil (10^{-5} cm/s). and the final moisture content can be found from Fig. 4. The results are quite similar to those for one-dimensional infiltration (1).

One cannot expect a perfect fit, if only because there is some lateral movement of moisture even in a soil lacking a transition layer. This also explains why there are two different moisture curves in Fig. 7, one for the hilltop (x = 0) and one for the valley bottom (x = 20).

In conclusion, there is no way of ascertaining beyond a shadow of doubt that the numerical solutions are perfectly accurate. However, after the computation of some 60 different problems with various changes in the parameters, the solution seems to be conformable and the results are reasonable. Furthermore, what is presently required of the solution is far less than perfect numerical accuracy; it should rather serve as an indication of correct trends. The numerical solution is used as an experimental tool. The conclusions from these numerical experiments should comply with a number of earlier analytical conjectures and a large volume of observations (6–9).

The following are lists of problems solved and some of the results.

Explanation and Notes About Results (Table 1)

Column 1.—In the problems mentioned here, the half-wavelength L is 20 m, 40 m, 2 m, and 0.2 m.

Column 2.—Different amplitudes are given for each wavelength. The first large group for L = 20 has only one amplitude, i.e., 2 m.

Column 3.—The thickness of the transition layer δ, includes all eight sublayers. In the first group for L = 20 m, it is either 0.45 m or 0 m (the latter indicating the absence of a transition layer).

Column 4.—Rain intensity P. In the first group for L = 20 m, its main values are 4 cm/h, 1 cm/h, 0.01 cm/h, and (a), the last indicating intermittent rain (problem 460). Note that the hydraulic conductivity of the subsoil is 10^{-5} cm/s = 0.036 cm/h. Thus the lowest intensity is 3.6 times smaller and the highest 270 times greater than the soil conductivity. In some problems the initial rain was increased gradually stepwise due to difficulties in convergance of the numerical solution. Therefore, P gives only the intensity of the main rainfall. It can easily be checked that the product of time T and intensity P does not produce the total rain D.

Columns 5, 6.—Average slope A/L and curvature A/L^2. They should have an important influence on the flow regime. However, the only results recorded here are the time and the total rain depth up to the onset of saturation and seepage, and these are not necessarily strongly affected by the topographic features.

Columns 7–9.—Total rain depth D_{sat}, time T_{sat}, and the number of calculation time steps TS_{sat} up to the first appearance of saturation within the profile. In all cases involving transition layers, moisture concentration was observed on the concave part. The reason for the absence of saturation will be analyzed in each case.

Columns 10–12.—Total rain depth D_{seep}, time T_{seep}, and the number of calculation time steps TS_{seep} for the spreading of saturation up to the soil surface and seepage in problems involving transition layers. In problems with no transition layer, T_{seep} and T_{sat} become identical.

In the case of thinner transition layers there is a tendency toward a decrease in the time gap between initial saturation and seepage.

Main Results from Table 1 and Figure 8

The appearance of saturation within the transition layer is the first notable result. It becomes manifest at any rain intensity, from low (problem 522) or intermittent (problem 460) to the highest (problem 815). The rainfall ranges from 0.01 cm/h–4 cm/h, while the conductivity of the subsoil is 0.036 cm/h.

In soils lacking a transition layer, saturation appeared only when the surface was flooded by high-intensity rain (problem 533, $D_{sat} = D_{seep}$). It never appeared with the low rainfall (problem 438). This is exactly as predicted by the classical theory.

At intermediate transition thicknesses (15 cm in problems 752 A and 752

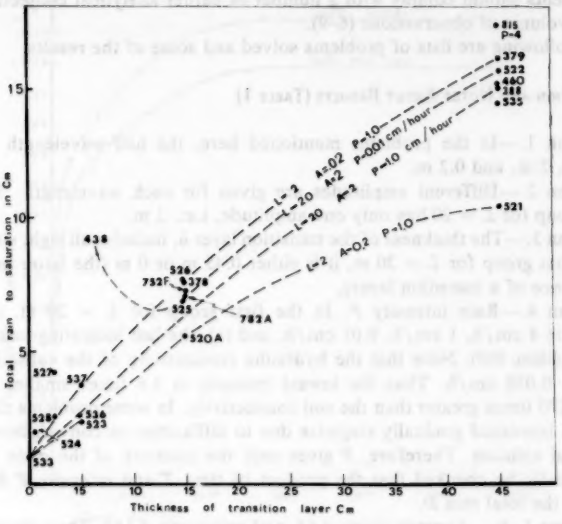

FIG. 8.—Cumulative Rain Depth Necessary for Onset of Saturation or Seepage in Gullied Soil

F, and 5 cm in problem 536), the times or total rains necessary for attainment of saturation are intermediate between those for thick transition layer (45 cm) and those in the case where there is no transition layer (problem 533).

Some of the results for the total rain necessary for saturation are presented in Fig. 8. Several facts stand out:

1. There is hardly any difference in the total rain necessary for the onset of saturation over an extremely wide range of rain intensities (problems 522, 388, and 812).
2. The thickness of transition layer has the main effect. For high-rain intensity, it is proportional to the total rain depth necessary for the onset of saturation.
3. In the case of thinner layers and very low rates of rain, no saturation will occur.

A similar conclusion can be drawn about the occurrence of seepage (saturation reaching the soil surface). There are two notable trends: (1) At lower rates of rainfall the total rain necessary for attainment of seepage is larger; and (2) the effect of a thick transition layer is to increase considerably the total rain prior to seepage, provided that its intensity is sufficiently high. If the rain is of low intensity, very thin layers will never attain a state of seepage.

These results are quite reasonable. There is a lateral movement of moisture that tends to increase the total water increment in the concave valley. However, whether saturation and seepage will actually occur depends on the interplay of several mechanisms. The added moisture spreads over a given soil depth. This depth increases over the course of time. For a given total rain the wetting depth is greater at a low rate of rainfall. Thus at low rates of rainfall there is more time for lateral motion but also more time for deeper moisture distribution.

The lateral discharge is dependent on the total thickness of the wetted

TABLE 2.—List of Problems Analyzed in Detail

Problem number (1)	Half cycle, in meters (2)	Amplitude, in meters (3)	Thickness of transition layer, in meters (4)	Main rain intensity, in centimeters per hour (5)
388	20	2	0.45	1
522	20	2	0.45	0.01
815	20	2	0.45	4
438	20	2	0	1
533	20	2	0	0.01
752 A	20	2	0.15	1
752 F	20	2	0.15	0.01

anisotropic or layered soil. Thus, the discharge with thin transition layers cannot be as high as that with thick transition layers. This is true at least over a sufficiently long time interval during which the wetting front penetrates beyond the thin transition layer. In a thick transition layer the lateral discharge has an opportunity to build up over a period. Therefore, thin layers may require less rain in order to attain saturation point, but if the rate of rain is low enough they may never reach saturation.

Details of Flow Regime

Table 2 is a partial list of problems whose solutions will be used in the present analysis. Each plot of the results has an identification label including the problem number at the upper right corner, the time T, the rain intensity P, the half-cycle length L, the rain depth D, the number of time steps in the program TS, the amplitude A, and the thickness of transition layer δ.

The results will be presented together with the development of the analysis. They will include moisture distribution, hydraulic head distribution, integral moisture accumulation, etc. In order to show the details of the head distribution, three vertical sections of the transition layer have been enlarged (Fig. 9): (1)

At the top of the hill; (2) in the region of maximum slope, and (3) at the valley bottom.

Fig. 10 shows the lines of equal head at a high rate of rainfall and after some 112 mm of rain have entered the soil. It is clear that at the wetting front the flow is normal to the transition layer. Behind the wetting front, streamlines (that would be approximately normal to the lines of equal head) clearly slope downstream. This is most pronounced in high slope (Section B).

In the upper diagram of Fig. 11 one can observe slanting flow in a transition layer, $\delta = 0.45$ m (problem 522). The lower diagram shows an almost vertical

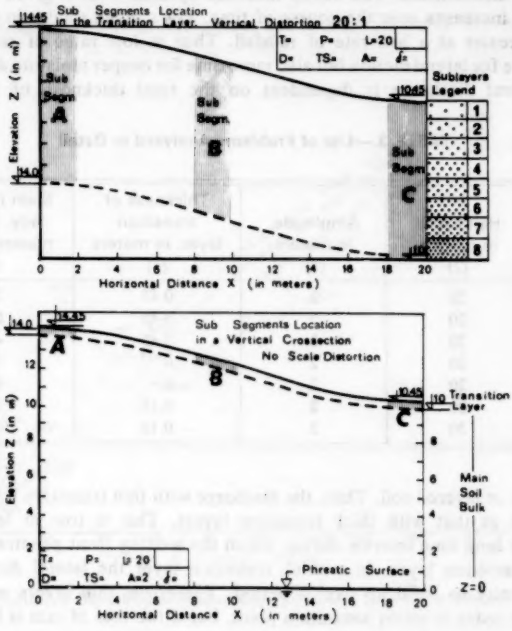

FIG. 9.—Segments A, B, and C in Transition Layer Enlarged for Discussion of Flow Direction

flow in a soil lacking a transition layer, $\delta = 0$ (problem 438). Both soils received rainfall of the same, very low intensity, equivalent to about one third of the subsoil hydraulic conductivity, and both diagrams represent sections of steepest slope after precipitation of about 260 mm of rain.

Fig. 12 shows the evolvement of the flow regime with time, by means of the lines of equal head, with rain of very high intensity (problem 815). It is interesting to note the elevations marked on the left side and right side of the diagrams. If the hydraulic head registered on the 150 g is lower than the elevation, the flow is under suction and may be unsaturated. On studying Fig. 12 and also Figs. 9–11, one can observe the high suction gradients at the wetting

front and ascertain that in all the examples the flow is under suction. Certainly there is no flooding or perched water formation anywhere. Nevertheless, there is a lateral flow component both when the rains greatly exceed the hydraulic conductivity and when they are much lower than it. In Fig. 12 one can see that at the onset of the rain the flow tends to be normal to the soil surface since suction gradients are predominant. Later, normal flow is maintained only within the wetting front. Lateral flow continues for quite a long time after the rain has stopped (the lowest part of Fig. 12).

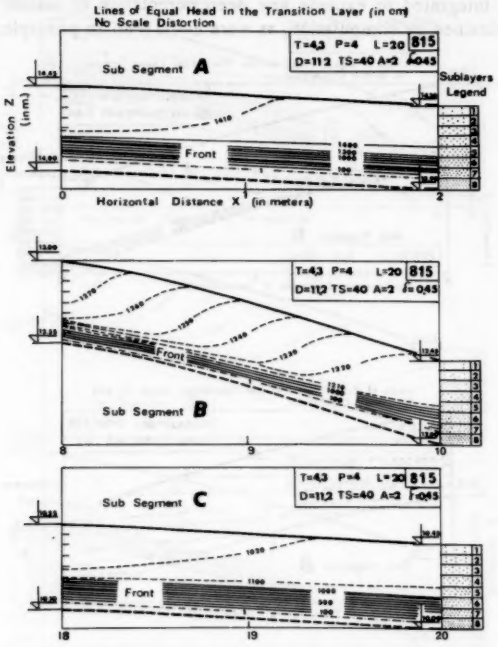

FIG. 10.—Segments A, B, and C: Lines of Equal Head (Problem 815); Head in Centimeters

On comparing Fig. 13 with the previous ones, one clearly notes how a soil lacking a transition layer at its surface differs from those with such a layer. In both, the flow starts more or less normal to the soil surface. After prolonged rain it tends to become vertical in the uniform soil. During drainage time after the rain has ceased, lateral flow seems to develop, but it is of negligible magnitude.

Relationship Between Slope and Lateral Flow Component

In previous parts of this report it has been shown that under steady-state infiltration the horizontal flow component is proportional to the slope.

One must now ask whether such a simple rule also applies in the case of a complex, nonsteady flow as dealt with here. To study this problem one has to integrate the moisture content Θ over a vertical column in order to obtain $w(xt) = \int \Theta(xzt)\,dz$. Then by conservation of mass

$$\frac{\partial}{\partial t} w(xt) - P = \frac{\partial Q(x)}{\partial x} \quad \ldots\ldots\ldots\ldots\ldots\ldots\ldots\ldots\ldots\ldots\ldots\ldots \quad (12)$$

in which P = the rate of rainfall. We assume the lower boundary of z over which Θ is integrated to exclude any deep percolation of water. The values of w were obtained by computation, as were $\partial w(xt)/\partial t$. In principle, this makes

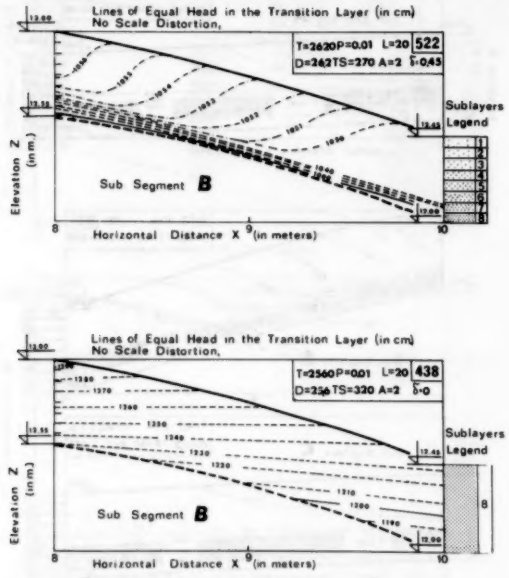

FIG. 11.—Middle Segment B of Steepest Slope: Lines of Equal Head in Uniform Soil (Problem 438) and Soil with Transition Layer (Problem 522)

possible the determination of $Q(x)$ by integration over x from the point $x = 0$ in which $Q(x) = 0$. One can now divide this calculated discharge at every point by the local slope. Table 3 is such a table for problem 522. Instead of the discharge we have used the weighted average of the horizontal hydraulic gradient, the latter being exactly proportional to the former.

It is quite evident that in the aforementioned case the horizontal gradient very closely follows the local slope. This conclusion is far from general. At most it serves as an indication that such proportionality between the horizontal flow and the slope is a possible rule of thumb. At the valley bottom, where more water accumulates, the gradient decreases. At the top of the hill, moisture depletion will also tend to limit the gradient.

FORMATION OF SATURATION AND SEEPAGE

From the numerous results we have chosen two sets to show the principal findings (Figs. 14, 15).

In these figures, four sequences of diagrams (from top to bottom) show four stages of flow within the top soil layer. The vertical scale of this layer has been enlarged in 20: 1 in order to show the details. Lines of equal moisture

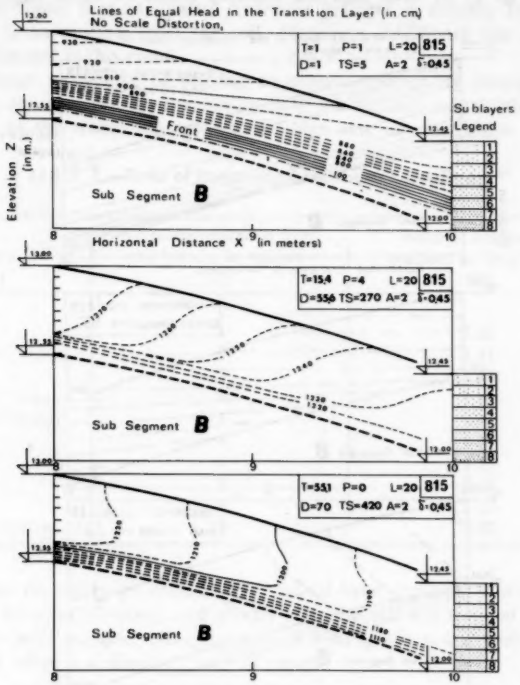

FIG. 12.—Middle Segment B of Steepest Slope (Lines of Equal Head): Problem 815 with Transition Layer and High-Intensity Rain at Three Different Times

are depicted, the moisture content being indicated on a volumetric basis. Zones of saturation are shaded. Owing to the enlargement of the vertical scale, flow directions should not be inferred from the lines of equal moisture.

The first sequence (Problem 522) in Fig. 14 shows early precipitation stages with the onset of moisture build up at the valley bottom. At some stage saturation occurs. As the rain continues the saturated area spreads upwards and sideways until it reaches the soil surface. After the cessation of the rain (drainage period), the zone of higher moisture is maintained for a long period despite respreading due to downward and lateral flow of the excess water. Saturation and seepage

occur despite the fact that the rain is equivalent to only about 1/3 of the hydraulic conductivity of the subsoil. The moisture depth accumulation in the concave parts greatly exceeds the average rainfall depth.

Problem 438 shown in Fig. 14 involves the same low rate of rainfall but no surface transition layer. There is no saturation, no seepage, and no runoff.

In Fig. 15 (problems 388 and 533) the comparison between soils with and without transition layers is repeated. The previous two problems differ from those in Fig. 14 by their high-rain intensity (some 30 times larger than the

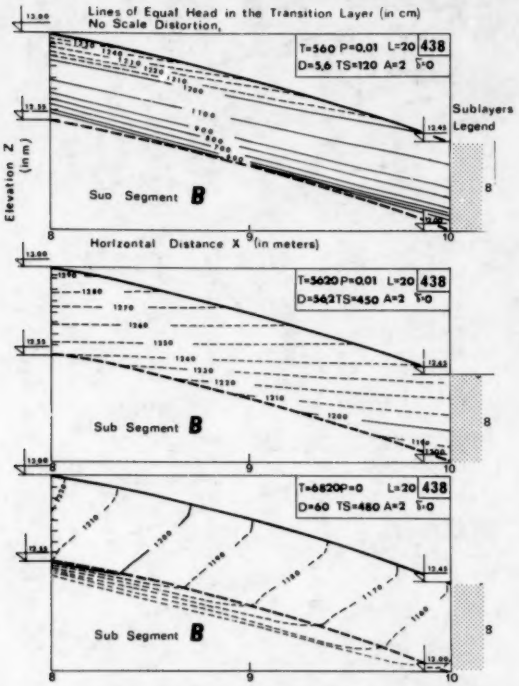

FIG. 13.—Middle Segment B of Steepest Slope (Head Distribution) Soil Lacking Transition Layer: Problem 438 at Three Different Times

hydraulic conductivity). Qualitatively, the same phenomenon occurs at both high and low rates of rainfall. If a transition layer is present, in both cases the rain first enters the soil. It then produces horizontal flow components, followed by moisture accumulation in concave spots. Saturation initially appears in such concave spots within the transition layer. Later, it spreads and reaches the surface in one place only, where runoff, in the usual sense of a well-defined surface flow, can start.

This leads us to a new and important conclusion. It has been argued previously

that surface saturation can be produced by rains that first enter the ground and then accumulate laterally. Here it is shown that in the presence of a surface transition layer this is the only possible mechanism. Every drop of rain, be it of high or low intensity, first penetrates into the soil. The classical model that predicts runoff only when the rainfall exceeds the local infiltration capacity fails not only in the case of low rates of rain. It is incorrect under all circumstances if we accept the surface transition layer as being a universal phenomenon.

Details of the flow at the valley bottom cannot be seen in Figs. 14–15. However, it has been found that an upward hydraulic gradient is actually formed and that there is an outflow from the soil. Moreover, additional rain is able to penetrate the soil at this point.

The seepage is capable of starting an erosive process by piping (seepage forces). In one example the seepage outflow was actually calculated (Fig. 16). According to the traditional models, the high rate of rain (about 110 times

TABLE 3.—Ratio of Horizontal Gradient to Local Slope

Place (1)	Horizontal distance from the hilltop, in meters (2)	Ratio of horizontal gradient to local slope (3)
Hilltop	0	
	1	1.02
	2	1.37
	3	1.48
	4	1.46
Steepest slope	5	1.45
	6	1.35
	7	1.35
	8	1.34
	9	1.20
Valley bottom	10	0.82

greater than the hydraulic conductivity) should have produced a water excess very soon after its inception, and shortly after the rain has stopped the runoff should also have stopped. Note the type of hydrograph actually obtained. As anticipated, there is a sizeable "tail" of runoff.

Gullies and Seepage Mechanism

Let us now consider a sinusoidal landscape similar to that in all the aforementioned solutions but with one difference. There is an eroded vertical cut at the valley bottom, (e.g., on the right-hand side of all the profiles shown in Figs. 14 and 15. The solution remains unchanged up to the time when saturation occurs. The exposed boundary at the cut acts as an impermeable one when under suction. It is then a streamline and does not differ from the symmetry line assumed in the original solution.

Seepage flow from the cut will start as soon as saturation is attained. This occurs much earlier than in the case where saturation has to reach an uneroded soil surface. Recall the saturation and seepage times or the total rain necessary

for the onset of saturation and seepage (in Table 1). For the present analysis these quantities may be interpreted as the total rain required for the onset of seepage from a soil with an undisturbed, smooth, continuous transition layer and those necessary for seepage from a truncated transition layer.

The conclusion is that gullies considerably shorten the time and reduce the total rain necessary for the onset of seepage outflow. In the presence of smooth,

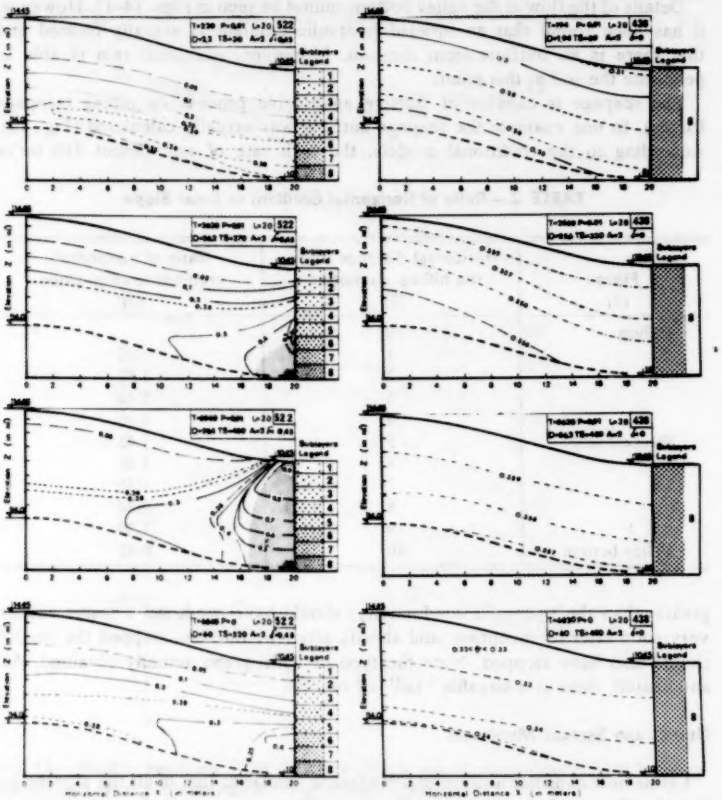

FIG. 14.—Lines of Equal Moisture Content Showing Stages of Moisture Accumulation

deep plough layers, a greater amount of rain is able to penetrate into the soil before the onset of seepage. From Table 4 one also notes the following: (1) The more gentle the slope (and the concavity), the more rain required to bring about saturation and seepage; and (2) the thicker the transition layer δ, the more rain necessary for the onset of saturation and seepage.

If seepage forces are the principal erosive mechanism, erosion can commence

as soon as seepage starts. According to the numerical solution, the upward and outward gradient may appear to be small. However, it should be noted that a slight, local dent in the soil surface can cause a local concentration of streamlines and greatly increased seepage forces. Once erosion has been initiated, the seepage gradients and outflow at the gully sidewall increase considerably and cause elongation, widening, and branching of the gully.

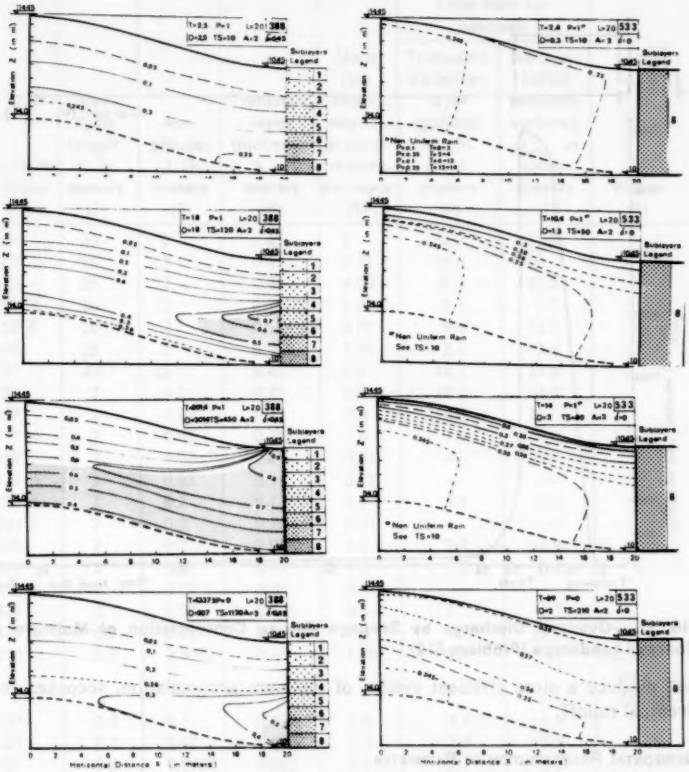

FIG. 15.—Lines of Equal Moisture Content Showing Stages of Moisture Accumulation

The foregoing offers an explanation for the formation of tunnel erosion so typical in many areas. In Israel it is pronounced, especially in the wind-blown loess soils of the south. It is a well-established fact that the initial bulk density of these soils is low. The delicate cohesive structure of the loess can collapse on saturation. The manifestation of such saturation in the profile is well demonstrated in the foregoing. The sites of its occurrence coincide exactly with those where underground tunnels were discovered in the loess area. When

the soil structure collapses a cavity is produced. Water seeps from the upper end of this cavity and reenters the soil at its lower end. When such eroded soil is transported the cavity is enlarged (the difference between the initial soil and the hydraulically redeposited soil). The tunnel is thus elongated and widened until its top caves in. Often it finds an outlet to a larger truncation.

Evidently erosion will progress at an increasing rate once it has been initiated. Moisture concentration will start erosion and runoff and the erosion in turn

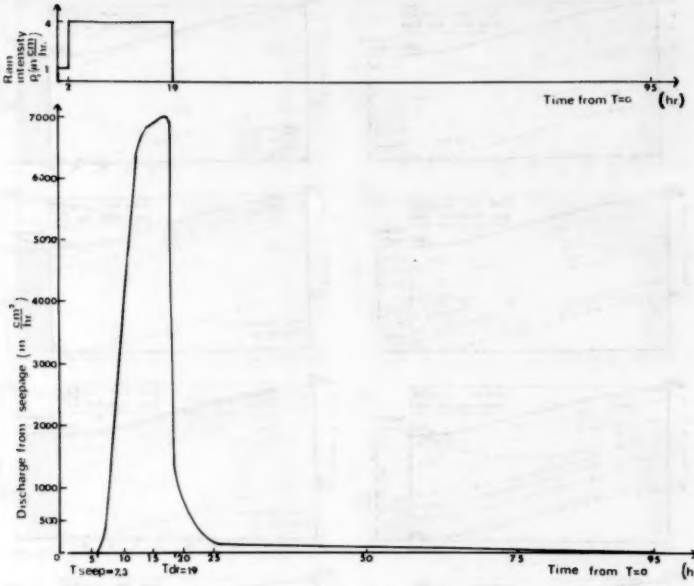

FIG. 16.—Overland Discharge by Seepage due to Concentration of Moisture in Concave Landscape (Problem 812)

will produce a more efficient system of moisture accumulation, seepage, and eventual runoff.

Horizontal Redistribution of Rainwater

Vertical integration of the moisture content, as in Eq. 12, was performed at 11 grid columns of the numerical solution. The initial value w_o at $t = 0$ was subtracted from this integral to give $\Delta w\ (t)$ resulting from the rain. The average $\bar{\Delta}w(t)$ was calculated and finally the ratio $\Delta w/\bar{\Delta}w$ was expressed. In cases where this ratio is unity, the local increment equals the average added rain. If the accumulation of moisture occurs, the ratio is higher than one. Figs. 17–20 show the results for five different cases. Let us first consider Fig. 17 for problem 388 (24 cm of rain/day). The curves in the lower part show moisture distribution during rainfall, e.g., at 2.5 h and 2.5 cm of rain there is some

uphill accumulation as the flow is normal to the soil surface and the force of gravity is still negligible compared to the pressure gradient. Later, the depth of the locally added water in the concave part (on the right) increases and

TABLE 4.—Onset of Runoff with and without Gullies

Problem number (1)	Half cycle length, L, in meters (2)	Amplitude, A, in meters (3)	Transition layer thickness, δ, in meters (4)	Main rain intensity, P, in centimeters per hour (5)	Total Rain for Seepage		Notes (8)
					Truncated transition layer (gullies), D_s, in centimeters (6)	No truncation (smooth surface), D_{seep}, in centimeters (7)	
388	20	2	0.45	1	14.9	21.3	
522	20	2	0.45	0.01	15.9	60	
815	20	2	0.45	4.00	17.2	23.2	
752 A	20	2	0.15	1.00	7.1	7.7	
752 F	20	2	0.15	0.01	8.0	12.0	
536	20	2	0.05	1.00	2.6	3.4	
535	40	12	0.45	1.0	14.3	19.0	
521	2	0.2	0.45	1.0	10.4	24.4	
379	2	0.02	0.45	1.0	16.0	38.0	
378 A	2	0.02	0.15	1.0	7.5	14.0	
379 I	2	0.02	0.45	0.01	—	—	
378 A	2	0.02	0.15	0.01	—	—	
520 A	2	0.2	0.15	1.0	5.6	8.4	
520 J	2	0.2	0.15	0.01	—	—	
523	2	0.2	0.05	1.0	2.4	2.9	
537	2	0.02	0.05	1.0	3.2	5.2	
537 B	2	0.02	0.05	0.01	—	—	
524	2	0.02	0.005	0.5	2	2.3	
525	0.2	0.02	0.15	1.0	7	15	
526	0.2	0.0002	0.15	13.0	8.8	—	run not long enough
527	0.2	0.1	0.025	1.0	4.8	4.6	
528	0.2	0.02	0.025	1.0	2.5	3.3	
529	0.2	0.0002	0.025	0.5	8.1	9.35	
530	0.2	0.1	0.005	0.5	2.0	2.0	
531	0.2	0.02	0.005	0.5	2.0	2.3	
532	0.2	0.0002	0.005	0.5	2.3	2.3	
525 P	0.2	0.02	0.15	0.01	—	—	
531 V	0.2	0.02	0.005	0.01	—	—	
532 W	0.2	0.0002	0.005	0.01	—	—	

even reaches twice the average. After the rain has stopped (upper part of the diagram, i.e., drainage), the build up of moisture continues in the lower, concave part, and depletion continues in the other parts. Fig. 18 relates to a very low

rate of rainfall (0.24 cm/day). The relative excess is very significant in the concave part, i.e., more than three times the average rain. Further concentration continues for some time after the rain has stopped. Despite deep drainage it is maintained for a relatively long period. After more than a year it is still twice the averae added rain. In all the previously mentioned problems, evaporation was ignored.

Problem 438 (Fig. 19) does not involve a transition layer and serves for the

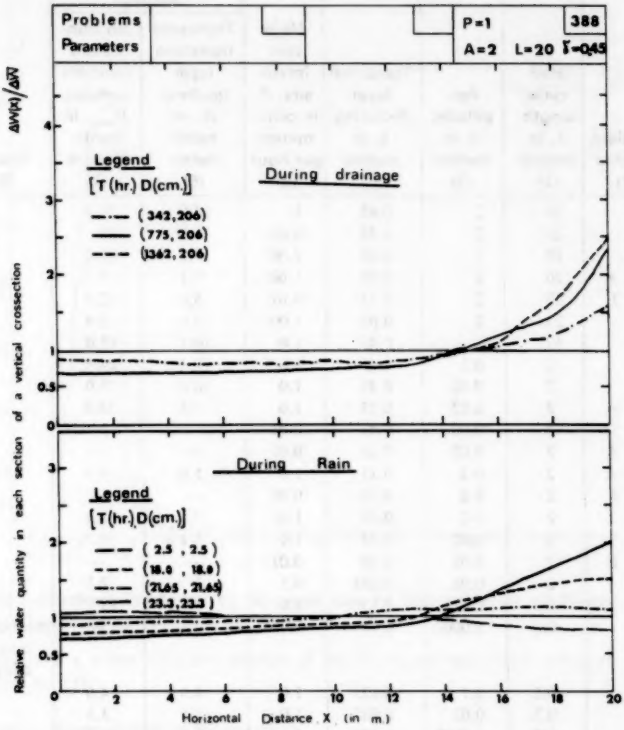

FIG. 17.—Horizontal Distribution of Relative Added Moisture Depth at Different Times: Problem 388

purpose of comparison. There is very little moisture accumulation and it is largely uphill. Fig. 20 exhibits the behavior at a very high rate of rainfall (40 mm/h–96 cm/day). It becomes evident that during the rain itself there is less time for lateral movement of moisture and the accumulation is less than that in problem 388. In both of the aforementioned problems the accumulation is less than that in problem 522. Later on, after the rain has stopped, there is still time for accumulation to develop.

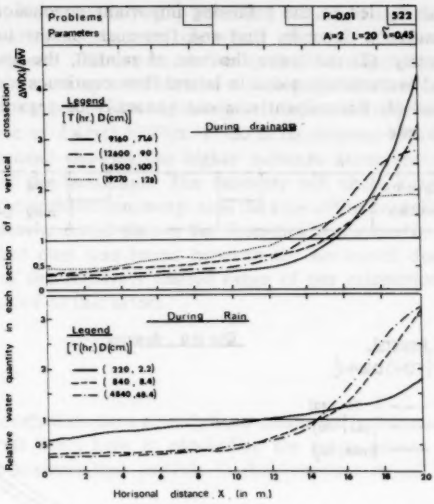

FIG. 18.—Horizontal Distribution of Relative Added Moisture Depth at Different Times: Problem 522

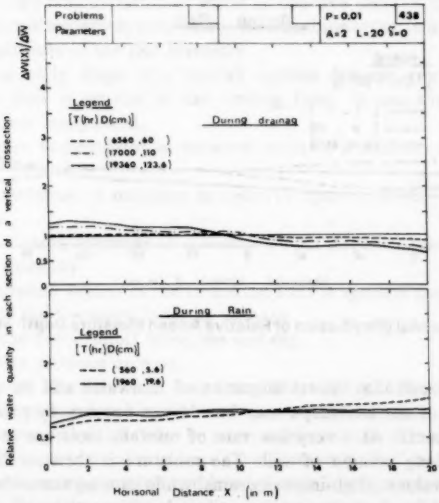

FIG. 19.—Horizontal Distribution of Relative Added Moisture Depth at Different Times: Problem 438

One is tentatively led to the following important conclusions: (1) Relative moisture accumulation depends, first and foremost, on the total rainfall and not on its intensity; (2) the lower the rate of rainfall, the greater the lateral accumulation; (3) accumulation due to lateral flow continues long after the rain has stopped; and (4) intermittent rain can generally be regarded as rain at a low, continuous rate.

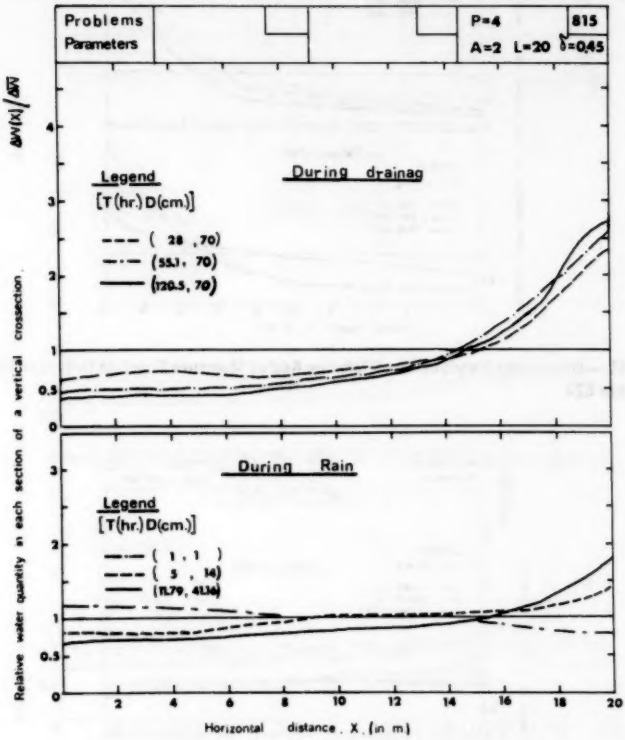

FIG. 20.—Horizontal Distribution of Relative Added Moisture Depth at Different Times: Problem 815

We should recall that lateral migration of rainwater and its accumulation in concave parts of the landscape may but do not necessarily produce saturation seepage and runoff. At a very low rate of rainfall, moisture accumulation can occur over a long column of soil. The moisture is then so distributed as to have low local values. High-intensity rains, while causing somewhat less moisture accumulation, have less time to penetrate deep into the soil. Thus, they are more liable to produce saturation and seepage (see Fig. 8).

In the numerical solution the rain was regarded as being uniformly distributed

over the surface. Note that in reality splashing raindrops and slanting rain may cause higher local concentrations, on which effect of the surface transition layer is superimposed. The latter can be by far the most important process, especially if it is bound up with erosion via seepage. Furthermore, this effect has been shown to apply over a wide range of slopes and curvatures.

The distribution of $\Delta w(xt)$ in Figs. 17–20 is reminiscent of a negative image of a surface sinusoid showing the higher moisture accumulation in the more concave parts of the landscape. The moisture will show a high, though not perfect correlation with the concavity, as in the case of the Beer-Sheba experiment (6). It should also be noted that in the foregoing a reasonable proportionality (but not a perfect one) was found between the horizontal discharge and the slope. In view of the relatively limited range of our calculations, they cannot serve as a full proof to this effect.

Conclusions

Many of the conclusions have already been mentioned in the preceding analysis. Let us summarize them here in concluding the entire report, paying special attention to the answers they provide to the questions raised in its first part (6):

1. Lateral flow does occur in the transition layer.
2. This lateral flow is roughly proportional to the slope.
3. It is also roughly proportional to the rain intensity itself.
4. It leads to the concentration of water in concave parts of the landscape.
5. Saturation will initially appear within the transition layer, in its most concave part, almost regardless of the rain intensity.
6. During the early stage of a rainfall suction prevails over the force of gravity and the flow is normal to the wetting front. It can thus give rise to a slight, uphill flow component.
7. No moisture accumulates in concave spots in a uniform soil during the rainfall time.
8. The accumulation of moisture in concave spots continues long after the rain has stopped.
9. The total excess moisture in a concave spot depends more on the total rain than on its intensity.
10. After saturation occurs in the transition zone it spreads and can approach the upper part of the transition layer as seepage.
11. Seepage can form runoff along the soil dip.
12. Seepage can produce erosion.
13. The fact that all of the rain first enters the soil and only then may partly seep out explains certain leaching phenomena as well as erosion.
14. The preceding explains why in many areas runoff actually commences only after a certain amount of rain has fallen, irrespective of its intensity.
15. It also explains why a thick and level plough layer prevents early runoff.
16. If a gully develops at the soil dip, seepage starts much earlier. This is especially significant in the case of low rates of rainfall.
17. For uniform water distribution in a field, the latter has to be smoothed

to a plane with no concave and convex spots.

Much work relating to all aspects of the new approach to surface hydrology is still necessary. We have raised sufficient doubts about the current formulation of certain hydrologic phenomena and furnished sufficient evidence in support of the new approach to justify further research. It could be directed at measuring soil properties at a point, characterization of a watershed as a whole, transformation of moisture accumulations into runoff and groundwater recharge, improved algorithms that will make possible the solution of three dimensional, nonsteady flow problems, correlation with present watershed data, etc.

Appendix I.—References

1. Braester, C., "Moisture Variation of the Soil Surface and the Advance of the Wetting Front During Infiltration of Constant Flux," *Water Resources Research*, Vol. 9, No. 3, 1973, pp. 687–694.
2. Neuman, S. P., "Galerkin Approach to Unsaturated Flow in Soils in Finite Element Methods in Flow Problems," J. T. Oden, et al., eds., *UAH Press*, University of Alabama, Huntsville, Ala., 1974, pp. 517–522.
3. Neuman, S. P., Feddes, R. A., and Bresler, E., "Finite Element Simulation of Flow in Saturated-Unsaturated Soil Considering Water Uptake by Plants," *Third Annual Report (Part I) Project No. A10-SWC-77*, Hydraulic Engineering Laboratory, Technion, Haifa, Israel, 1974.
4. Neuman, S. P., Feddes, R. A., and Bresler, E., "Finite Element Analysis of Two-Dimensional Flow in Soils Considering Water Uptake by Roots, I. Theory," *Proceedings*, Soil Science Society of America, Vol. 39, No. 2, 1975, pp. 224–230.
5. Sinai, G., and Zaslavsky, D., "Rainflow in the Soil and Near its Surface, Observations, Models and Solutions," *Publication No. 264*, Faculty of Agricultural Engineering, Technion, Haifa, Israel, 1976.
6. Zaslavsky, D., and Sinai, G., "Surface Hydrology: I—Explanation of Phenomena," *Journal of the Hydraulic Divison*, ASCE, Vol. 107, No. HY1, Proc. Paper 15958, Jan., 1981, pp. 1–16.
7. Zaslavsky, D., and Sinai, G., "Surface Hydrology: II—Distribution of Raindrops," *Journal of the Hydraulic Division*, ASCE, Vol. 107, No. HY1, Proc. Paper 15959, Jan., 1981, pp. 17–35.
8. Zaslavsky, D., and Sinai, G., "Surface Hydrology: III—Causes of Lateral Flow," *Journal of the Hydraulic Division*, ASCE, Vol. 107, No. HY1, Proc. Paper 15960, Jan., 1981, pp. 37–52.
9. Zaslavsky, D., and Sinai, G., "Surface Hydrology: IV—Flow in Sloping, Layered Soil," *Journal of the Hydraulic Division*, Vol. 107, No. HY1, Proc. Paper 15961, Jan., 1981, pp. 53–64.

Appendix II.—Notation

The following symbols are used in this paper:

A = amplitude of surface elevation;
D = total rain;
H = subsoil thickness;
K = hydraulic conductivity;
L = length of half-cycle in soil surface elevation; differential operator;
n = porosity of soil;
P = rain intensity, in centimeters per hour;
Q = discharge;

T = total rain time;
TS = number of time steps;
t = time;
V = volume;
w = total water depth in column;
x = coordinate;
z = elevation, in z direction;
δ = thickness of transition layer;
Θ = volumetric moisture content;
ϕ = hydraulic head; and
ψ = pressure head.

Subscripts

i = relating to ith soil layer; ith coordinate;
j = relating to jth coordinate;
sat = to saturation;
seep = up to onset of surface seepage;
d = at end of rain; and
f = end of program run.

Superscripts

R = isotropic term of K, pressure head dependent; and
s = anisotropic constant term of K, saturated K.

JOURNAL OF THE HYDRAULICS DIVISION

MULTIPORT SLEEVE VALVE DEVELOPMENT AND APPLICATION

By Philip H. Burgi,[1] Edward O. Green,[2] and Raoul E. Thibault[3]

INTRODUCTION

The design and construction of long aqueducts to supply municipal and industrial water have presented the need to develop a control valve and energy dissipator that would be compatible with the aqueduct system. A valve design is needed that will: (1) Adequately dissipate high energy flow at small discharges; and (2) pass the maximum design flow with a minimum of energy loss. The aqueduct would dissipate the majority of available energy in line losses when operating under full design discharge flow conditions and the control valve would dissipate the majority of excess energy when operating under a low-flow condition.

Flow control stations on many long aqueducts have generally been limited to pressure head differentials of approximately 15 m. This head restriction resulted from the cavitation damage associated with the use of butterfly valves when used for throttling at high head differentials. If a valve and associated energy dissipator could be developed to accommodate pressure head differentials exceeding 15 m, the number of "control stations" required along an aqueduct could be reduced, resulting in significant cost savings. With these needs in mind, the Division of Research and the Division of Design at the Bureau of Reclamation's (now Water and Power Resources Service) Engineering and Research Center, in Denver, Colo., initiated a research program in 1972 to develop a more versatile control valve and energy dissipator.

[1]Hydr. Engr., United States Dept. of Interior, Water and Power Resources Service, Engrg. and Research Center, P.O. Box 25007, Building 67, Denver Federal Center, Denver, Colo. 80225.

[2]Retired; formerly Supervisory Mech. Engr., United States Bureau of Reclamation, Denver, Colo.

[3]Supervisory Civ. Engr., United States Dept. of Interior, Water and Power Resources Service, Engrg. and Research Center, P.O. Box 25007, Building 67, Denver Federal Center, Denver, Colo. 80225.

Note.—Discussion open until June 1, 1981. To extend the closing date one month, a written request must be filed with the Manager of Technical and Professional Publications, ASCE. Manuscript was submitted for review for possible publication on March 12, 1980. This paper is part of the Journal of the Hydraulics Division, Proceedings of the American Society of Civil Engineers, © ASCE, Vol. 107, No. HY1, January, 1981. ISSN 0044-796X/81/0001-0095/$01.00.

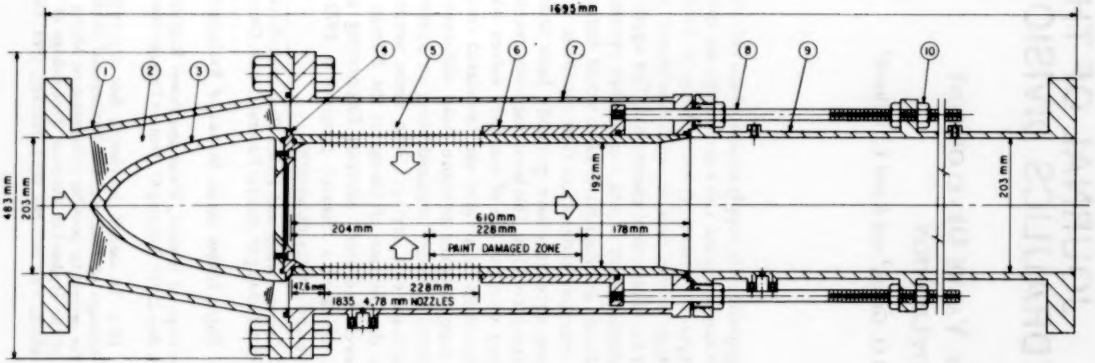

VALVE PARTS LIST

1	UPSTREAM BODY
2	SUPPORT FIN
3	CONE
4	SEAT RING
5	PERFORATED SLEEVE
6	CONTROL SLEEVE
7	MAIN BODY
8	OPERATING STEM
9	DOWNSTREAM BODY
10	OPERATING NUTS

203 mm BAILEY POLYJET VALVE
(1 mm = 0.0394 in)

FIG. 1.—200-mm Bailey Polyjet Valve

On Nov. 6, 1979, the Bureau of Reclamation was renamed the Water and Power Resources Service of the U.S. Department of the Interior. The new name more closely identifies the agency with its principal functions—supplying water and power. Some of the references listed in this paper were prepared prior to adoption of the new name; all references to the Bureau of Reclamation or any derivative thereof are to be considered synonymous with the Water and Power Resources Service.

This paper presents the laboratory results of tests conducted to determine the discharge coefficients and overall valve performance of two 200-mm sleeve valves. The essential components of a sleeve valve are two concentric cylinders. One cylinder is stationary and the other serves as a control sleeve traveling

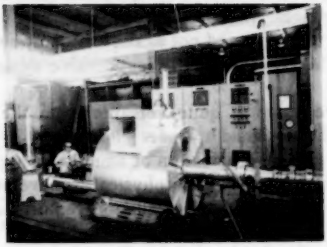

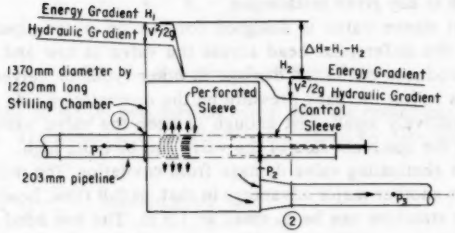

FIG. 2.—200-mm Horizontal Multijet Sleeve Valve

across the open ports of the stationary cylinder. The first valve tested was the Bailey Polyjet valve. As can be seen in Fig. 1 the control for the Bailey valve consists of a cylindrical sleeve that travels over a smaller diameter stationary cylinder with regulating ports. The second valve tested was the horizontal multiport sleeve valve developed in the laboratory, Fig. 2. The outer cylinder of this valve is fixed and contains the regulating ports; the inner, smaller diameter movable cylinder is the control sleeve.

Application of Multiport Sleeve Valves

Previous studies (2) on a 50-mm model of a multiport sleeve valve and a vertical stilling well indicated that such a valve could meet the control requirements stated previously. In a study reported by Miller (6), Glenfield and Kennedy,

Ltd., described a submerged valve similar to the Wanship sleeve valve (4). They developed a new device which could be attached to their standard sleeve valve resulting in a ported sleeve valve. Miller also noted an improvement in energy dissipation resulting from the small individual jets leaving the valve.

The MWD (Metropolitan Water District) of Southern California (5) conducted tests on an improved submerged discharge valve (without ports), but found, that at pressure heads in excess of 30 m, cavitation damage occurred on the bottom plate of the valve and edges of the control sleeve. To develop a valve that could control high energy flows, the concept of flow nozzles was used. MWD engineers developed an outer sleeve containing a large number of small nozzles and attached it to a sleeve valve under study. The nozzles produce a flow acceleration through the outer sleeve; thus cavitation does not occur in the metal flow passages. As the jets exit the valve, cavitation occurs in the water surrounding the valve and not against the flow surfaces. The developmental stages of the MWD "multijet" sleeve valve design were summarized by Watson (9).

The multiport sleeve valve is quite versatile from the designer's point of view. The ports can be designed to meet almost any hydraulic requirement. It can regulate flows from fine regulation of small discharges to maximum flow with minimum pressure head loss. The physical arrangement of the valve can be varied to meet a wide range of installation requirements. It is adaptable to various types of operating mechanisms with different mounting positions. The sleeve valve can operate over a wide range of pressure heads including a wide variation at any given installation.

The multiport sleeve valve is designed for use on water pipeline pressure systems where the differential head across the valve at low and intermediate flows usually produces cavitation damage in other types of valves. What this, in effect, means is that the back pressure on the downstream side of the sleeve valve can be relatively small, just enough to keep the valve submerged while the pressure on the upstream side of the valve can be quite high.

In addition to eliminating valve damage from cavitation, the multiport sleeve valve also offers another major advantage in that, at full flow, head loss through the entire valve structure can be as small as 1.5 m. The low head loss features can yield significant savings in costs of pipe. The ability to dissipate high-pressure heads enables the designer to use fewer rate-of-flow control stations along an aqueduct.

The multiport concept of valve control has permitted designers to consider controlling high-pressure head flows, ranging from 150 to 300 m at one installation. Previously, such high-pressure head flow was controlled using several steps of energy reduction to prevent cavitation damage to the control valves.

Hydraulic Considerations

Two appealing flow characteristics of a valve using the multiport concept are:

1. The flow and energy are dissipated quite rapidly upon leaving the valve, thus requiring a relatively small energy dissipation structure.
2. The inevitable process of formation and collapse of cavitation bubbles,

which occurs during throttling of high energy flow, can be controlled to occur in the water surrounding the valve and not against the flow surfaces of the valve or energy dissipation chamber.

Jet velocity deceleration rate is related to port size. The location of the "cavitation bubble collapse zone" is related to the port exit shape and its relative proximity to other ports. Fig. 3 shows the flow pattern developed by a submerged jet (7). Albertson (1) and Yevdjevich (11) examined the characteristics of a submerged jet. Albertson described the phenomena as two stages: zone of flow establishment and zone of established flow. In the zone of flow establishment, the core of the submerged jet is penetrated by viscous shear until the center-line velocity begins to decrease. Thus the jet decelerates while the fluid surrounding the jet gradually accelerates. The zone of established flow is defined as that

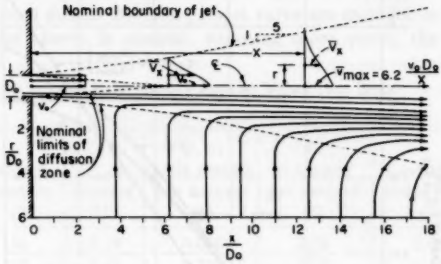

FIG. 3.—Submerged Jet Flow Patterns

zone where the entire jet becomes turbulent and the center-line velocity begins to decelerate. The center-line velocity V_m is defined by Albertson as

$$V_m = 2.28\, V_o \sqrt{\frac{B_o}{X}} \quad \text{(slotted port)} \quad \ldots\ldots\ldots\ldots\ldots\ldots\ldots\ldots (1)$$

$$V_m = 6.2\, V_o \frac{D_o}{X} \quad \text{(circular port)} \quad \ldots\ldots\ldots\ldots\ldots\ldots\ldots\ldots (2)$$

in which V_m = jet center-line velocity at distance X; V_o = jet exit velocity = $C_d\sqrt{2g\Delta H}$; B_o = slot width; D_o = circular port diameter; X = distance from exit port along jet center line; C_d = discharge coefficient of port; and ΔH = pressure head differential across port.

From Eq. 2 it is evident that for a circular port, the distance X from the port, needed to reduce the jet velocity V_m to a certain fraction of the jet exit velocity V_o, is directly related to the port diameter D_o. Thus a reduction in the port diameter by one-half would reduce the distance X required to produce the same center-line velocity V_m by one-half. Ports as small as 3.2 mm have been used on some multiport valves. Therefore, for a head of 150 m, the jet velocity could be reduced from 51 m/s at the exit port to 4.0 m/s in a distance of 250 mm, using a 3.2-mm-diam port.

Investigation of Multiport Sleeve Valves

Hydraulic Laboratory Testing.—The Water and Power Resources Service Hydraulic Laboratory's high head test facility was used for laboratory tests of two multiport valves. The facility consists of a seven stage vertical turbine pump driven by a 186-kW d-c motor. The rectifying unit and motor speed control converts a-c into d-c. needed for the motor and provides speed selection from 200 to 1,800 rpm. Rate of flow is measured with a 200-mm venturi meter permanently installed 3 m downstream from the pump outlet. A 200-mm, motor-operated valve was used to control the downstream pressure on the test valve.

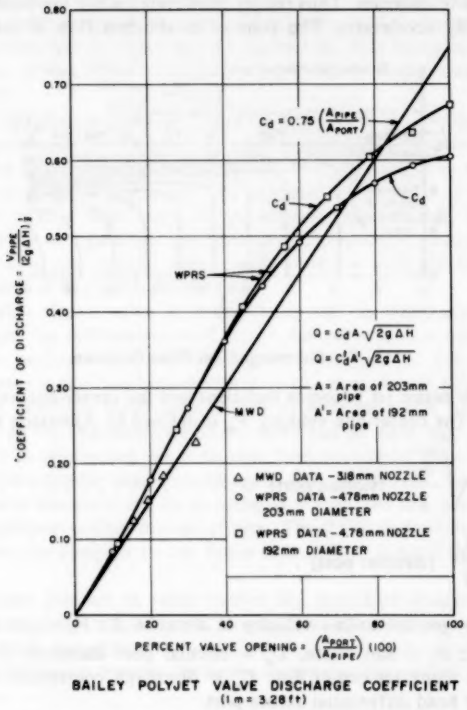

FIG. 4.—Bailey Polyjet Valve Discharge Coefficient

Bailey Polyjet Valve.—Tests were conducted on a 200-mm test valve provided by the Chas. M. Bailey Co., Inc., 1301 59th Street, Emeryville, Calif. 94608 (Fig. 1). The purpose of the test was to determine the performance characteristics of the valve under the two operating conditions previously discussed; namely, energy dissipation at low-flow conditions and minimal energy loss at design flows.

The control for the Bailey valve consists of a cylindrical sleeve located inside the annular chamber of the valve that travels over the ports. Movement of the sleeve controls the open port area and, thus, the valve discharge. The flow passes inward through the 1,835, 4.78-mm ports, then along the inside of the perforated sleeve into the downstream pipe, which is the same diameter as the inlet pipe.

Tests were conducted to determine the discharge coefficient, C_d, for the Bailey valve. The discharge coefficient curves based on the 203-mm-diam pipe inlet area and the 192-mm-diam perforated sleeve area are shown in Fig. 4. Since all 1,835 ports were the same size and configuration, it would appear that the overall valve flow characteristics would be the same as the local flow characteristics of each port. This would result in a linear relationship between the valve coefficient of discharge C_d and the area ratio: A_{port}/A_{pipe}. As indicated on Fig. 4, this was not the case. Test results conducted by the MWD of Southern California (10) on a similar 200-mm polyjet valve are included in Fig. 4.

As the control sleeve is opened, exposing more ports, the flow near the

TABLE 1.—Bailey Polyjet Valve Test Data

Valve opening, in percent (1)	H_u, in meters (2)	H_d, in meters (3)	Q, in cubic meters per second (4)	V, in meters per second (5)	Cavitation index = σ^a (6)	Time, in hours (7)
5	136	2.19	0.066	2.04	0.08	2.0
10	107	5.85	0.122	3.78	0.14	2.0
15	70.1	4.18	0.151	4.66	0.19	2.0
20	46.0	4.15	0.167	5.15	0.30	1.5
30	25.3	4.05	0.171	5.27	0.59	2.0

[a]$\sigma = (H_d - H_v)/(H_u - H_d)$; $H_v = -8.47$ m (atmospheric pressure at the Water and Power Resources Service test facility); and H_d = downstream pressure head.

upstream end of the perforated sleeve passes the upstream ports in an effort to satisfy the downstream flow demand. The resultant approach velocity and pressure drop near the upstream ports causes a reduction in the flow through these ports. This phenomenon is similar to that which occurs in manifold pipes.

To evaluate potential cavitation damage to the 200-mm polyjet test valve, the inside flow surfaces of the ported sleeve were painted with a white concrete curing compound. In earlier tests concrete curing compound proved to be an excellent indicator of the location and degree of pitting of a metal surface resulting from cavitation bubble collapse. Table 1 presents the test data for the polyjet valve for sleeve openings of 5, 10, 15, 20, and 30%. Pressure head on the valve was measured 1.83 m upstream (H_u) and 1.73 m downstream (H_d) from the valve. The vapor pressure H_v at the Water and Power Resources Service laboratory elevation is equivalent to -8.47 m of water.

The high head vertical turbine pump head was designed to deliver a maximum flow of approximately 0.17 m^3/s. Therefore, the cavitation damage tests were limited to valve openings between 5 and 30% and cavitation index, $\sigma = (H_d - H_v)/(H_u - H_d)$, values ranging from 0.08 to 0.59, respectively. Fig. 5 shows

the resulting paint removal (small pockmarks) on the internal flow surfaces of the ported sleeve under the 15% valve opening test condition described in Table 1. The photograph shows cumulative damage from the 5% opening up to and including the 15% open level. (The scratch lines on the paint in the damaged area were caused by insertion of a mirror for photographs.)

The cavitation damage shown on Fig. 5 is typical of locations where individual cavities implode near the flow surface. The damage was located in a zone which extended 152 mm downstream from the ports to 76 mm into the port zone, Fig. 1. Although the valve was operated at an extremely low sigma value ($\sigma = 0.08$) for the 5% test, there was no apparent cavitation damage. The majority of paint removal occurred at the 10 and 15% valve openings. Results

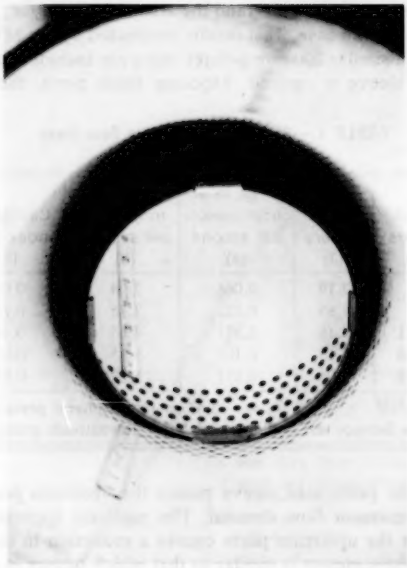

FIG. 5.—Looking Upstream at Ported Sleeve Valve Surface

indicate that the cavitation damage in the test of this particular valve is related to the quantity of vapor bubbles produced as well as the pressure head relationship. The amount of paint removal would increase for greater valve openings at low sigma values. However, on long pipelines, the majority of the energy head would be dissipated in upstream pipe losses at larger valve openings, resulting in higher sigma values with less cavitation potential. It is most likely that the critical point, with respect to cavitation damage for polyjet valves on long aqueducts with high friction losses, will be in the range of 10 to 15% open. In general, the polyjet valve performed well when operated within the manufacturer's suggested pressure head ranges.

Horizontal Multiport Sleeve Valves.—Prior to the tests described herein,

multiport sleeve valve designs could not be found that fully satisfied the design criteria desired by the Service, that is, a valve that will dissipate high energy flows in a low-flow condition and deliver design flows with a minimum energy loss at the valve. Although previous designs function quite well as pressure-reducing valves, most do not emphasize minimal energy loss when delivering design flows.

The 200 mm laboratory test valve discharged into a 1,370-mm-diam, 1,220-mm-long stilling chamber. The basic concept of the valve and stilling chamber is illustrated in Fig. 2. Flow enters the valve from the high-pressure side and is discharged outward through the perforated body of the valve into the stilling chamber. A cylindrical sleeve located inside the valve body travels over the perforated section of the valve, controlling the port area and thus the valve discharge. The flow is discharged into the downstream pipeline at the lower end of the stilling chamber.

The concept of a linear relationship between sleeve travel and valve discharge was also sought as a desired characteristic in the new design. Such a valve would provide better control characteristics on long aqueducts where water hammer presents a potential problem. Fig. 6 shows ideal valve characteristics

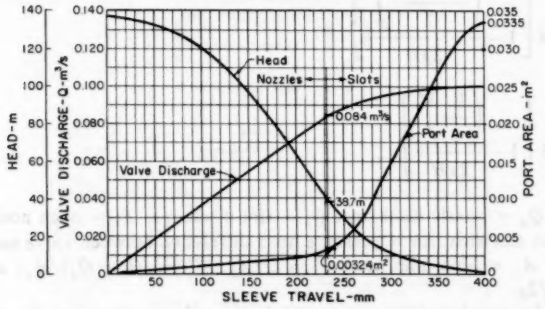

FIG. 6.—Ideal Multijet Sleeve Valve Characteristics

as a function of sleeve travel for a 200-mm pipeline where the static upstream pressure head is 137 m. A 200-mm-horizontal multiport sleeve valve with nozzles and slots for ports is proposed. As the valve is opened and the port area slowly increases, the valve discharge increases linearly with sleeve travel. This increase in valve discharge results in a reduced upstream pressure head due to friction losses in the long aqueduct. When the valve sleeve has been opened 230 mm, it has completed the function of a pressure reducing valve and assumes the role of a low-head-loss control valve. At this point the valve port area increases rapidly with sleeve travel but this produces a diminishing increase in discharge due to the low available pressure head across the valve. When the valve port area equals the 200-mm pipe area, the pressure head differential, ΔH, has decreased to 1.1 m across the valve, resulting in a discharge coefficient C_d of approximately

$$C_d = \frac{\dfrac{Q}{A}}{\sqrt{2g\Delta H}} = 0.68 \qquad (3)$$

in which Q = valve discharge; A = port area; and ΔH = pressure head differential across the valve. The key to the multiport design is the proper placement of the ports along the several turns of a spiral that extends along the length of the valve to produce a nearly linear relationship between the valve discharge and travel.

Pressure heads were measured at pressure taps P_1, P_2, and P_3 (Fig. 2) and corrected for a pressure differential, ΔH, between the upstream flange of the sleeve valve, H_1, and the downstream 200-mm pipe flange, H_2. Eqs. 4 and 5 were used to calculate the discharge through the nozzles and slots, respectively

$$Q_n = C_n A_n \sqrt{2g\Delta h} \qquad (4)$$

$$Q_s = C_s A_s \sqrt{2gH} \qquad (5)$$

$$C_n = 0.94 \left[1 - \frac{\left(\dfrac{V + V'}{2}\right)^2}{2gH} \right] \qquad (6)$$

$$C_s = 0.85 \left[1 - \frac{\left(\dfrac{V'}{2}\right)^2}{2gH} \right] \qquad (7)$$

in which Q_n = nozzle discharge; Q_s = slot discharge; A_n = open nozzle area; A_s = open slot area; Δh = pressure head difference between valve and stilling chamber; A_p = pipe inlet area; $V = Q/A_p$; $V' = (Q - Q_n)/A_p$; and $H = \Delta h + V^2/2g$.

When the nozzles alone are exposed, the velocity term on the right side of Eq. 6 is negligible since the velocity head is small with respect to the total available energy, H. As the control sleeve opens, the total energy term decreases due to friction losses in the upstream aqueduct, and the velocity term increases. Thus the nozzle and slot coefficients, C_n and C_s, decrease in value to reflect the phenomena of a manifold where the majority of the valve discharge is released through the downstream ports of the valve.

Eqs. 6 and 7 are similar to the equations presented by Vigander (8) and Enger (3) dealing with large diffusers and manifolds. They are empirical equations based on the results of laboratory studies conducted on the 200-mm test valves.

The investigation included studies conducted on the two-ported (nozzle and slots) valve sleeve shown in Fig. 7. The sleeve travel versus port area relationship curves for the two configurations and the polyjet valve are shown in Fig. 8. The Bailey polyjet valve has a linear relationship between port area and sleeve travel. The area for the slotted port configuration increases at a somewhat slower rate initially. The area for the valve with nozzles and slots increases very slowly at the start of the sleeve travel and then rapidly increases once

the slots are exposed, yielding a linear relationship between the sleeve travel and valve discharge.

The use of nozzles or orifices for the discharge ports should be carefully considered. The present spiral arrangement of the ports results in the partial blockage of some of the ports when the valve is used to control the flow. Further laboratory investigations should be conducted to determine the pressure head-nozzle diameter relationship where cavitation occurs in large nozzle flow passages. Until such laboratory investigations have been conducted, it is suggested that an orifice design [similar to that shown in Fig. 7(*b*)] instead of the nozzle design be considered for ports 19 mm in diameter or larger (2).

Data for the head loss coefficient K are plotted with respect to percent valve

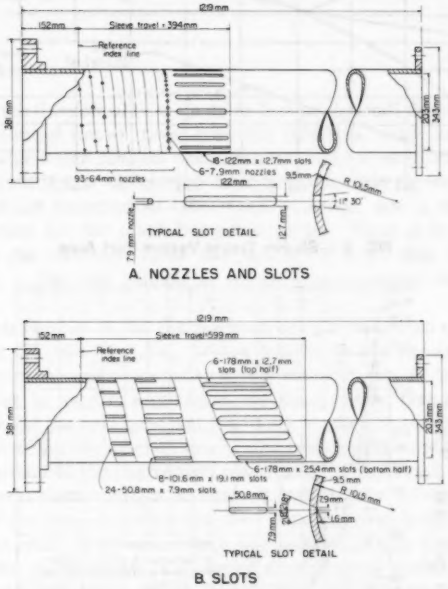

FIG. 7.—Dimensional Sketches of Ported Valve Sleeves

opening (100 × port area/pipe area) on Fig. 9 for both port configurations shown in Fig. 7. The head loss coefficient K is based on the pressure head differential, ΔH, between the upstream valve flange and the 200-mm pipe flange downstream of the stilling chamber. The loss coefficient, therefore, includes the total system loss for the control structure. The Bailey polyjet valve data are also plotted on Fig. 9.

Computer Model.—Presently, multiport sleeve valve designs include a large number of apertures in the valve body. To reduce manufacturing costs and to obtain a better flow control characteristic, the Service's sleeve valve design utilizes the fact that pipe friction head losses can be approximated for various

flows by using the equation $H_f = KQ^2$, in which K = constant for a particular pipeline and $Q = CA\sqrt{2gH}$. Using this approach, a computer program (2) (U.S. customary units) has been developed to locate and space nozzles along

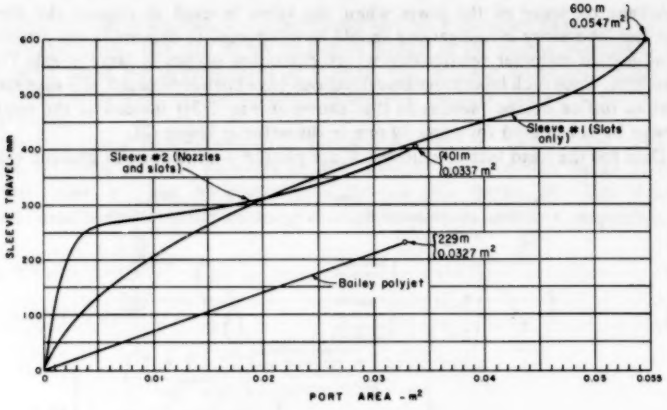

FIG. 8.—Sleeve Travel Versus Port Area

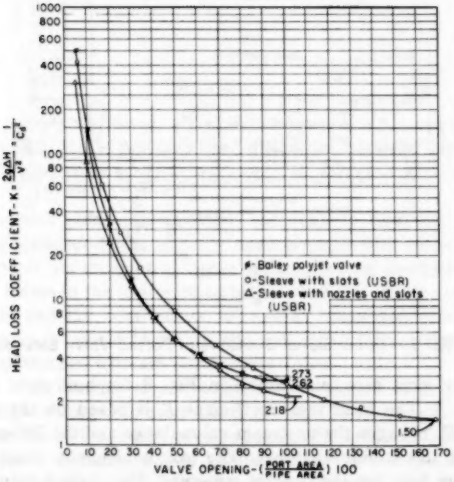

FIG. 9.—Head Loss Coefficient

a spiral around the valve body such that a linear change in flow is maintained through the zone of the nozzles. As the control sleeve is retracted to expose more apertures, the number and/or diameter of the nozzles is increased until

the largest diameter nozzle is equal to the wall thickness of the valve body. When a point is reached where the computed number of nozzles cannot meet the minimum spacing requirements along the spiral in a quadrant that is being incremented, then the program automatically changes its output from nozzles to a preselected number of longitudinal slots. The length of the slots is computed by short intervals such that at the final length, full flow is achieved: that is, when the control sleeve is retracted past the end of the last slot [Fig. 7(*a*)]. The differential area, Aq, of each set of nozzles in a quadrant along the spiral is determined by use of the well-known orifice equation, $Q = CA\sqrt{2g\Delta H}$. The linear change in flow is obtained by setting a uniform rate of change between spiral peaks; hence the change for a quadrant can be calculated. Rewriting the orifice equation, we have

$$A_t = \frac{Q_n}{C_n\sqrt{2g\Delta H}} \qquad (8)$$

in which Q_n = the theoretical flow (in cubic feet per second) through the nozzles based on the control sleeve travel from the reference index line [Fig. 7(*a*)]; $C_n = 0.94$, a value which remains constant until slots are included in the output; $2g = 64.32$ ft/s^2; ΔH = differential head in feet across the sleeve valve for the quadrant being incremented. (For each quadrant, ΔH is reduced by the total pipe friction for the reach being considered. Since Q is a function of distance from the reference index line and $H_f = KQ^2$, then $H = H_{static} - KQ^2$); and A_t = the total amount of nozzle area in square feet required to pass flow Q_n.

From this relationship, A_q for the quadrant being incremented can be obtained by subtracting the total area, A_n, of the nozzles in the preceding quadrants from A_t. Because A_q will not exactly match with the sum of the areas of the nozzles that can be used in a quadrant, the small excess area is added to the calculated area for the next quadrant before its number of nozzles is computed.

The physical model test program was used to evaluate the empirical coefficients used and has produced good agreement with discharges indicated in the computer model. The linear change in Q is maintained until the control sleeve is retracted to the zone of the slots. At this point, flow is approximately 82% of the design flow. The end result is a valve which can achieve design flow with a much smaller number of apertures. It is hoped that physical model testing can be continued to evaluate larger design flows where two or more multiport sleeve valves would be required in a flow control structure.

Mechanical Considerations.—The heart of the sleeve valve is two concentric cylinders. The outer cylinder or body is fixed and contains the regulating ports; the inner, unperforated movable cylinder is the control sleeve. It fits closely inside the body and is moved longitudinally to cover and uncover the ports providing regulation of flow. Minimal practical clearances are provided between the body and sleeve to control leakage. No seals or packings have been used on the sleeve. A guard valve upstream of the sleeve valve provides tight shutoff when no flow is desired and the sleeve valve is closed. If minimal leakage is important, piston rings are provided on the sleeve. The Metropolitan Water District of Southern California designed their valves for tight closure (5,9). Packings are provided on the end of the sleeve which does not move across

the regulating ports and a fixed seal is mounted in the body to seal the other end of the sleeve when the valve is closed.

The valve ports can be varied in size, type, and spacing to meet a wide range of requirements. According to MWD round nozzles are limited in size as their diameter cannot be larger than the body shell thickness because of changes which occur in jet characteristics. Because of the limitation on size, a large number of nozzles is required. Ports can be machined as slots with the same taper as the round nozzles. The width of the slots has the same limitations as the diameter of the nozzles with respect to cavitation damage, and the length is limited by the physical strength of the body shell. Because of the taper, these ports must be reamed from the inside of the cylindrical body. This is a difficult and expensive machining process. A 200-mm valve is considered the smallest that can be machined from the inside.

In river or reservoir outlet work installations where the water may carry debris large enough to plug the nozzle-type ports, ports that are designed as sharp-edged orifices are utilized. These ports have parallel sides for the first 1.5 to 7 mm of depth from the inside of the body [Fig. 7(*b*)]. To eliminate any possibility of cavitation on the sides of the port, the remainder of the port is flared out at a 45° angle.

The size and shape of the ports can be specified to suit specific requirements. Port shapes have been made round, oblong, and longitudinal. In general, the size of a port is limited by the physical strength of the body shell. However, the larger the port, and in turn the jet, the greater the outward distance (perpendicular to the valve body) that is required to dissipate the energy of the jet. For this reason, the ports should be kept as small as practicable consistent with the size of expected debris that must be passed.

Port size and spacing may be varied to meet specific hydraulic requirements. As noted previously, valves used in long municipal-industrial pipelines gain benefits from linear discharge characteristics even though the effective energy head at the valve drops rapidly as the discharge increases. It has already been shown that this requirement can be easily met by varying spacing and size of the nozzles and, when effective head drops sufficiently, changing to slots. This general principle can be used for other discharge characteristics. As an example, valves requiring fine regulation of small off-season discharge can have a few small ports as required for the off-season releases. The remainder of the ports can be longer and spaced closer together to give needed regulation of normal releases with minimum sleeve travel. As port size increases, it is necessary to place ports diametrically opposite to maintain hydraulic balance of the valve.

The sleeve valve lends itself to many physical arrangements. The most efficient and straightforward is the horizontal valve of the general type used in the Service laboratory test and shown in Fig. 2. In this type, the stem attached to the control sleeve is extended downstream through packings to the valve operator. Thus all moving parts of the sleeve are downstream of and unaffected by the water flow. The sleeve is hydraulically balanced. The only unbalance is the hydraulic load on the valve stem. Since this stem load and friction are the only loads to be overcome, the operating mechanisms can be relatively small.

Sleeve valves are adaptable to many types of operating mechanisms. The Service has used a gear type with torque-limiting switches, hydraulic cylinders,

and even a hand-operated gear lift for a remote installation without power.

A vertical arrangement has been used for some valves with the flow being discharged downward into a square stilling well (Fig. 10). This is a good arrangement for valves with large ports as the distance required to dissipate the jet energy is much greater. The bottom of the stilling well and the lower walls should be steel lined and the well sized to allow jet velocities as high as 12 m/s to impinge on the steel liner. The stilling well will very effectively dissipate the remaining energy of the jets. However, with this arrangement the incoming water flow must pass through a 90° elbow and the valve operator

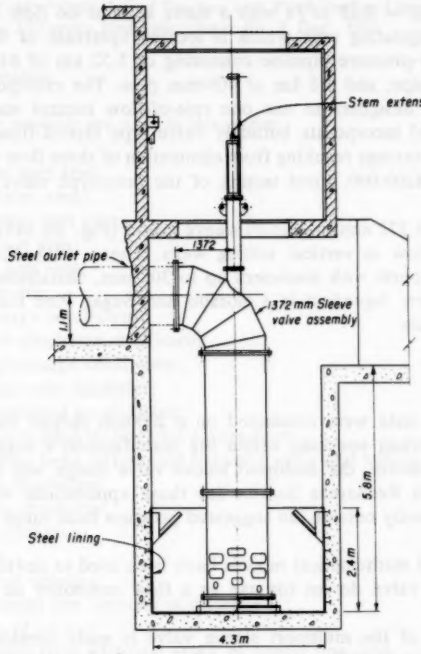

FIG. 10.—Typical Multiport Sleeve Valve in Vertical Stilling Well

is mounted on top of the elbow. Thus the control stem is in the water passage and the water must flow through the inside of the control sleeve. The valve interior must be streamlined to impede water flow as little as practical and to provide adequate support to the stem. The Service's experience has shown that vibrations can cause fatigue and breaking of a stem. Flow velocity through the elbow and sleeve must be kept low and, when at maximum valve opening, should not exceed 11 m/s.

From the mechanical standpoint, sleeve valves are fairly simple devices. However, there are features that prevent them from being classified as inexpen-

sive. The body, sleeve, and stem must be made from corrosion-resistant materials. The sleeve and body must be carefully and closely fitted. As noted before, the ports are difficult and expensive to machine. The stainless steel body also creates a machining problem.

Prototype Installations and Experience

A 356-mm-diam prototype horizontal multiport sleeve valve has been installed in the Deep Red Run rate-of-flow control station near the end of the Frederick Aqueduct of the Service's Altus Project in Oklahoma. The valve is designed for $Q = 0.23$ m^3/s with a static head at no flow of 70 m. From the Frederick regulating tank which is located upstream of the valve, there is a gravity flow-pressure pipeline consisting of 5.52 km of 610-mm pipe, 6.4 km of 458-mm pipe, and 3.8 km of 406-mm pipe. The multiport sleeve valve has allowed the designers to use one rate-of-flow control station in lieu of four which would incorporate butterfly valve type rate-of-flow controllers. It is estimated that savings resulting from elimination of three flow control stations are well above $200,000. Field testing of the prototype valve is planned for the near future.

Several large (1,372 mm) multiport sleeve valves (Fig. 10) have been designed for control of flow in vertical stilling wells. These valves have circular or elliptical-shaped ports with diameters up to 305 mm. Installations are planned for the Mt. Elbert Aqueduct in Colorado and Sugar Pine Dam River outlet works in California.

Conclusions

1. Laboratory tests were conducted on a 200-mm polyjet valve. The valve performed well when operated within the manufacturer's suggested pressure head ranges. However, the multiport sleeve valve design will be used by the Water and Power Resources Service for those applications where operation may be intermittently outside the suggested pressure head range for the polyjet valve.
2. Physical and mathematical models have been used to develop a horizontal multiport sleeve valve design for use as a flow controller on long aqueduct systems.
3. The design of the multiport sleeve valve is quite versatile and can be used in a wide variety of flow regulation situations.

Appendix I.—References

1. Albertson, M. L., Dai, Y. B., Jensen, R. A., and Rouse, H., "Diffusion of Submerged Jets," *Transactions*, ASCE, Vol. 115, Paper No. 2409, 1950, p. 639.
2. Burgi, P. H., "Hydraulic Model Studies of Vertical Stilling Wells," *REC-ERC-73-3*, Bureau of Reclamation, Denver, Colo., Feb., 1973.
3. Enger, M. C., and Levy, M. L., "Pressure in Manifold Pipes," *Journal American Water Works Association*, Vol. 21, Mar., 1929, p. 659.
4. Falvey, H. T., "Hydraulic Model Studies of the Wanship Dam Vertical Stilling Wells, Weber Basin Project, Utah," *Report No. Hyd-481*, Bureau of Reclamation, Denver, Colo., Jan., 1962.
5. Johnson, D., "Sleeve Valves," Institute on *Control of Flow in Closed Conduits*,

Colorado State University, Fort Collins, Colo., Aug., 9–14, 1970, (published 1971).
6. Miller, E., "The Submerged Discharge Valve," *Glenfield Gazette*, No. 229, Feb., 1969.
7. Rouse, H., "Jet Diffusion and Cavitation," *Journal of the Boston Society of Civil Engineers*, Vol. 53, No. 3, 1966.
8. Vigander, S., Elder, R. A., and Brooks, N. H., "Internal Hydraulics of Thermal Discharge Diffusers," *Journal of the Hydraulics Division*, ASCE, Vol. 96, No. HY2, Proc. Paper 7085, Feb., 1970, pp. 509–527.
9. Watson, W. W., "Evolution of Multijet Sleeve Valve," *Journal of the Hydraulics Division*, ASCE, Vol. 103, No. HY6, Proc. Paper 13006, June, 1977, pp. 617–631.
10. Winn, W. P., "Test and Evaluation of 8-inch Bailey Polyjet Valve," Report No. 874, Metropolitan Water District of Southern California, Oct., 1970.
11. Yevdjevich, V. M., "Diffusion of Slot Jets with Finite Orifice Length-Width Ratios," *Colorado State University Hydraulics Paper No. 2*, Dec., 1965.

Appendix II.—Notation

The following symbols are used in this paper:

A_n = nozzle port area;
A_p = pipe inlet area;
A_q = quadrant port area;
A_s = slot port area;
A_t = total port area;
B_o = slot width;
C_d = discharge coefficient;
C_n = nozzle discharge coefficient;
C_s = slot discharge coefficient;
D_o = circular port diameter;
g = gravitational acceleration;
ΔH = pressure head differential across port;
Δh = pressure head differential between valve and stilling chamber;
Q = valve discharge;
Q_n = nozzle discharge;
Q_s = slot discharge;
$V = Q/A_p$;
V_o = jet exit velocity;
V_m = jet center line velocity at distance X;
$V' = (Q - Q_n)/A_p$;
X = distance from exit port along jet center line; and
σ = cavitation index.

JOURNAL OF THE
HYDRAULICS DIVISION

TECHNICAL NOTES

Note.—Discussion open until June 1, 1981. To extend the closing date one month, a written request must be filed with the Manager of Technical and Professional Publications, ASCE. This paper is part of the Journal of the Hydraulics Division, Proceedings of the American Society of Civil Engineers, © ASCE, Vol. 107, No. HY1, January, 1981.

Technical Notes

To provide a place within ASCE for publication of technical ideas that have not advanced, as yet, to the point where they warrant publication as a Proceedings paper in a *Journal*, the publication of Technical Notes was authorized by the Board of Direction on October 16–18, 1967, under the following guidelines:

1. An original manuscript and two copies are to be submitted to the Manager of Technical and Professional Publications, ASCE, 345 East 47th Street, New York, N.Y., 10017, along with a request by the author that it be considered as a Technical Note.
2. The two copies will be sent to an appropriate Technical Division or Council for review.
3. If the Division or Council approves the contribution for publication, it shall be returned to Society Headquarters with appropriate comments.
4. The technical publications staff will prepare the material for use in the earliest possible issue of the *Journal*, after proper coordination with the author.
5. Each Technical Note is not to exceed 4 pages in the *Journal*. As an approximation, each full manuscript page of text, tables, or figures is the equivalent of one-half a *Journal* page.
6. The Technical Notes will be grouped in a special section of each *Journal*.
7. Information retrieval abstracts and key words will be unnecessary for Technical Notes.
8. The final date on which a Discussion should reach the Society is given as a footnote with each Technical Note.
9. Technical Notes will not be included in *Transactions*.
10. Technical Notes will be included in ASCE's annual and cumulative subject and author indexes.

The manuscripts for Technical Notes must meet the following requirements:

1. Titles must have a length not exceeding 50 characters and spaces.
2. The author's full name, Society membership grade, and a footnote reference stating present employment must appear on the first page of the manuscript. Authors need not be Society members.
3. The manuscript is to be submitted as an original copy (with two duplicates) that is typed double-spaced on one side of 8-1/2-in. (220-mm) by 11-in. (280-mm) white bond paper.
4. All mathematics must be typewritten and special symbols must be properly identified. The letter symbols used must be defined where they first appear, in figures or text, and arranged alphabetically in an Appendix.—Notation.
5. Standard definitions and symbols must be used. Reference must be made to the lists published by the American National Standards Institute and to the *Authors' Guide to the Publications of ASCE*.
6. Tables must be typed double-spaced (an original ribbon copy and two duplicate copies) on one side of 8-1/2-in. (220-mm) by 11-in. (280-mm) paper. An explanation of each table must appear in the text.
7. Figures must be drawn in black ink on one side of 8-1/2-in. (220-mm) by 11-in. (280-mm) paper. Because figures will be reproduced with a width of between 3 in. (76 mm) to 4-1/2 in. (110 mm), the lettering must be large enough to be legible at this width. Photographs must be submitted as glossy prints. Explanations and descriptions must be made within the text for each figure.
8. References cited in text must be typed at the end of the Technical Note in alphabetical order in an Appendix.—References.
9. Dual units, i.e., U.S. Customary followed by SI (International System) units in parentheses, should be used throughout the paper.

RE-EXAMINATION OF NIKURADSE ROUGHNESS DATA

By William R. Brownlie,[1] A. M. ASCE

INTRODUCTION

Two sets of flow resistance data are commonly used in the evaluation of friction factors for pipes and open channels. The data compiled by Colebrook and White for commercial pipes were used by Moody to construct his well known friction factor diagram (3, Fig. 5.32). A similar diagram based on the data of Nikuradse (1) for sand-roughened pipes appears in most texts of fluid mechanics (2, Fig. 108 and 3, Fig. 5.31), however, with a much more limited range of relative roughness and Reynolds number than the Moody diagram. While the Colebrook and White data are appropriate for commercial pipe applications, the Nikuradse data, with its sand roughness, may be more applicable for problems involving open channels with uniform-sand beds for which grain friction factor is required. This note describes an inconsistency in the original presentation of some of the Nikuradse data and provides a Moody-type diagram with some engineering applications for a range of the data believed to be valid. The data are reviewed here because they appear in many classical texts of fluid mechanics for engineers (e.g., 2, 3).

ORIGINAL DATA

The experiments reported by Nikuradse were conducted using pipes with diameters of 2.474 cm, 4.94 cm, and 9.94 cm. Roughness was created by gluing uniform sands to the pipes. In all, five sands were used, with mean diameters ranging from 0.01 cm–0.16 cm, to give six values of relative roughness (grain diameter over pipe diameter). Uniformity of sand grains was created by sieving, resulting in a typical geometric standard deviation of 1.02 for the grain-size distributions. Measurements in the pipes were taken using an approach length of approximately 40 pipe diam.

The data has traditionally been presented graphically in two different forms following the original presentation of Nikuradse (1). In the Moody-type form, friction factor is plotted against Reynolds number on a log-log scale with a different curve and set of data points for each of the six values of relative roughness. In the alternate form, by transforming the plotting coordinates, the

[1]Grad. Research Asst., W. M. Keck Lab. of Hydr. and Water Resources, Calif. Inst. of Tech., Pasadena, Calif. 91125.

Note.—Discussion open until June 1, 1981. To extend the closing date one month, a written request must be filed with the Manager of Technical and Professional Publications, ASCE. Manuscript was submitted for review for possible publication on April 25, 1980. This paper is part of the Journal of the Hydraulics Division, Proceedings of the American Society of Civil Engineers, © ASCE, Vol. 107, HY1, January, 1981. ISSN 0044-796X/81/0001-0115/$01.00.

six curves are collapsed to one curve as in Fig. 1.

Fig. 1 shows data from 90 runs randomly selected from the 362 that are published. The figure also shows the Colebrook transition function upon which the Moody diagram is based. Since the equivalent sand roughness of the Colebrook and White data was calibrated to the Nikuradse data in the fully rough regime, the two curves converge to the same asymptote on the right side of Fig. 1.

An inconsistency in the original data presentation can be seen by comparing the two plot types (1, Figs. 9 and 11) with the data tables. The data in the tables cover the range of parameters shown in Fig. 1; however, all points plotted on the original diagram do not appear in the tables. Conversely, all of the data in the tables are not shown in the original diagram, but they do conform closely to the curve in Fig. 1. On the other hand, the Moody-type diagram shows data with Reynolds numbers as low as 500 whereas the lowest Reynolds

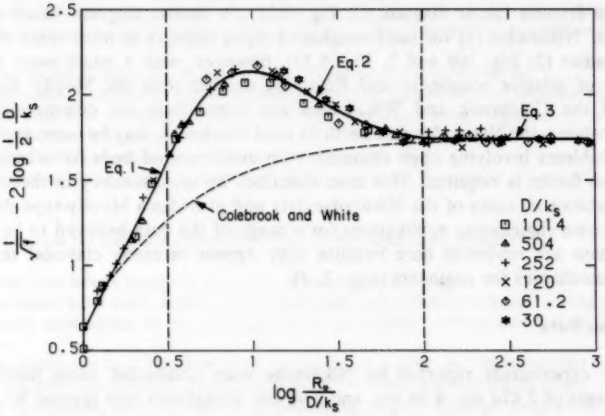

FIG. 1.—Comparison between Nikuradse Resistance Data and Colebrook and White Transition Function (about 25 percent of Published Data are Shown)

number given in the tables is 4,300. Furthermore, the two diagrams are consistent only for Reynolds numbers greater than 10,000. Finally, the unpublished data are somewhat suspect because they show a smooth transition from turbulent to laminar flow occurring at a Reynolds number of about 2,000, for all given values of relative roughness. Such a condition seems unlikely due to the nature of the physical transition.

Flow Resistance Chart

The Moody-type flow resistance chart shown in Fig. 2 was derived from the curve fitted to the data points in Fig. 1. Although there are inconsistencies in the original diagrams, the experiments appear to have been carefully conducted and the data in the tables are reasonable. Reynolds numbers lower than 10,000 have been omitted.

It is hoped that Fig. 2 will be a useful and accurate tool for engineers. The chart can be used for side-wall corrections as well as for separating total resistance into grain resistance and form resistance. For open channel flow calculations, pipe diameter D should be replaced by $4r$ in which r = hydraulic radius.

Fig. 2 is based on three equations which apply to different domains along the abscissa of Fig. 1:

$$\frac{1}{\sqrt{f}} - 2\log\frac{1}{2}\frac{D}{k_s} = 0.705 + 2\log\frac{R_* k_s}{D} \ldots \quad \text{for} \quad \log\frac{R_* k_s}{D} < 0.5 \ldots\ldots (1)$$

$$\frac{1}{\sqrt{f}} - 2\log\frac{1}{2}\frac{D}{k_s} = \sum_{i=0}^{6} A_i \left(\log\frac{R_* k_s}{D}\right)^i \ldots \quad \text{for} \quad 0.5 \le \log\frac{R_* k_s}{D} \le 2.0 \qquad (2)$$

$$\frac{1}{\sqrt{f}} - 2\log\frac{1}{2}\frac{D}{k_s} = 1.74 \ldots \quad \text{for} \quad \log\frac{R_* k_s}{D} > 2.0 \ldots\ldots\ldots\ldots (3)$$

in which $R_* = \sqrt{f/8}\, R$; f = friction factor; D = pipe diameter; k_s = the sand grain roughness (equivalent to grain diameter); R = Reynolds number;

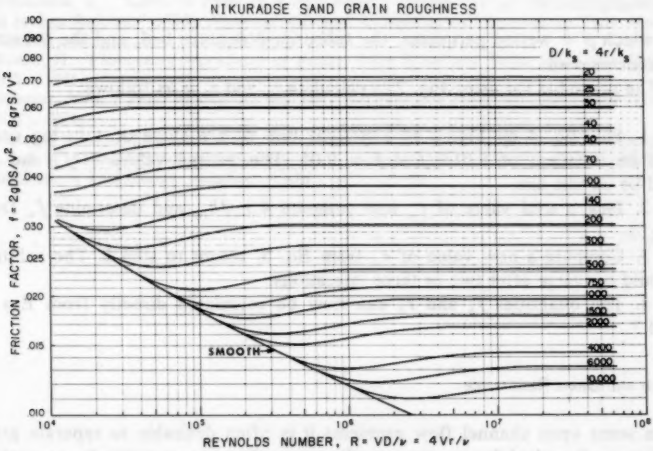

FIG. 2.—Friction Factor Diagram, for Pipes of Diameter, D, or Channels of Hydraulic Radius, r

and A_i = empirical constants. Eq. 1 is for smooth pipes, and relative roughness can be removed by factoring both sides of the equation. Eq. 2 was fitted by the writer to the transition data from the smooth to the rough regime, with the coefficients A_0 through A_6 defined as 1.3376, −4.3218, 19.454, −26.480, 16.509, −4.9407, 0.57864, respectively. Eq. 3 describes the fully rough regime where friction factor is a function of relative roughness only.

Side-Wall Correction

Fig. 2 can be used to perform a side-wall correction for flow at a given R, in flumes with a known friction factor, f, and roughness, k_s, using a procedure analogous to the smooth-wall procedure described by Vanoni and Brooks (4). From the derivation given in Ref. 4, the following equations can be obtained:

$$R_w = \frac{R}{f} f_w \quad \ldots \quad (4)$$

$$r_w = \frac{r}{f} f_w \quad \ldots \quad (5)$$

$$f_b = f + \frac{p_w}{p_b}(f - f_w) \quad \ldots \quad (6)$$

$$r_b = \frac{r}{f} f_b \quad \ldots \quad (7)$$

in which p = wetted perimeter; the subscript b denotes bed, and the subscript w denotes wall.

The procedue for using Fig. 2 to calculate r_w and r_b is as follows:

1. Plot Eq. 4 on Fig. 2 as a straight line with a slope of 1 in log units, and an intercept of $0.01R/f$ at $f = 0.01$. The desired values of f_w and R_w will lie on this line.
2. Pick a trial value of r_w and compute $4\, r_w/k_{sw}$ and determine f_w from Fig. 2.
3. Compute a new value of r_w from Eq. 5, return to step 2. The solution should converge after two or three interations.
4. The quantities f_b and r_b can now be calculated directly from Eqs. 6 and 7.

Form and Grain Resistance

In some open channel flow problems it is often desirable to separate grain resistance from bed-form resistance. Two procedures are possible for separating the bed shear stress into its two components. Either the slope may be broken into components or the hydraulic radius of the bed may be broken into components. Vanoni and Brooks (4) have presented a graphical solution of the Einstein-Barbarosa approach which divides the hydraulic radius into two components. Fig. 2 could also be used to carry out this procedure by applying a technique similar to that of the side-wall correction procedure just described. However, a more convenient and perhaps more conceptually reasonable approach is to divide the energy slope into two components.

The following equations can be used with Fig. 2 to perform this procedure:

$$S' = \frac{f'_b V^2}{8 g r_b} \quad \text{(8)}$$

$$S'' = S - S' \quad \text{(9)}$$

$$f''_b = f - f'_b \quad \text{(10)}$$

in which S' and f'_b = the energy slope and bed friction factor, respectively, resulting from grain resistance; and S'' and f''_b = those quantities resulting from form drag, for a flow with a given velocity and bed hydraulic radius. The quantity f'_b can be determined directly from Fig. 2, given R_b and $4r_b/k_s$. The remaining quantities can be calculated from Eqs. 8, 9, and 10.

Acknowledgements

The preparation of this note was suggested by Norman H. Brooks and based upon work supported by the National Science Foundation, under Grant CME 79-20311. Special thanks to A. Massengale.

Appendix.—References

1. Nikuradse, J., "Laws of Flow in Rough Pipes," (translation of "Stromungsgesetze in rauhen Rohren," 1933), *National Advisory Committee for Aeronautics Tech Memo 1292,* Washington, D.C., 1950, 62 pp.
2. Rouse, H., *Elementary Mechanics of Fluids,* John Wiley and Sons, Inc., New York, N.Y., 1946.
3. Streeter, V. L., *Fluid Mechanics,* 5th ed., McGraw-Hill Book Co., Inc., New York, N.Y., 1971.
4. Vanoni, V. A., and Brooks, N. H., "Laboratory Studies of the Roughness and Suspended Load of Alluvial Streams," *Sedimentation Laboratory Report No. E68,* California Institute of Technology, Pasadena, Calif., 1957, 121 pp.

River Bed Aggradation due to Overloading

By Subhash C. Jain,[1] M. ASCE

Introduction

The water and sediment discharges in natural streams evolved over geologic time are in "equilibrium" and produce no objectionable scour or deposition. However, many factors, both man made and natural, can contribute to the imbalance between the supply of sediment to and the sediment transport capacity of a river, which in turn can lead to degradation/aggradation along the river reaches. The channel bed along some reaches of the Missouri River has been progressively degrading and aggrading since about 1960 (3). Reliable, quantitative estimates of the future rate and extent of long-term degradation and aggradation would be invaluable to river-management planning.

Aggradation in a stream due to increase in sediment load was studied analytically and experimentally and recently reported by Soni et al. (4). When their analytical results failed to agree with their experimental data, they empirically modified the value of the aggradation coefficient to achieve conformity between predicted and measured bed profiles. The nonconformity between the analytical and experimental results were attributed to the several simplifications made in the analysis. The writer, in a discussion of their paper (2), pointed out an error in the boundary condition of their analytical model. This paper presents the analytical solution of the aggradation problem for a more appropriate boundary condition. The analytical results are compared with the laboratory experimental data of Soni et al. (4).

Theoretical Analysis

Consider a uniform flow with a mean flow velocity U_0 and mean flow depth h_0 in a wide rectangular alluvial channel as shown in Fig. 1. The equilibrium sediment transport "rate" under the uniform flow condition is equal to G_e and the bed slope is S_0. Let the sediment supply rate at a section $x = 0$ be increased by a constant rate ΔG. The bed level for $x \geq 0$ will rise with time due to increase in the sediment load. The differential equation for the bed level obtained by Soni et al. (4) is

[1]Assoc. Prof. in Energy Div., and Research Engr. in Inst. of Hydr. Research, The University of Iowa, Iowa City, Iowa 52242.

Note.—Discussion open until June 1, 1981. To extend the closing date one month, a written request must be filed with the Manager of Technical and Professional Publications, ASCE. Manuscript was submitted for review for possible publication on May 8, 1980. This paper is part of the Journal of the Hydraulics Division, Proceedings of the American Society of Civil Engineers, © ASCE, Vol. 107, No. HY1, January, 1981. ISSN 0044-796X/81/0001-0120/$01.00.

$$\frac{\partial z}{\partial t} = K_0 \frac{\partial^2 z}{\partial x^2} \qquad (1)$$

in which the aggradation coefficient K_0 is given by

$$K_0 = \frac{1}{3} \frac{b\, G_e}{S_0(1 - \lambda)} \qquad (2)$$

In Eqs. 1 and 2 z = depth of deposition at time t at a distance x from the origin; λ = the porosity of the sediment; and b = the exponent in the sediment transport law:

$$G = a\, U^b \qquad (3)$$

in which G = total sediment transport rate at any cross section in absolute volume per unit width of the channel; V = mean flow velocity; and a = constant.

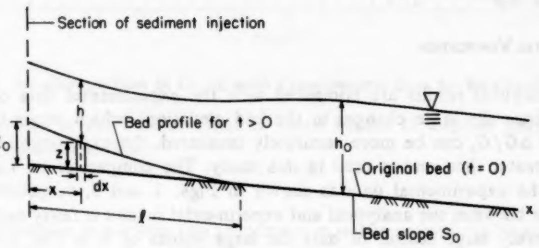

FIG. 1.—Definition Sketch

The initial and boundary conditions for the aggradation problem under consideration are

$$z(x, 0) = 0 \quad \text{for} \quad x \geq 0 \qquad (4)$$

$$-K_0 \frac{\partial z}{\partial x}(0, t) = \frac{\Delta G}{(1 - \lambda)} \quad \text{for} \quad t > 0 \qquad (5)$$

in which ΔG = the increased volumetric sediment supply rate per unit width. The explanation for the boundary condition (Eq. 5) is given in Appendix I. The forms of the governing equation (Eq. 1) and the initial and boundary conditions (Eqs. 4 and 5) are exactly similar to those of heat conduction in a semi-infinite solid with a constant heat flux across the surface. The solution of the differential equation for the prescribed initial and boundary conditions is (1):

$$z = \frac{2\Delta G}{K_0(1 - \lambda)} \left[\left(\frac{K_0 t}{\pi} \right)^{1/2} \exp\left(-\frac{x^2}{4K_0 t} \right) - \frac{x}{2} \operatorname{erfc}\left(\frac{x}{2\sqrt{K_0 t}} \right) \right] \qquad (6)$$

$$\text{in which} \quad \operatorname{erfc}(\eta) = \frac{2}{\sqrt{\pi}} \int_\eta^\infty e^{-u^2}\, du \qquad (7)$$

The bed elevation at $x = 0$ is given by

$$z_0 = \frac{2\Delta G}{K_0(1-\lambda)}\left(\frac{K_0 t}{\pi}\right)^{1/2} \quad \ldots\ldots\ldots\ldots\ldots\ldots\ldots\ldots\ldots\ldots\ldots\ldots\ldots\ldots (8)$$

which can be rearranged in nondimensional form as

$$\frac{z_0}{\sqrt{K_0 t}} = \frac{2}{\sqrt{\pi}}\frac{\Delta G}{K_0(1-\lambda)} \quad \ldots\ldots\ldots\ldots\ldots\ldots\ldots\ldots\ldots\ldots\ldots\ldots\ldots\ldots (9)$$

The bed profile in the nondimensional form is given by

$$\frac{z}{z_0} = [e^{-\eta^2} - \eta\sqrt{\pi}\ \mathrm{erfc}(\eta)] \quad \ldots\ldots\ldots\ldots\ldots\ldots\ldots\ldots\ldots\ldots\ldots\ldots\ldots\ldots (10)$$

in which $\eta = x/(2\sqrt{K_0 t})$.

Furthermore, the length of aggradation, l, on the assumption that aggradation ends where $z/z_0 = 0.01$ (from Eq. 10) is given by

$$l = 3.20\sqrt{K_0 t} \quad \ldots\ldots\ldots\ldots\ldots\ldots\ldots\ldots\ldots\ldots\ldots\ldots\ldots\ldots\ldots\ldots (11)$$

Experimental Verification

The analytical results are compared with the experimental data of Soni et al. (4). Since the large changes in the bed elevations which occur for higher values of $\Delta G/G_e$ can be more accurately measured, the experimental data for $\Delta G/G_e$ greater than one is used in this study. The comparison of Eqs. 9 and 10 with the experimental data is shown in Figs. 2 and 3, respectively. The agreement between the analytical and experimental results is fairly satisfactory. The relatively large scatter of data for large values of η in Fig. 3 is due to

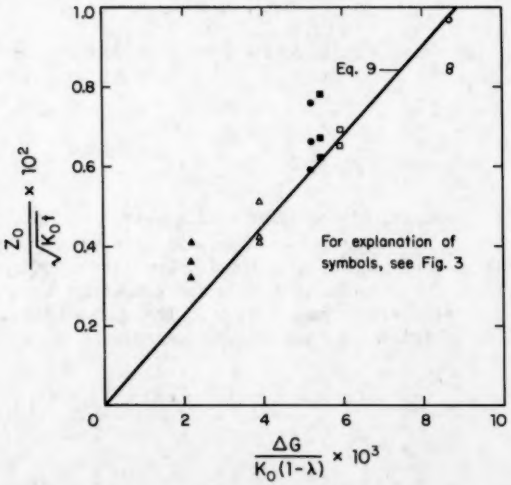

FIG. 2.—Comparison of Eq. 9 with Available Experimental Data

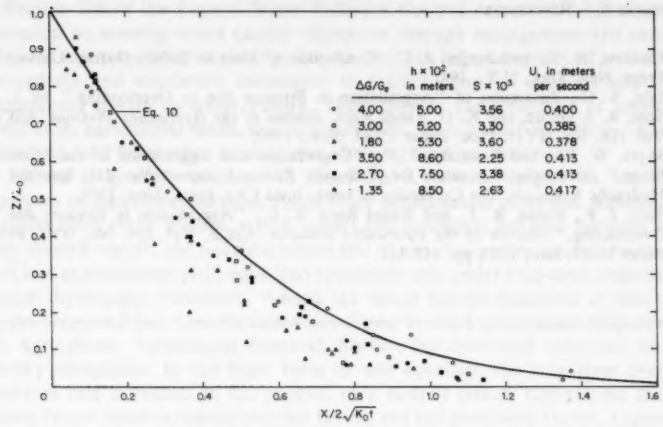

FIG. 3.—Comparison of Eq. 10 with Experimental Data for Bed Profiles

possible errors in the measurement of small depths of deposit near the end of the aggradation profile.

Conclusions

The aggradation in a stream due to increase in sediment load can be analytically determined from Eqs. 9 and 10. The analytical results are in agreement with the available experimental data.

Appendix I.—Boundary Condition

The volume of sediment between the initial bed profile ($t = 0$) and the bed profile at time t (see Fig. 1) must be equal to the volume of additional sediment supplied at $x = 0$ during time t, i.e.:

$$\Delta G t = \int_0^\infty (1 - \lambda)\, z\, dx \quad \ldots \quad (12)$$

The time derivative of Eq. 12 yields

$$\Delta G = (1 - \lambda) \int_0^\infty \frac{\partial z}{\partial t}\, dx \quad \ldots \quad (13)$$

Substitution for $(\partial z)/(\partial t)$ from Eq. 1 and integration gives

$$\Delta G = (1 - \lambda)\, K_0 \left(\frac{\partial z}{\partial x}\right)_0^\infty \quad \ldots \quad (14)$$

Eq. 14 reduces to Eq. 5 since

$$\frac{\partial z}{\partial x}(\infty, t) = 0$$

Appendix II.—References

1. Carslaw, H. S., and Jaeger, J. C., *Conduction of Heat in Solids*, Oxford University Press, New York, N.Y., 1947.
2. Jain, S. C., discussion of "Aggradation in Streams due to Overloading," by J. P. Soni, R. J. Garde, and K. G. Ranga Raju, *Journal of the Hydraulics Division*, ASCE, Vol. 106, No. HY11, Proc. Paper 15784, Nov., 1980.
3. Sayre, W. W., and Kennedy, J. F., "Degradation and Aggradation of the Missouri River," *International Institute for Hydraulic Research Report No. 215*, Institute of Hydraulic Research, The University of Iowa, Iowa City, Iowa, June, 1978.
4. Soni, J. P., Garde, R. J., and Ranga Raju, K. G., "Aggradation in Streams due to Overloading," *Journal of the Hydraulics Division*, ASCE, Vol. 106, No. HY1, Proc. Paper 15147, Jan., 1980, pp. 117–132.

Sediment Yield from Cultivated Lands: Selected Bibliography

By Frank D. Masch,[1] Michael A. Ports,[2] Members, ASCE, and A. R. Robinson,[3] F. ASCE

Introduction

Quantitative estimates of sediment yield from all sources of uncontrolled erosion in the United States have been cited at rates varying from 500,000,000 tons to over four billion tons annually. Although there are wide variations in estimates attributable to individual sources, there is unanimity in the recognition that continued uncontrolled erosion produces serious environmental problems in downstream rivers and reservoirs and in other areas where the sediments are deposited. Ultimately, eroded sediments use up the capacity of reservoirs, lakes, and ponds, restrict streams and drainageways, reduce crop yields, adversely affect aquatic and terrestrial ecosystems, and reduce recreational and consumptive use of waters through increased turbidity and increased treatment and removal costs. Sediments also act directly as pollutants by themselves and when they transport sorbed mineral nutrients, pesticides, herbicides, and pathogenic organisms and viruses.

[1]Stottler Stagg and Assoc., Architects Engineers Planners Inc., 4538 Centerview Drive, Suite 151, San Antonio, Tex. 78228.
[2]Federal Energy Regulatory Commission, Washington, D.C.
[3]Consulting Engr., Laurel, Md.

Note.—Discussion open until June 1, 1981. To extend the closing date one month, a written request must be filed with the Manager of Technical and Professional Publications, ASCE. Manuscript was submitted for review for possible publication on July 8, 1980. This paper is part of the Journal of the Hydraulics Division, Proceedings of the American Society of Civil Engineers, © ASCE, Vol. 107, No. HY1, January, 1981. ISSN 0044-796X/81/0001-0124/$01.00.

Section 208 of the Federal Water Pollution Control Act of 1972 has focused attention on meeting water quality objectives through management and control of point and nonpoint sources of pollution. This has led to a variety of evaluation procedures and simulation techniques to predict nonpoint loadings and their subsequent effects on water quality. These include the prediction of sediment yield from agricultural lands, construction sites, silvicultural operations, mining activities, and from other existing and changing land use practices.

Efforts to quantify sediment in runoff have centered largely on statistical analyses of measured sediment yields from experimental plots and watersheds. Results from these studies, which reflect the combined linkages between land use, rainfall-runoff, and soil detachment and transport are often used to determine soil loss and sediment yield equations applicable only under long-term, reasonably steady hydrologic conditions. Among the better known equations of this type is the Universal Soil-Loss Equation developed by the United States Department of Agriculture, Agricultural Research Service for cultivated soils east of the Rocky Mountains. In the basic form of this equation, the long term average soil-loss rate is related to the product of a rainfall factor, topographic factor, cover factor, erosion control practice factor, and soil erodibility factor. Typically, when used to predict nonpoint loadings, the Universal Soil Loss Equation times a sediment delivery ratio is used to estimate the sediment load or yield, and source loadings for various pollutants are then generally assumed proportional to the sediment load. By computing these rates over a period of time, pollutagraphs or histographs of various water quality constituents are determined. However broad or detailed the output from such nonpoint load generators, the estimates remain limited by the assumptions and conditions for which the sediment yield equation was developed. However, recent progress in sediment yield modeling has improved predictions and has added some deterministic predictors to the previously empirical relationships.

It is recognized that a variety of constraints for both designated and non-designated areawide waste treatment management studies often precluded more than a cursory analysis of sediment runoff from agricultural and cultivated lands. Still, the environmental effect of erosion and sediment runoff is potentially very significant. Fortunately, Section 208 planning is a continuing process and opportunities for improved analysis should exist. For this reason, the American Society of Civil Engineers Sedimentation Committee of the Hydraulics Division believes it is desirable to make available sources of more recent information from which improved predictors of sediment yield from agricultural lands can be developed. To assist in the dissemination of this information, a bibliography of selected references has been compiled on behalf of the Sedimentation Committee.

Appendix.—Bibliography

"Soil Erosion and Sedimentation," *Proceedings of the National Symposium on Soil Erosion and Sedimentation by Water*, American Society of Agricultural Engineers Publication 4-77, American Society of Agricultural Engineers, St. Joseph, Mich., 1977.

American Society of Civil Engineers, *Sedimentation Engineering, Manual No. 54*, American Society of Agricultural Engineers Manual and Report on Engineering Practice, American Society of Civil Engineers, 1975.

Bennett, H. H., *Soil Conservation,* McGraw-Hill Book Co., Inc., New York, N.Y., 1939.

Blakely, B. D., Coyle, J. J., and Steel, J. G., "Erosion on Cultivated Land," *The Year Book of Agriculture,* United States Department of Agriculture, Washington, D.C., 1957, pp. 290–307.

Robinson, A. R., "Relationship Between Soil Erosion and Sediment Delivery," Erosion and Solid Matter Transport in Inland Waters. Paris, France Symposium IAHS-AISH, Publication No. 122, 1977.

"Soil Erosion: Prediction and Control," Soil Conservation Society of America, Ankeny, Iowa, 1977.

"Universal Soil Loss Equation: Past, Present, and Future," *Soil Science Society of America Special Publication No. 8,* Soil Science Society of America, Madison, Wisc., 1979.

Stewart, B. A., Wischmeier, W. J., Woolhiser, D. A., Caro, J. H., and Frere, M. H., "Control of Water Pollution from Cropland," "A Manual for Guideline Development," Vol. I; also "An Overview," Vol. II, *ARS-H-5-1* and *2,* United States Government Printing Office, Washington, D.C., 1975.

Proceedings of the Federal Interagency Sedimentation Conference, Misc. Publ. 970, United States Department of Agriculture, Agricultural Research Service, Washington, D.C., 1975.

"Present and Prospective Technology for Predicting Sediment Yield and Sources," *ARS-S-40,* United States Department of Agriculture, Agricultural Research Service, Washington, D.C., 1975.

"Sedimentation," *National Engineering Handbook,* Section 3, United States Department of Agriculture, Soil Conservation Service, Washington, D.C., 1971.

"Procedure for Computing Sheet and Rill Erosion for Project Areas," *SCS TR No. 51,* United States Department of Agriculture, Soil Conservation Service, Washington, D.C., 1975.

"Guide for Predicting Rainfall-Erosion Losses from Agricultural Land in Maryland and Delaware," *Conservation Planning 1-78,* United States Department of Agriculture, Soil Conservation Service, College Park, Md., 1978.

Proceedings of the Third Federal Interagency Sedimentation Conference, PB-245 100, Sedimentation Committee, Water Resources Council, Washington, D.C., 1976.

Wischmeier, W. H., and Smith, D. D., "Predicting Rainfall Erosion Losses, A Guide to Conservation Planning," United States Department of Agriculture, *Agriculture Handbook No. 537,* Washington, D.C., 1978.

Flow Investigations in Two Pumping Pits

By G. K. Nathan[1]

Introduction

Model studies with pumping pits to predict the possible flow conditions in a prototype have become increasingly important due to use of more pumps in a limited size pumping pit and high flow rate pumps. Tullis (5) has considered in detail the associated hydraulic problems in model studies, and stressed the need for systematic studies and publication of such results. The hydraulic problems that affect the performance of a pump are surface and submerged vortices, air entrainment in the inflow, and swirl and asymmetric flow in pump intakes.

In this study, relationships between hydraulic problems and various dimensionless groupings, and Reynolds number effect on the determination of swirl angle and the axial velocity distribution in the pump intake are investigated with two simple pumping pits. Also, a quantitative method is attempted to determine the best configuration of one of the pumping pits.

Theoretical Considerations

The performance of a pump represented by its efficiency (η) is affected by the adverse effects in a pumping pit (2) and this efficiency will be different from the design efficiency (η_d) of a pump. If an ideal pumping pit is designed, then both efficiencies would be the same and the ratio (η/η_d) leads to unity. Using dimensional analysis and taking note of the numbers that have been identified to affect the hydraulic problems in a pumping pit, the following expressions can be obtained:

$$\left(\frac{\eta}{\eta_d}\right) = f\left(\frac{\rho V D}{\mu}, \frac{V}{\sqrt{gD}}, \frac{\mu V}{\tau}, \frac{L_1}{D}, \frac{L_2}{D}, \ldots \frac{L_n}{D}\right) \quad \ldots\ldots\ldots\ldots\ldots (1)$$

in which D = a diameter of pump intake; g = acceleration due to gravity; $L_1 \ldots L_n$ = linear dimensions of pumping pit; V = velocity of inflow; μ = kinematic viscosity; ρ = density; and τ = surface tension of fluid.

Therefore, for complete similarity of a geometrically similar model, all three numbers have to be satisfied. The Froude number can be satisfied quite easily,

[1]Sr. Lect., Faculty of Engrg., Univ. of Singapore, Kent Ridge, Singapore 0511, Republic of Singapore.

Note.—Discussion open until June 1, 1981. To extend the closing date one month, a written request must be filed with the Manager of Technical and Professional Publications, ASCE. Manuscript was submitted for review for possible publication on April 8, 1980. This paper is part of the Journal of the Hydraulics Division, Proceedings of the American Society of Civil Engineers, © ASCE, Vol. 107, No. HY1, January, 1981. ISSN 0044-796X/81/0001-0127/$01.00.

and when $(\mu V/\tau)_m = (\mu V/\tau)_p$, "equal-velocity" simulation is obtained if the same fluid is used for the model (m) and the prototype (p) (1). It is rather difficult to have Reynolds number simulation and thus a critical value of 5×10^5 is chosen to simulate flow conditions at the pump intake.

Pumping Pits and Experimental Setup

Details of pumping pits are given in Fig. 1 where continuous lines show the original pumping pit and broken lines the modifications. The dry dock pumping pit (DDP-pit) has one vertical axis and a mixed flow pump of capacity 474.9 gal/s (1,800 L/s). The return activated sludge pumping pit (RASP-pit) has two identical vertical axis, axial flow pumps of capacity 105.5 gal/s (400 L/s) each, and is symmetrically placed.

Model scale ratios of 1:8.750 and 1:4875 were selected for DDP-pit and RASP-pit respectively, taking into consideration the availability of standard pipes and

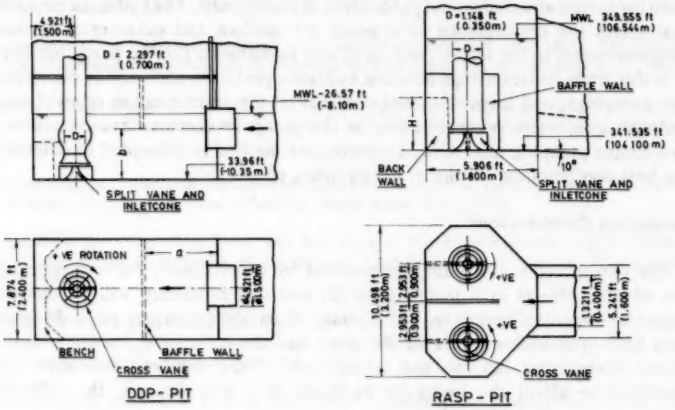

FIG. 1.—Line Diagram of Pumping Pits, Broken Line Showing Modifications to Original Pumping Pits

suitability of a minimum model size for simulation of flows conditions at different modelling laws. Geometrically similar models were made with plywood and transparent material (perspex) was used for walls and pipe of 3.15 in. (80 mm) diam to visualize the flow within the pumping pits.

A standard experimental setup (2) was used. It had a pair of antiswirl vanes and a constant speed pump. The swirl near the pump intake was measured using a vortometer (3) and it can be shown that $\tan \phi = U/V_t$ in which ϕ = swirl angle; U = tip velocity; and V_t = mean axial velocity (4). Axial velocity profiles at the intake were measured using a log linear velocity rake.

Experimental Results and Analysis

Experiments were conducted with models of both pumping pits at flow rates

corresponding to Froude, "equal-velocity," and critical Reynolds number simulations and at intermediate values. Part of the investigation was flow visualization within the models using dyes and tufts, and the other part was determination of swirl angle with and without modifications. The acceptable configurations which had the best flow conditions were determined by the usual trial and error approach and in the case of the DDP-pit model. The best configuration was also found by determining the efficiency of the pump used in the model study. For the best configuration of pumping pits the velocity profiles were also determined. Different problems were identified with both models, the DDP-pit had air entrainment, surface undulation, and surface and submerged vortices, while the RASP-pit had high swirl angle and submerged vortices.

Flow Conditions and Swirl Angle.—In the DDP-pit, introduction of a bench reduced the strength of vortices and a baffle wall eliminated the vortices formed

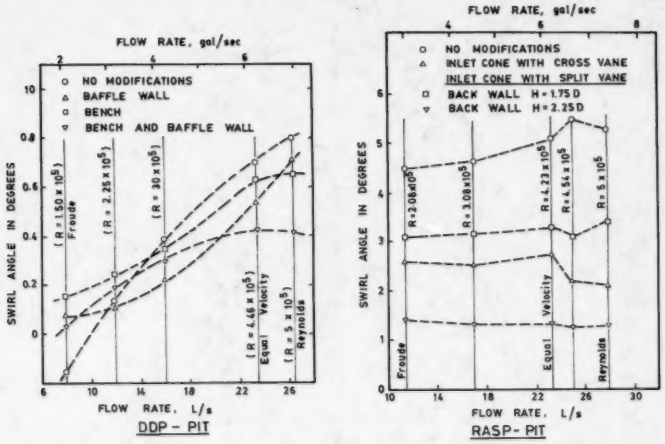

FIG. 2.—Relationship of Swirl Angle with Reynolds Number Variation

at the back wall corners; between the bellmouth and the pit invert a submerged vortex persisted which was eliminated by introducing an inlet cone with a split vane.

The RASP-pit had a high swirl angle which could have been reduced to a lower value using a cross vane within the bellmouth, but it was not acceptable to the user of pumps. Therefore different types of modifications such as back wall, cross vane at the pit invert, etc. were attempted. Finally an inlet cone with a split vane and a back wall reduced the swirl angle to within an acceptable limit. The inlet cone also eliminated the submerged vortices between the bellmouth and the pit invert. As the pumps were symmetrically placed, the same values for swirl angle and velocity profiles were obtained but the direction was mirror symmetric as shown in Fig. 1.

In both pumping pits the swirl angle increased with the Reynolds number

but the variation is small. Fig. 2 shows that the modifications on a DDP-pit have very little effect on the swirl angle, but substantial difference is seen with the RASP-pit. This shows that the cross vane within the bellmouth is very effective in controlling the swirl angle in the pump intake. The swirl angle obtained for the final configuration of models is less than 2°, which was a stipulated requirement of the pump manufacturer.

Velocity Profiles at Intake.—The design performance of a pump could not be met and would be affected by the type of velocity profiles at the inlet of the impeller. The velocity profiles were determined for the best configuration of both pumping pits at flow rates corresponding to critical Reynolds number

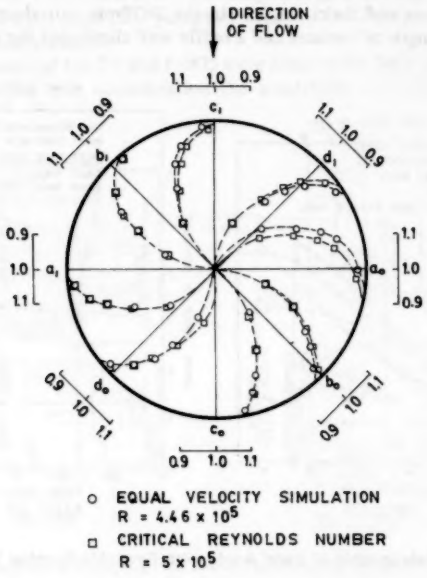

FIG. 3.—Normalized Velocity Profiles at Dry Dock Pump Intake Determined at Different Vertical Planes

and "equal-velocity" simulation. Fig. 3 shows the normalized velocity distribution with respect to the center velocity of the DDP-intake which is almost the same. Similar results were obtained with the RASP-intake. Therefore it can be concluded that the critical Reynolds number satisfactorily simulates the velocity profiles of the prototype. Also, velocity profiles would depend on the size of the intake and thus the model ratio.

Efficiency as a Parameter.—The best configuration is usually determined subjectively by observing the flow conditions. In this investigation for various positions of the baffle wall, the efficiency of the pump used in the model study of the DDP-pit was determined at "equal-velocity" simulation. Fig. 4

shows that the relative efficiency (η/η_d) has an optimum position for the baffle wall, which incidently coincides with the position determined by the trial and error method. The variation of efficiency of the pump used in the model study is mainly caused by the air entrainment in the inflow.

Surface and Submerged Vortices.—At a flow rate corresponding to Froude simulation, surface circulation around the suction inlet(s) were noticed in both pits. When the flow rate was increased towards the "equal-velocity" simulation, dimples which were formed in the RASP-pit remained as weak vortices, while those in the DDP-pit became strong intermittent air entraining vortices. Showing that when the velocity in the model pit approaches that in the prototype, the intensity of vortices adversely affects the performance of only one pit.

Submerged vortices are detectable at Froude simulation using a dye, but it can be seen in most cases without any aid if the experiment is conducted at a high flow rate. Velocity profile measurement also leads to detection of the

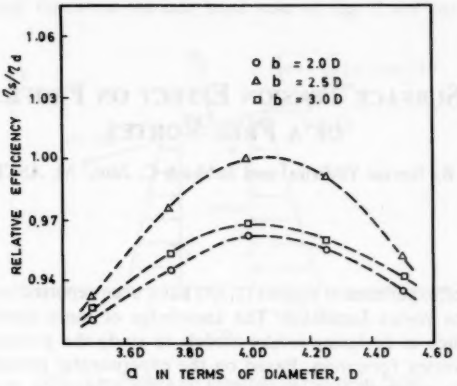

FIG. 4.—Variation of Relative Efficiency of Pump Determined at Different Positions of Baffle Wall in Dry Dock Pumping Pit

submerged vortex which causes localized distortion of the velocity profiles in the pump intake.

Conclusions

The swirl angle measurement is only slightly affected by the variation of the Reynolds number, and the critical Reynolds number of 5×10^5 gives satisfactory simulation of the velocity profiles at the pump intake. The model pump efficiency may be used as a parameter to determine the best modification quantitatively. From the model investigation it appears that it is preferable to conduct the study at different flow rates corresponding to Froude "equal-velocity" and critical Reynolds number simulations which would lead to a better assessment of the performance of a prototype pump pit.

Appendix.—References

1. Kenn, M. T., and Zanker, K. T., "Aspects of Similarity for Air Entraining Water Flows," *Nature*, Vol. 213, No. 5071, Jan., 1967, pp. 59–60.
2. Patterson, I. S., and Campbell, G., "Pumps Intake Design Investigations," *Proceedings of the Institution of Mechanical Engineers*, Vol. 182, Part 3M, 1967–1968, pp. 1–10.
3. Prosser, M. J., "The Hydraulic Design of Pump Sumps and Intakes," British Hydromechanics Research Association, Cranfield, England, July, 1977, pp. 40–41.
4. Siekmann, H., and Holzhuter, E., "Pump Intake Design of High Specific Speed Pumps," Klern, Schanzhn and Becker AG, Frankenthal, West Germany, Oct., 1973, pp. 2–8.
5. Tullis, J. P., "Modeling in Design of Pumping Pits," *Journal of the Hydraulics Division*, ASCE, Vol. 105, No. HY9, Proc. Paper 14812, Sept., 1979, pp. 1053–1063.

Surface Tension Effect on Profile of a Free Vortex

By Nevzat Yildirim[1] and Subhash C. Jain,[2] M. ASCE

Introduction

A number of experimental studies (1,3,4) have been reported on the similitude in free-surface vortex formation. The knowledge of these similitude relations is of importance in designing intake models to study the prototype conditions that lead to vortex formation. Based on the experimental results (1,3,5) it has been generally accepted that the surface tension effects on the formation of the free surface vortex are not important in most test systems. In this technical note, the effect of the surface tension on the surface profile of a free vortex is examined analytically.

Governing Equations

Consider a differential element HEFG of a rotating fluid with the forces acting on it, as shown in Fig. 1. Equations of motion for the differential element in the z and r directions, respectively, can be written as

[1]Grad. Student, Iowa Inst. of Hydr. Research, The Univ. of Iowa, Iowa City, Iowa 52242.
[2]Research Engr. Iowa Inst. of Hydr. Research, The Univ. of Iowa, Iowa City, Iowa 52242.

Note.—Discussion open until June 1, 1981. To extend the closing date one month, a written request must be filed with the Manager of Technical and Professional Publications, ASCE. Manuscript was submitted for review for possible publication on July 8, 1980. This paper is part of the Journal of the Hydraulics Division, Proceedings of the American Society of Civil Engineers, © ASCE, Vol. 107, No. HY1, January, 1981. ISSN 0044-796X/81/0001-0132/$01.00.

$$\sigma \frac{d}{dr}\,[r \sin \psi] - \rho g z r + (p - p_o) r = 0 \quad \ldots\ldots\ldots\ldots\ldots\ldots\ldots\ldots (1)$$

and $$-\frac{1}{2}\frac{d}{dr}\,[(2p - \rho g z) z r] + \frac{1}{2}(2p - \rho g z) z + p_o r \frac{dz}{dr}$$

$$+ \left\{ \sigma \frac{d}{dr}\,[r \cos \psi] - \sigma \sec \psi \right\} = -\frac{\Gamma^2}{4\pi^2 r^2} \rho z \quad \ldots\ldots\ldots\ldots\ldots\ldots\ldots\ldots (2)$$

in which σ = surface tension; p = pressure at the bottom of the element; p_o = atmospheric pressure; ρ = fluid density; g = acceleration due to gravity; ψ = surface angle; and Γ = circulation.

The various terms in Eq. 1 are the resultant force due to the surface tension, the weight of the element, and the resultant of the pressure forces acting on the free surface and the bottom of the element in the vertical direction. The first and second terms on the left hand side of Eq. 2 are the resultants of

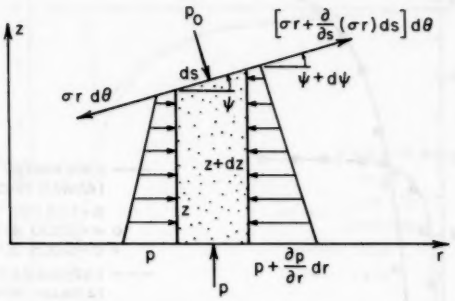

FIG. 1.—Forces on Element of Rotating Fluid

the pressure forces acting on the tangential faces and radial faces of the element, respectively. The third term is the pressure force due to atmospheric pressure acting on the free surface of the element, and the fourth term is the resultant force due to surface tension in the radial direction. The term on the right hand side is the product of the mass and the acceleration of the element. For the free vortex, the tangential velocity is assumed to be inversely proportional to the radial distance, r.

The elimination of $(p - p_o)$ from Eqs. 1 and 2 and some trigometric manipulations give

$$(\sigma r \cos^3 \psi) z''' + \sigma \cos^3 \psi (1 - 3r \cos^2 \psi\, z' z'') z'' - \rho g r z'$$

$$-\frac{\sigma}{r} \sin \psi + \frac{\rho \Gamma^2}{4\pi^2 r^2} = 0 \quad \ldots\ldots\ldots\ldots\ldots\ldots\ldots\ldots\ldots\ldots (3)$$

which after dividing by $\sigma r \cos^3 \psi$ and using the transformation $z = C - \xi$ reduces to

$$\xi''' + \frac{1}{r}\left[1 - \frac{3r\xi'\xi''}{(1+\xi'^2)}\right]\xi'' + \frac{\rho g}{\sigma}(1+\xi'^2)^{3/2}\xi' - \frac{\xi'}{r^2}(1+\xi'^2)$$

$$+ \frac{\rho g B}{\sigma r^3}(1+\xi'^2)^{3/2} = 0 \quad \ldots\ldots\ldots\ldots\ldots\ldots\ldots\ldots\ldots\ldots\ldots\ldots\ldots\ldots (4)$$

in which C = a constant; ξ = the drop in the free surface; $B = \Gamma^2/4\pi^2 g$; and primes represent derivatives with respect to r.

Eq. 4 is an ordinary, nonlinear, differential equation. An analytical solution of this equation is difficult to obtain. Therefore it was solved numerically using the Runga-Kutta method. For a third order equation, three boundary conditions are needed. At large r, the curvature of the free surface is small, and the

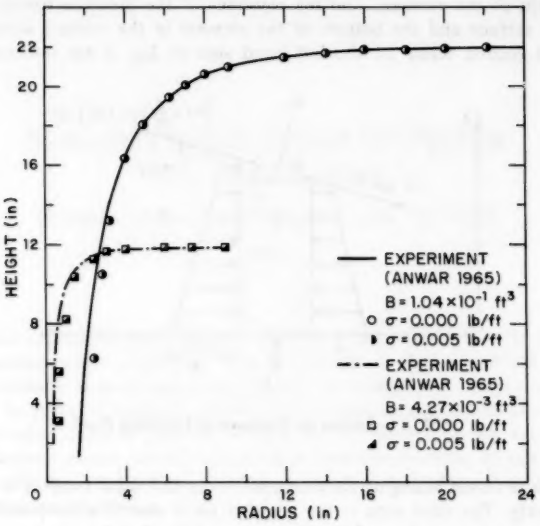

FIG. 2.—Measured and Calibrated Surface Profiles

effect of the surface tension can be neglected. Thus the boundary conditions at large r can be assumed to be the same as those without the surface tension.

For $\sigma = 0$, Eq. 3 reduces to

$$\xi' = -\frac{B}{r^3} \quad \ldots\ldots\ldots\ldots\ldots\ldots\ldots\ldots\ldots\ldots\ldots\ldots\ldots\ldots\ldots\ldots (5)$$

which on integration yields

$$\xi = \frac{B}{2r^2} \quad \ldots\ldots\ldots\ldots\ldots\ldots\ldots\ldots\ldots\ldots\ldots\ldots\ldots\ldots\ldots\ldots (6)$$

The boundary condition, $\xi = 0$ at $r \to \infty$ is used in integrating Eq. 6. The curvature at any point, r, can be obtained by differentiating Eq. 5 with respect to r such that

$$\xi'' = \frac{3B}{r^4} \qquad (7)$$

The following boundary conditions at $r = r_0$ are, therefore, used to solve Eq. 4:

$$\xi_0 = \frac{B}{2r_0^2}; \quad \xi_0' = -\frac{B}{r_0^3}; \quad \xi_0'' = \frac{3B}{r_0^4} \qquad (8)$$

The comparisons of the solution of Eqs. 4 and 6 with the free-vortex surface profiles measured by Anwar (2) are shown in Fig. 2. There is no effect of

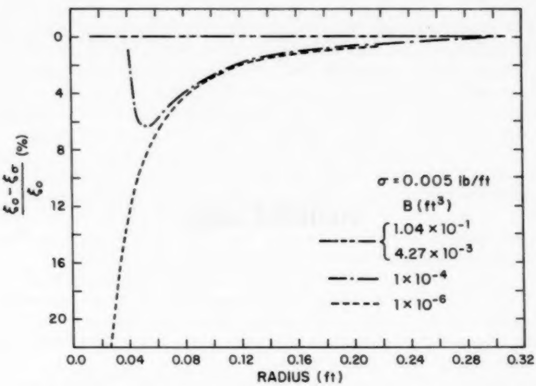

FIG. 3.—Change in Surface Drop due to Surface Tension

the surface tension on the surface profile for these values of circulation ($B = 0.104$ ft^3 and 0.00427 ft^3).

The variation of the normalized difference between the surface drops without surface tension (ξ_0) and with surface tension (ξ_σ) for several values of circulation is shown in Fig. 3. The effect of the surface tension for the low values of the circulation becomes significant, particularly near the core. The effect of the surface tension increases with the decrease in the circulation.

Conclusion

The effect of the surface tension on the free-vortex surface profile becomes significant at low values of the circulation and may give rise to some scale effects in model studies on vortex formation.

APPENDIX.—REFERENCES

1. Jain, A. K., Ranga Raju, K. G., and Garde, R. J., "Vortex Formation at Vertical Pipe Intakes," *Journal of the Hydraulic Division*, ASCE, Vol. 104, No. HY10, Proc. Paper 14104, Oct., 1978, pp. 1429–1445.
2. Anwar, H. O., "Flow in a Free Vortex," *Water Power*, Apr., 1965, pp. 153–161.
3. Daggett, L. L., and Keulegan, G. H., "Similitude in Free Surface Vortex Formations," *Journal of the Hydraulic Division*, ASCE, Vol. 100, No. HY11, Proc. Paper 10941, Nov. 1974, pp. 1565–1581.
4. Quick, M. C., "Scale Relationships Between Geometrically Similar Free Spiral Vortices," *Civil Engineering and Public Works Review*, Part I, Sept., 1962, Part II, Oct., 1962, p. 1319.
5. Yildirim, N., "Effect of a Surface Layer on Free Surface Vortex," thesis presented to the University of Iowa, at Iowa City, Iowa, in July, 1978, in partial fulfillment of the requirements for the degree of Master of Science.

JOURNAL OF THE
HYDRAULICS DIVISION

DISCUSSION

Note.—This paper is part of the Journal of the Hydraulics Division, Proceedings of the American Society of Civil Engineers, © ASCE, Vol. 107, No. HY1, January, 1981. ISSN 0044-796X/81/0001-0139/$01.00.

Discussions

Discussions may be submitted on any Proceedings paper or technical note published in any *Journal* or on any paper presented at any Specialty Conference or other meeting, the *Proceedings* of which have been published by ASCE. Discussion of a paper/technical note is open to anyone who has significant comments or questions regarding the content of the paper/technical note. Discussions are accepted for a period of 4 months following the date of publication of a paper/technical note and they should be sent to the Manager of Technical and Professional Publications, ASCE, 345 East 47th Street, New York, N.Y. 10017. The discussion period may be extended by a written request from a discusser.

The original and three copies of the Discussion should be submitted on 8-1/2-in. (220-mm) by 11-in. (280-mm) white bond paper, typed double-spaced with wide margins. The length of a Discussion is restricted to two *Journal* pages (about four typewritten double-spaced pages of manuscript including figures and tables); the editors will delete matter extraneous to the subject under discussion. If a Discussion is over two pages long it will be returned for shortening. All Discussions will be reviewed by the editors and the Division's or Council's Publications Committees. In some cases, Discussions will be returned to discussers for rewriting, or they may be encouraged to submit a paper or technical note rather than a Discussion.

Standards for Discussions are the same as those for Proceedings Papers. A Discussion is subject to rejection if it contains matter readily found elsewhere, advocates special interests, is carelessly prepared, controverts established fact, is purely speculative, introduces personalities, or is foreign to the purposes of the Society. All Discussions should be written in the third person, and the discusser should use the term "the writer" when referring to himself. The author of the original paper/technical note is referred to as "the author."

Discussions have a specific format. The title of the original paper/technical note appears at the top of the first page with a superscript that corresponds to a footnote indicating the month, year, author(s), and number of the original paper/technical note. The discusser's full name should be indicated below the title (see Discussions herein as an example) together with his ASCE membership grade (if applicable).

The discusser's title, company affiliation, and business address should appear on the first page of the manuscript, along with the *Proceedings* paper number of the original paper/technical note, the date and name of the *Journal* in which it appeared, and the original author's name.

Note that the discusser's identification footnote should follow consecutively from the original paper/technical note. If the paper/technical note under discussion contained footnote numbers 1 and 2, the first Discussion would begin with footnote 3, and subsequent Discussions would continue in sequence.

Figures supplied by the discusser should be designated by letters, starting with A. This also applies separately to tables and references. In referring to a figure, table, or reference that appeared in the original paper/technical note use the same number used in the original.

It is suggested that potential discussers request a copy of the *ASCE Authors' Guide to the Publications of ASCE* for more detailed information on preparation and submission of manuscripts.

DILUTION IN A VERTICAL ROUND BUOYANT JET[a]

Closure by Nikolas E. Kotsovinos[5]

The writer would like to thank the discussers for their interest in the paper and for their valuable comments. The writer thinks that high values of σ are probably caused by experimental errors due to: (1) Stratification of the ambient water; and (2) boundary or free surface effects. The writer's opinion is that accurate measurements in concentration, velocity and their turbulence characteristics are necessary to resolve questions about the details of the buoyant jet behavior in the plume region. However, it is worthy to point out that Eq. 6 (or Eq. 11) is based on various assumptions and simplifications and therefore even the most accurate experimental data would not have to follow the curve of Eq. 11 in Fig. 1.

Errata.—The following corrections should be made to the original paper:

Page 796, Eq. 4: Should read $\frac{\Delta\rho_M(x)}{\rho_\alpha} = \alpha\, T_M(x)$ instead of $\frac{\Delta\rho_M(x)}{P_0} = \alpha\, T_M(x)$

TWO-DIMENSIONAL BUBBLE PLUMES[b]

Errata

The writer is grateful to W. Hall C. Maxwell for drawing his attention to errors in the expressions for the Reynold's Number, R, and the Weber Number, W.

Errata.—The following corrections should be made in the original paper:

Page 142, Table 1, Col. 6: Should read "500, 49, 10.3, 8.2, and 21" instead of "300, 13.4, 5.2, 1.3, 0.62, and 2.6"

Page 146, paragraph 1 line 5: Should read "$R = \beta_o / g\nu$ is a form of Reynolds

---

[a]May, 1978, by Nikolas E. Kotsovinos (Proc. Paper 13723).

[5]Prof., School of Engrg., Democritus Univ. of Thrace, Xanthi, Greece.

[b]February, 1979, by David L. Wilkinson (Proc. Paper 14385).

[2]Visiting Lect. in Civ. Engrg., School of Engrg., Univ. of Canterbury, Christchurch 1, New Zealand.

number; and $W = \rho\beta_o^{4/3}/\sigma g$ is a form of Weber number." instead of "$R = \beta_o^{4/3}/g\nu$ is a form of Reynolds number; and $W = \rho\beta_o^2/\sigma g$ is a form of Weber number."

(These changes do not affect other calculations or conclusion in the paper.)

Hydraulic Resistance of Artificial Strip Roughness[a]

Closure by Donald W. Knight[6] and J. Alasdair Macdonald[7]

The writers are grateful to Eric Valentine, R. Fuentes, and J. J. Garcia, for their comments. The topic of nonuniform roughness is still clearly one of considerable interest. One of the issues raised by all the discussers concerns the shape of the roughness elements. In the writers' experiments, the roughness elements were carefully machined to a square cross section such that $b = k = 3$ mm, i.e., $b/k = 1$, in which b = width of element. The additional data presented by Valentine, which confirm the general usefulness of Eq. 11, have $b/k = 4$ and $\lambda/k = 8$. The data presented by Fuentes and Garcia have $b/k = 0.52$, 1.0, and 10.0 for varying λ/k. In both sets, the values of the coefficient, C_3, differ somewhat from those suggested by the writers. Evidence from experimental work in pipes with different transverse two-dimensional ribs (26) strongly suggests that the parameter b/k has an effect upon the roughness by as much as 25% or more. Generally the friction factor increases with decreasing b/k for given λ/k and h/k values. The variation of C_3 with λ/k should therefore reflect this as pointed out by Fuentes and Garcia. The writers' curve is of course only valid for $b/k = 1$. However, the trend indicated in Fig. 11, with the discussers' additional data, does not appear to be consistent. Although the data points for $b/k = 0.52$ are below those for $b/k = 1$, the data points for $b/k = 10$ appear to lie on the same curve as those for $b/k = 1$. The reasons for the discrepancy between the writers' and discussers' $b/k = 1$ results at large λ/k values is not apparent. The determination of C_3 as suggested by Sayre and Albertson is subject to a certain amount of error, but it is unlikely that all the discrepancy may be attributed to this cause. Until more data are published in a similar format it is unlikely that this problem will be resolved.

The comments about the inadequacies of current sidewall correction procedures are thoroughly endorsed by the writers. The boundary shear results undertaken by the writers (25) clearly demonstrate some shortcomings. The first writer is continuing his studies in nonuniform roughness by examining momentum transfer in symmetric and asymmetric sections using a wind tunnel and a flume. The boundary will be differentially roughened and it is hoped that this will shed some light on these basic correction procedures. It is a source of astonishment

[a]June, 1979, by Donald W. Knight and J. Alasdair Macdonald (Proc. Paper 14635).

[6]Lect., Civ. Engrg., Univ. of Birmingham, P.O. Box 363, Birmingham B15 2TT, England.
[7]Asst. Engr., Soar Div., Severn Trent Water Authority, Leicester, England.

that we know so little about shear distribution in simple cross sections considering the importance of open channel flow to so many problems. The writers are grateful to have Ref. 22 drawn to their attention. As regards viscous effects, apart from presenting the data in the form of Figs. 2 and 3, no further analysis was undertaken. Until a more rational sidewall correction procedure is formulated there seems to be little point in examining this issue due to the complex interaction of various parameters.

Appendix.—References

25. Knight, D. W., and Macdonald, J. A., "Open Channel Flow with Varying Bed Roughness," *Journal of the Hydraulics Division*, ASCE, Vol. 105, No. HY9, Proc. Paper 14839, Sept., 1979, pp. 1167–1183.
26. "Losses Caused by Friction in Straight Pipes with Systematic Roughness Elements," *ESDU Data Item No. 79014*, Engineering Sciences Data Unit, London, England, Sept., 1979, pp. 1–40.

Shear-Stress Distribution in Stable Channel Bends[a]

Closure by Mamdouh A. Nouh[4] and Ronald D. Townsend[5]

The writers thank Hooke for emphasizing the role of sediment transport rate over the entire bend in shaping the bed topography. The contention that the shape of any stable channel is a consequence of the balancing of the prevailing shear stress and the sediment transport rate is correct.

The important fact, however, is that for flow through bends, secondary circulation is an intrinsic feature and is accompanied by and concurrent with asymmetry of velocity and shear distribution. Interestingly for flow through rigid boundary laboratory channel bends (3), high shear-stress zones along the inner bank at entry shifting to the outer bank at exit occur with the development of a pronounced dead (decelerating) water zone. Because in this instance no point bar exists along the down-valley bank nor scour hole along the up-valley bank, the suggestion that the velocity gradient (and consequently bed shear-stress) is higher or lower consequent to smaller or greater depth of flow is not valid.

The locus of the bed shear maxima, however, is associated with the path of the longstream high velocity filament which has a characteristic swing from the inner bank to the outer bank (3,11). This has also been observed for highly curvilinear and accelerating flow through end-dump constrictions (12,13).

The writers agree with the discusser that more detailed studies to assess the role of the secondary flow in a bend in shaping the local channel geometry (or not?) must be undertaken. In this context it is perhaps worth noting that

---

[a]October, 1979, by Mamdouh A. Nouh and Ronald D. Townsend (Proc. Paper 14898).
[4]Post-doctoral Student, Dept. of Civ. Engrg., Univ. of Calgary, Calgary, Alberta, Canada.
[5]Prof., Dept. of Civ. Engrg., Univ. of Ottawa, Ottawa, Ontario, Canada K1N 9B4.

recent analytical approaches to the problem (1,8) employ the radial velocity component to arrive at the steady-state transverse bed profile.

APPENDIX.—REFERENCES

11. Bathurst, J. C., Thorne, C. R., and Hey, R. D., "Secondary Flow and Shear Stress at River Bends," *Journal of the Hydraulics Division*, ASCE, Vol. 105, No. HY10, Proc. Paper 14906, Oct., 1979, pp. 1277–1295.
12. Das, B. P., "Stability of Rockfill in End-Dump River Closures," *Journal of the Hydraulics Division*, ASCE, Vol. 98, No. HY11, Proc. Paper 9381, Nov., 1972, pp. 1947–1967.
13. Das, B. P., "Bed Scour at End-Dump Channel Constrictions," *Journal of the Hydraulics Division*, ASCE, Vol. 99, No. HY12, Proc. Paper 10228, Dec., 1973, pp. 2273–2291.

CALCULATION OF STRONGLY CURVED OPEN CHANNEL FLOW[a]

Discussion by Habib O. Anwar[4] and James G. Rodger[5]

The authors have obtained an excellent agreement between the experimental results and those of their numerical K-ϵ model. Although it was not mentioned in the paper, the model with its auxiliary algebraic equations can only be used when the flow is isotropic for which the coefficient C_μ, C_1, C_2, σ_K and σ_ϵ remains universally constant, otherwise the model must be "tuned" by adjusting the numerical values of the constants, which, usually differ from experimental values. The writers have, however, evaluated the constant, C_μ, from measurements conducted in a laboratory flume on a two-dimensional flow (35) and from field data obtained in the Great Ouse Estuary (Ref. 36, United Kingdom). The global Reynolds numbers for these flows were 9×10^4 and 4×10^6, respectively. It was found that the laboratory C_μ value, depending on y, varied between 0.008 and 0.08 ($C_\mu = 0.008$, near the free surface) and the field value of C_μ measured at $y = 1.14$ m varied between 0.08 and 0.012. The energy spectra showed the existence of a $-5/3$ distribution (35,36), but further examination showed that the flows were anisotropic (36). The C_μ value in a homogeneous isotropic turbulent shear flow (38) is about 0.11; in a turbulent boundary layer with zero pressure gradient (39), depending on y/δ, δ being the boundary layer thickness, C_μ was 0.075 and 0.059 for $y/\delta = 0.1$ and 0.9, respectively. The C_μ value used by the authors was 0.09. These results show clearly that the constant, C_μ, depending on the flow, can vary considerably.

The K-ϵ model, although successful in describing isotropic turbulence with

---

[a]October, 1979, by Michael A. Leschziner and Wolfgang Rodi (Proc. Paper 14927).

[4]Principal Scientific Officer, Dept. of the Environment, Hydr. Research Station, Wallingford, Oxon OX10 8BA, England.
[5]Sr. Scientific Officer, Dept. of the Environment, Hydr. Research Station, Wallingford, Oxon OX10 8BA, England.

the universal constants, could not be applied, as aforementioned, without some tuning to more general flow problems. Therefore, it is not obvious that the results from a K-ϵ model compared with those from other simpler turbulence models, e.g., Prandtl mixing length approach (41), could justify the additional computational effort required to solve the K and ϵ equations.

The authors in Eq. 4 have assumed, by analogy with laminar flow, that the Reynolds stress is proportional to the rate of strain. Prandtl (41), on the other hand, postulated by analogy with Rayleigh's investigation on the stability of curved flow that the Reynolds stress, being positive, is proportional to the vorticity (37); what changes would the authors expect had Prandtl's suggestion been used?

Appendix.—References

35. Anwar, H. O., and Atkins, R., "Turbulence Measurements in a Simulated Tidal Flow," ASCE, *Journal of the Hydraulics Division*, Vol. 106, No. HY8, Proc. Paper 15609, Aug., 1980, pp. 1273–1289.
36. Anwar, H. O., "The Study of the Turbulent Structure in a Tidal Flow," in press.
37. Anwar, H. O., "Turbulent Flow in a Vortex," *Journal of Hydraulic Research*, Vol. 7, No. 1, 1969, pp. 1–29.
38. Champagne, F. H., Harris, V. G., and Corrsin, S., "Experiments on Nearly Turbulent Flow," *F. Fluid Mech.*, Vol. 41, Part 1, 1970, pp. 81–139 (see also "Turbulence," Bradshaw, ed., section 6, Springer-Verlag, Berlin, Germany, 1976).
39. Klebanoff, P. S., "Characteristics of Turbulence in a Boundary Layer with Zero Pressure Gradient," *Report No. 3178*, National Advisory Committee for Aeronautics, Washington, D.C., 1954.
40. Odd, N. V. M., and Rodger, J. G., "Vertical Mixing in Stratified Tidal Flows," ASCE, *Journal of the Hydraulics Division*, Vol. 104, No. HY3, Proc. Paper 13599, Mar., 1978, pp. 337–351.
41. Prandtl, L., "Einfluss stabilisierender Kräfte auf die Turbulenz," *Gesammelte Abhandlungen*, Zweiter Teil, Springer-Verlag, Berlin, Germany, 1961, pp. 778–785.

Longitudinal Dispersion in Rivers[a]

Discussion by Mustafa Gögüş[2]

Recent investigations (31,32) have shown that the dispersion process in natural rivers cannot be accurately predicted by the well-known Fickian dispersion theory. The concentration-time distribution curve is generally found to be skewed with a sharper rise and more prolonged fall in the initial period. The author has proposed a dispersion model with two coefficients to reduce the discrepancies between field data and the Fickian theory. Application of this model to natural

[a]January, 1980, by Spyridon Beltaos (Proc. Paper 15118).
[2]Research Asst., Iowa Inst. of Hydr. Research, The Univ. of Iowa, Iowa City, Iowa 52240.

streams shows good agreement between the data and the model. The practical advantage of the method using several $\bar{C}$ versus t curves at fixed cross sections to determine ΔT values with a higher accuracy rather than $\bar{\sigma}_t^2$ should be emphasized. However, the writer would like to discuss a few points which do not seem to be clear in the development of the model and presentation of results.

The value of α is given as 5.55 and assumed to be a universal constant. However, it is not explained how this constant quantity was obtained. The coefficient α can be calculated either numerically or using the definition of α as given in Eq. 30. For a numerical solution, Eq. 22 can be rearranged for $\bar{C}/\bar{C}_p = 0.5$, introducing $t_p = x/V$, and $T = t/t_p$ as follows:

$$T \exp(1 - T) = 0.5^{\beta} \quad \ldots \quad (38)$$

Solutions of Eq. 38 for a known value of β give T_1 and T_2 which correspond to t_1 and t_2 on the $\bar{C}$ versus t curve, respectively. Since $\Delta T = T_2 - T_1$ and $\Delta T = (\alpha\beta)^{1/2}$, one can easily calculate α. According to the writer's calculation

TABLE 1.—Application of Model to Fischer's Flume Data

Fischer's data (1)	X_1, in meters (2)	X_2, in meters (3)	$\bar{\sigma}_{t_1}^2$, in seconds^2 (4)	$\bar{\sigma}_{t_2}^2$, in seconds^2 (5)	V, in meters per second (6)	ΔT_1, in seconds (7)	ΔT_2, in seconds (8)	L_T,* in meters (9)	From Eq. 30 α_1 (10)	From Eq. 30 α_2 (11)	From Eq. 15 L, in meters (12)	From Eq. 15 β (13)
Series 2800	16.07	26.11	369	651	0.251	12.3	—	30.9	0.410	—	2.954	0.300
Series 2900	16.08	26.12	111	179	0.454	6.0	18.0	28.1	0.324	1.810	<0.0	—
Series 3100	17.50	29.45	130	241	0.444	10.2	30.0	23.1	0.800	3.734	3.559	0.258

*Taylor length, L_T, is calculated from Eq. 7.
Note: 1 m = 3.281 ft.

it was found that for $0.00700 < \beta < 0.01400$, $\alpha \simeq 5.55$, and α increases slightly beyond this range. Use of Eq. 30 to define α requires known values of ΔT and $\bar{\sigma}_t^2$ from observed $\bar{C}$ versus t curves. Although ΔT can be found fairly accurately, determination of accurate $\bar{\sigma}_t^2$ from experimental data is difficult since $\bar{\sigma}_t^2$ is very sensitive to the tail region of $\bar{C}$ versus t curves. It is possibly for this reason that the author did not present any value of α directly computed from measured values of ΔT and $\bar{\sigma}_t^2$.

Fischer's experiments (15) conducted in laboratory flumes should nearly satisfy the condition of one-dimensionality required for the application of the author's model. Values of α were computed using Eq. 30 for series 2800, 2900, and 3100 of Fischer's experiments, and are presented in Table 1. The α values obtained are seen to be much smaller than 5.55, and to increase with increasing X. It is possible that α would eventually reach the value of 5.55.

In the aforementioned experiments, ΔT is not proportional to x; therefore, it is unlikely that Fischer's measurements were conducted in the linear range. Therefore, values of β and L were calculated from Eq. 15 using the data measured at two locations, X_1, and X_2, and the Taylor length, L_T was calculated using Eq. 7. The results of these computations are also included in Table 1. The following comments can be made:

1. The values of β are much larger than those suggested by the author.
2. The length L is less than one third of L_T that was found by the author using field data.
3. Since X_1 and X_2 are greater than $3L$ in Fischer's experiments considered herein, the corresponding $\bar{C}$ versus t curve should be in the Fickian range according to the author's criterion. On the other hand, X_1 and X_2 are still significantly smaller than L_T, and, thus, they are within the intermediate range. This is

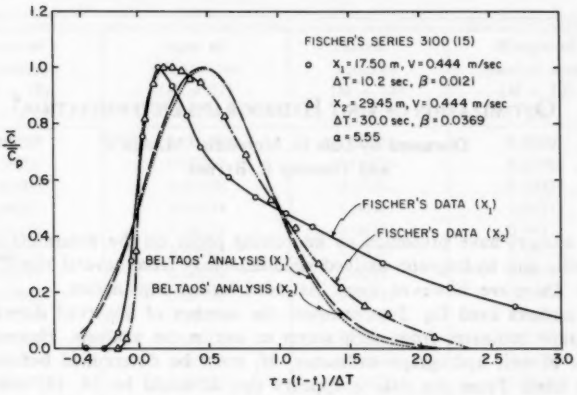

FIG. 10.—Comparison of Fischer's Data with Proposed Model Prediction

also confirmed by the fact that the $\bar{C}$ versus t curves for the aforementioned experiments are very skewed (more skewed at $X = X_1$, than at $X = X_2$).

It was then assumed that the low values for α as calculated above were due to inaccurate determination of $\bar{\sigma}_t^2$. The method proposed by the author for the determination of β and L from Eq. 31 was thus attempted, using the ΔT values at the two measuring stations in series 2900 and 3100, and $\alpha = 5.55$. However, for these two particular series no finite value for L can be obtained. If indeed the L values were so large as to be much greater than the flume length, Fischer's experiments then would have been all conducted in the linear range, which is in contradiction with the observation that ΔT is not proportional to X. Furthermore, when the data of series 3100 at $X = X_1$ and $X = X_2$ are compared with the prediction of Eq. 25 with $\alpha = 5.55$ and β obtained from Eq. 27, it can be seen from Fig. 10 that the agreement is very poor at $X = X_1$, although somewhat better at $X = X_2$.

No satisfactory explanation for the discrepancy between Fischer's experimental data and the author's model prediction can be offered since on the one hand, no flaw was discovered in the author's analysis, and on the other hand, Fischer's data are widely accepted as being reliable. The author's comments on the possible source for the disagreement discussed here would be extremely welcomed.

Appendix.—References

31. McQuivey, R. S., and Keefer, T. N., "Convective Model of Longitudinal Dispersion," *Journal of the Hydraulics Division*, ASCE, Vol. 102, No. HY10, Proc. Paper 12478, Oct., 1976, pp. 1409–1424.
32. McQuivey, R. S., and Keefer, T. N., "Dispersion-Mississippi River Below Baton Rouge, La.," *Journal of the Hydraulics Division*, ASCE, Vol. 102, No. HY10, Proc. Paper 12490, Oct., 1976, pp. 1425–1437.

Optimization of Unit Hydrograph Determination[a]

Discussed by Dale D. Meredith,[6] M. ASCE and Timothy E. Byrnes[7]

The authors have presented an interesting paper on the determination of a composite unit hydrograph derived simultaneously from several runoff hydrographs. There are, however, items that need further explanation.

The authors used Eq. 2 to compute the number of observed direct runoff hydrograph ordinates from each storm to use in the analysis. However, the number of unit hydrograph ordinates, M, must be determined before Eq. 2 can be used. From the data it appears that M could be 14, 18, and 16 for storms A, B, and C, respectively. The authors chose $M = 16$ without explaining how or why this value was chosen.

It is relatively easy to formulate the problem such that the optimal number of unit hydrograph ordinates can be obtained simultaneously with the values of the ordinates. Choose M somewhat larger than the largest value indicated by the data, e.g., here choose $M = 20$. Then Eq. 2 can be used to determine the number of direct runoff hydrograph ordinates required. If the number of required ordinates is greater than the number of observed ordinates then the additional ordinates are assumed to be zero, e.g., here the last six runoff hydrograph ordinates for storm A would be 0. This formulation increases the number of decision variables and the number of constraints. However, Eqs. 16 and 17 are still valid. The number of nonzero unit hydrograph ordinates in the linear programming solution will be the optimal number of unit hydrograph ordinates.

---

[a]January, 1980, by Larry W. Mays and Lynn Coles (Proc. Paper 15129).

[6]Prof., Dept. of Civ. Engrg., Parker Engrg. Building, State Univ. of New York at Buffalo, Buffalo, N.Y. 14214.
[7]Water Resources Planner, U.S. Army Corps of Engrs., Buffalo Dist., Buffalo, N.Y.

Using the formulation presented here the optimal value of M is 17 for storms A, B, and C. The resulting unit hydrograph is shown in Col. 2 of Table 6.

The authors stated that: "least squares methods cannot guarantee nonnegative ordinates of the derived unit hydrographs. The linear programming method has nonnegativity constraints that eliminate any occurrence negative ordinates." Least squares methods that guarantee nonnegative ordinates of the derived unit hydrographs can be used. The procedure is simply to formulate the problem as a nonlinear programming problem with nonnegative constraints. Statisticians call this restricted least squares. The formulation is the same as for the linear programming problem except that the objective function is now nonlinear. Nonlinear programming algorithms are now available at most commercial computer installations.

TABLE 6.—Derived Unit Hydrographs for Different Programming Models for Storms A, B, and C, in inches per hour[a]

Sum of differences (M = 16) (1)	Sum of differences (M = 17) (2)	Least squares (M = 17) (3)	Weighted least squares (M = 15) (4)
0.00292	0.00279	0.00125	0.00307
0.00707	0.00737	0.01055	0.01086
0.03406	0.03406	0.03012	0.03034
0.04295	0.04294	0.04427	0.04373
0.04154	0.04158	0.04151	0.04171
0.03216	0.03203	0.03301	0.03252
0.02297	0.02298	0.02321	0.02306
0.01963	0.01930	0.01818	0.01776
0.01397	0.01402	0.01494	0.01580
0.01207	0.01204	0.01151	0.01137
0.00764	0.00771	0.00804	0.00794
0.00570	0.00572	0.00531	0.00464
0.00364	0.00363	0.00387	0.00425
0.00165	0.00159	0.00223	0.00211
0.00109	0.00089	0.00083	0.00085
0.00096	0.00084	0.00072	
	0.00052	0.00047	

[a]1 in./h = 25.4 mm/h.

The nonlinear programming model objective function was stated as a least squares fit, i.e.:

$$\text{Min} \sum_{i=1}^{I} \sum_{n=1}^{N_i} (z_{i,n}^2 + v_{i,n}^2) \quad \ldots \ldots \ldots \ldots \ldots \ldots \ldots \ldots \ldots \ldots \quad (18)$$

with M chosen as indicated in the foregoing. The solution was obtained using an available nonlinear programming algorithm (23) and is shown in Col. 3 of Table 6. Again the optimal value of M is 17.

The nonlinear programming model objective function was then stated as a weighted least squares fit, i.e.:

$$\text{Min} \sum_{i=1}^{I} \sum_{n=1}^{N_i} d_{i,n} (z_{i,n}^2 + v_{i,n}^2) \quad \ldots \ldots \ldots \ldots \ldots \ldots \ldots \ldots \ldots \ldots \quad (19)$$

in which $d_{i,n}$ = a weighting factor used by the U.S. Army Corps of Engineers in computing optimal unit hydrograph ordinates (24) and is computed as

$$d_{i,n} = \frac{(Q_{i,n} + \bar{Q}_i)}{2\bar{Q}_i} \quad \ldots \ldots \ldots \ldots \ldots \ldots \ldots \ldots \ldots \ldots \quad (20)$$

where $\bar{Q}_i$ = the mean of the ordinates for the ith direct runoff hydrograph. The optimal value of M for this model is 15 and the resulting unit hydrograph is shown in Col. 4 of Table 6. The author's unit hydrograph is shown in Col. 1 for comparison.

The authors state that: "An important factor in deriving unit hydrographs is to properly define the peak and time to peak." In order to evaluate the

TABLE 7.—Peak of Direct Runoff Hydrographs for Various Unit Hydrographs, in inches per hour[a]

Unit hydrograph used (1)	Storm A (2)	Storm B (3)	Storm C (4)
Sum of differences (M = 16)	0.08890	0.02560	0.09228[b]
Sum of differences (M = 17)	0.08888	0.02560	0.09207[b]
Least squares (M = 17)	0.09025	0.02623	0.09081[c]
Weighted least squares (M = 15)	0.09023	0.02600	0.09046[c]
Observed	0.08800	0.02560	0.08900

[a]1 in./h = 25.4 mm/h.
[b]Two time intervals after observed peak.
[c]One time interval after observed peak.

results from the programming models the four unit hydrographs in Table 6 were then used to compute direct runoff hydrographs for storms A, B, and C. The peaks for these computed hydrographs are shown in Table 7 along with the observed peaks for comparison. The linear programming models (sum of differences) resulted in a peak greater and two time periods later than the observed peak for storm C. The nonlinear programming models (least squares and weighted least squares) resulted in a more accurate estimate of the peak for storm C but in slightly larger peaks for storms A and B.

Therefore, from this preliminary analysis it appears that the nonlinear programming models may be more accurate than the linear programming models because peak weighting can be preformed. In addition the models appear to be more accurate when the number of unit hydrographs ordinates are determined by the model rather than a priori.

Further study should be done to evaluate these programming models. It would also be useful if the models could be formulated to obtain the optimal unit hydrograph for several storms when the input data are observed precipitation and total runoff hydrograph ordinates. Ref. 24 can be used to determine an optimal unit hydrograph for a single storm event with a weighted least squares fit.

APPENDIX.—REFERENCES

23. Cohen, C., and Stein, J., *Multi Purpose Optimization System, User's Guide, Manual No. 320,* Version 3, Northwestern University, Evanston, Ill., 1976.
24. *HEC-1, Flood Hydrograph Package, User's Manual,* Corps. of Engineers, Hydrologic Engineering Center, Jan., 1973.

EXTENDED SET OF COMPONENTS IN PIPE NETWORKS[a]

Discussion by Michael A. Collins,[3] M. ASCE

The author has presented an interesting overview of hydraulic network analysis, drawing particular attention to the treatment of control type elements, such as check valves and pressure reducing valves, and providing a systematic description of the proper network topology to be used when such elements are presented in a network.

The author, in his conclusion, raises the important issue of solution uniqueness, and appropriately implies there remain questions to be answered in regard to this issue. In networks without control elements and in which the head loss-discharge characteristics for all elements are monotonic, it can be guaranteed that a unique solution exists (9). The results of Ref. 9 can also be readily extended to networks in which the only control elements are simple check valves since, as has been demonstrated (10,11), a network containing both unidirectional elements, such as check valves, and bidirectional elements, such as pipes with simple frictional losses, can be modeled by an equivalent network consisting of solely unidirectional elements and the results of Ref. 9 apply to such a unidirectional network.

Other types of control elements, which for modeling certain modes of operation require a changing of the network topology beyond the simple replacement of bidirectional elements by two equivalent but oppositely directed unidirectional elements, indeed appear to offer the opportunity to yield nonunique steady state solutions (8). This potential nonuniqueness arises, of course, because when the network topology is altered one essentially has another network problem, and there appears to be no reason yet proposed why one solution to a steady-state network should rule out a solution to another different, albeit similar, steady-state network.

In networks wherein the control elements are pressure reducing valves, even when a unique solution does exist, the criteria as described by the author to identify the proper solution do not appear to this writer to be complete. The remainder of this discussion addresses this apparent deficiency.

---

[a]January, 1980, by M. Chandrashekar (Proc. Paper 15130).

[3]Prof. of Civ. Engrg., Civ. and Mech. Engrg. Dept., School of Engrg. and Applied Sci., Southern Methodist Univ., Dallas, Tex. 75275.

Three criteria are given, of which only two are of concern here: (1) If $H_e < H_{set}$ and $H_j < H_i$, then the pressure reducing valve is inactive; and (2) if $H_e > H_{set}$ and $H_j < H_i$, then the pressure reducing valve is active and the admittance is changed from y_k to $\bar{y}_k$. Because one does not necessarily know if a unique solution does exist, one should consider all the possibilities of alternative operating modes of the pressure reducing valves. One might argue that if one initially finds that $H_e < H_{set}$, one needs to go no further. This seems plausible, but if one admits to the possibility of nonuniqueness, this assumption certainly could miss a possible steady-state solution. But suppose one does accept the premise that if the first criteria ($H_e < H_{set}$) is satisfied one has the correct solution, then the author's criteria would imply that if it is found that $H_e > H_{set}$ then the proper solution corresponds to an active mode of operation for the pressure reducing valve. But what happens if there is more than one pressure reducing valve and thus there exists the possibility

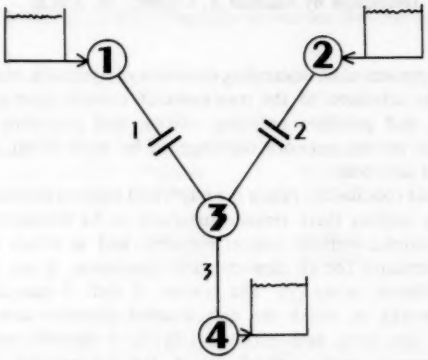

FIG. 12.—Example Network with Two Pressure Reducing Valves

of one valve being active and the others being inactive? In this case the author's criteria appear incomplete.

To readily demonstrate the point being raised as well as identify the missing component in the author's criteria, consider the simple four node network of Fig. 12 consisting of three pipes, of which two have pressure reducing valves. Nodes 1, 2, and 4 are reservoirs with fixed heads of 100, 100, and 0 units of head, respectively. For simplicity and without loss of generality, flows, heads, and admittances will be described without reference to any specific set of units with the understanding a consistent set of units is being used. Pipe element number 3 between nodes 3 and 4 is assumed to be described by Eq. 3 with $y_3 = 0.200$.

The pressure reducing valves in elements 1 and 2 prevent excessive pressure at node 3. The control set head in the valve in pipe 1 is $H_{set} = H_{set,1} = 90.7$ while that for the pressure reducing valve in pipe 2 is $H_{set} = H_{set,2} = 90$. Note that the different set heads for the two valves do not make the problem unrealistic since the network of Fig. 12 could be considered to be a simplification of some more complex network with more pipes and nodes between the pressure

reducing valves and node 3. When these pressure reducing valves are inactive, $y_1 = 0.200$ and $y_2 = 0.250$. Both pressure reducing valves are located midway along the pipe on which they occur, i.e., $\bar{L}_1/L_1 = \bar{L}_2/L_2 = 0.5$, in which L_k = the length of pipe k; and $\bar{L}_k$ = the distance along pipe k from its downstream end to the pressure reducing valve [see Fig. 4(*a*)]. Since the author implies that admittance for an active pressure reducing valve is modeled as a simple pipe (see Eq. 11) in which the effective admittance $\bar{y}_k$ is based on $\bar{L}_k$, it follows that $\bar{y}_k = y_k(L_k/\bar{L}_k)^{0.54}$. Thus $\bar{y}_1 = 0.291$ and $\bar{y}_2 = 0.363$.

A tentative solution (in the sense that it is not known a priori whether the solution will satisfy the author's criteria) can be obtained from a continuity equation for node 3 expressed in terms of head losses:

$$y_1^*(H_1^* - H_3)^{0.54} + y_2^*(H_2^* - H_3)^{0.54} = y_3 H_3^{0.54} \quad \ldots\ldots\ldots\ldots\ldots (25)$$

in which the heads H_1^* and H_2^* have been introduced to denote the fact that these heads will have different values according to the operation of the pressure reducing valves. The variable, y_k^*, is merely y_k or $\bar{y}_k$ depending on whether the pressure reducing valve is inactive or active, respectively.

It is apparent that four cases are possible:

Case 1.—Both pressure reducing valves are inactive; thus $H_1^* = H_1 = 100$ and $H_2^* = H_2 = 100$.

Case 2.—The pressure reducing valve in pipe 1 is active but the other valve is inactive; thus $H_1^* = H_{\text{set},1} = 90.7$ and $H_2^* = H_2 = 100$.

Case 3.—The pressure reducing valve in pipe 2 is active but the other valve is inactive; thus $H_1^* = H_1 = 100$ and $H_2^* = H_{\text{set},2} = 90$.

Case 4.—Both pressure reducing valves are active; thus $H_1^* = H_{\text{set},1} = 90.7$ and $H_2^* = H_{\text{set},2} = 90.0$.

The tentative solution for each case is obtained from Eq. 25 using a simple

TABLE 7.—Summary of Alternative Tentative Solutions for Example Network of Fig. 12*

Case (1)	H_3 (2)	Pipe, k (3)	H_e^* (4)	q_k (5)	y_k (6)	$\bar{y}_k$ (7)	y_k^u (8)	H_e (9)
1	81.7840	1	90.8920	0.9587	0.200	—	0.2908	90.8920
1	81.7840	2	90.8920	1.1984	0.250	—	0.3635	90.8920
1	81.7840	3	—	2.1571	0.200	—	—	—
2	81.6872	1	90.7000	0.9539	—	0.291	0.2910	90.9760
2	81.6872	2	90.8436	1.2018	0.250	—	0.3635	90.8436
2	81.6872	3	—	2.1557	0.200	—	—	—
3	81.2095	1	90.6048	0.9749	0.200	—	0.2908	90.6048
3	81.2095	2	90.0000	1.1740	—	0.363	0.3386	91.2318
3	81.2095	3	—	2.1489	0.200	—	—	—
4	81.2518	1	90.7000	0.9785	—	0.291	0.2935	90.5403
4	81.2518	2	90.0000	1.1710	—	0.363	0.3370	91.2732
4	81.2518	3	—	2.1495	0.200	—	—	—

*If the y_k column is blank, pressure reducing valve is activated; if the $\bar{y}_k$ column is blank, pressure reducing valve is not active.

Newton Raphson iteration procedure. Results are summarized in Table 7. The variable, H_3, is the computed head at node 3 while q_k in Col. 5 is the discharge computed from this head, the admittances y_k or $\bar{y}_k$, and the upstream (or downstream in the case of pipe 3) heads appropriate to the assumed operating mode of the pressure reducing valve. The variable H_3^* is the head at the downstream side of the pressure reducing valve. In the case of inactive valve operation it is merely the average of H_3 and the reservoir head since the valve is midway between the reservoir and node 3. In the case of active operation of a valve $H_e^* = H_{set}$. The variable y_k^u is the apparent admittance that must exist upstream of the pressure reducing valves in view of the computed discharge and the tabulated valve of H_e^*. The variable, H_e, on the other hand, is the head at the upstream side of the pressure reducing valve as computed from the discharge, the upstream reservoir head, and admittance y_k adjusted for the shorter length of pipe upstream of the valve; these latter admittances being merely equal to y_k^u of case 1.

It is seen from Table 7 that case 1, for which both valves are inactive, yields heads at the pressure reducing valve which exceed H_{set}. Thus, by the author's criteria, this case is not the proper solution. But examination of the other cases shows, as well, that H_e does not simultaneously satisfy $H_e < H_{set}$ for both valves in any case. Thus, the author's criteria as given would imply no solution. It would appear another physical condition, not apparently explicitly cited by the author, is necessary. Physically, a pressure reducing valve becomes active by increasing the effective head loss coefficient across the valve, i.e., the valve admittance decreases. Thus, for a physically acceptable solution, it would be necessary that for each active pressure reducing valve y_k^u be less than the y_k^u for the inactive operation of the valve. Table 7 shows that case 3 satisfies this criterion and is thus apparently the correct solution.

This writer would therefore suggest that the author's second criteria be replaced with the following:

> If criterion number 1 is not satisfied, then a solution in which for each active pressure reducing valve the apparent upstream admittance is less than the corresponding inactive value of the upstream admittance is an acceptable solution, provided $H_i > H_j$.

Of course, these criteria still do not indicate which solution is the proper solution when nonunique solutions are found.

Appendix.—References

8. Collins, M. A., "Pitfalls in Pipe Network Analysis Techniques," *Transportation Engineering Journal*, ASCE, Vol. 106, No. TE5, Proc. Paper 15675, Sept. 1980, pp. 507–521.
9. Collins, M. A., Cooper, L., and Kennington, J. L., "Multiple Operating Points in Complex Pump Networks," *Journal of the Hydraulics Division*, ASCE, Vol. 105, No. HY3, Proc. Paper 14452, Mar., 1979, pp. 229–244.
10. Collins, M. A., Cooper, L., Helgason, R. V., and Kennington, J. L., "Solution of Large Scale Pipe Networks by Improved Mathematical Approaches," *Technical Report IEOR 77016-WR 77001*, Southern Methodist University, Dallas, Texas, Aug., 1978.
11. Collins, M. A., Cooper, L., Helgason, R., Kennington, J., and LeBlanc, L., "Solving the Pipe Network Analysis Problem Using Optimization Techniques," *Management Science*, Vol. 24, No. 7, Mar., 1978, pp. 747–760.

TIDAL HYDRAULICS IN ESTUARINE CHANNELS[a]

Discussion by Zbigniew W. Kundzewicz[2]

The author has presented an interesting and novel contribution to tidal hydraulics. The writer would like to raise several points that in his opinion deserve discussion.

The author began his paper with the statement that "Intuition tells us that alternating tidal flow in an estuarine channel has similarities to alternating current flow in an electrical circuit." As intuition is not an objective research tool, this analogy can be proved by comparing the mathematical equations describing certain electrical and hydraulic systems (10,11).

Furthermore, the dimensional analogates for DC flow (Eqs. 3 and 4), suggested by the author, are confirmed in the analysis of similarities between the mathematics of basic electrical and hydraulic laws. As has been shown in Ref. 10, Kirchhoff's first law generally corresponds to the continuity equation (conservation of mass) in open channel hydraulics, and the Kirchhoff's second law corresponds to the momentum equation for steady, and uniform, open channel flow.

The author introduced a lumped, electrical analogy model to describe the velocity-head relationship in each of two gauged cross sections of the Intracoastal Waterway. The physical phenomena occurring in each of these cross sections were represented by means of an electrical resonant circuit forced by a sinusoidal voltage source.

However it is difficult to understand why this particular series circuit structure was a priori assumed to model the hydraulic phenomena in question. The lumped circuit, suggested by the author, cannot account for the transformation of a flow along the reach. The applicability of this approach is limited to modeling the amplitude-phase relationship between velocity and head of tidal flow at a given section. Indeed, even at a single section, the proposed analogy is doubtful between measured tidal head and an ideal voltage source, independent of conditions in the electrical system. The sinusoidal forcing functions (analogous to harmonic sources of electricity) appearing in the system of flow in the analyzed waterway are physically located at its two boundaries. Velocities and depths of flow in intermediate cross sections are the distributed system responses to the ocean inlet conditions and to the tributary inflows. The process of flow transformation along the waterway can be modeled by a distributed electrical analog circuit.

Based on the harmonic linearization of the resistance term (procedure identical to the author's development of the "equivalent damping coefficient"), Ippen (9) modeled the tidal flow in estuaries by means of the telegraphers equations

[a]February, 1980, by Robert M. Snyder (Proc. Paper 15202).

[2]Alexander von Humboldt Foundation Fellow, Inst. Wasserbau III, Univ. of Karlsruhe, Federal Republic of Germany; also Research Hydro., Inst. of Geophysics, Polish Academy of Sci., Warszawa, Poland.

introduced in electrical engineering for a transmission line. The electrical-hydraulic analogies go even further; as shown by the writer in Ref. 10, the frictionless linear channel flow system is mathematically identical to an LC transmission line, and the linear parabolic flow model (diffusion analogy) is mathematically identical to an RC transmission line.

The amplification of the tidal head, in the area where measurements were taken, can probably be explained by variations in the channel geometry (i.e., decrease of channel width), and accounted for in a distributed electrical model.

Moreover, the meaning of the new term "DC flow," and its relation to the well established terms like "steady" and "uniform" have not been precisely stated.

As seen in Fig. 2, the agreement of calculations with the recorded data, for the case of 57 acres, is questionable. In fact, the tidal current leads the tidal head in the first segment of sinusoid presented in Fig. 2 and so contradicts the calculated results.

Appendix.—References

9. Ippen, A. T., ed., *Estuary and Coastline Hydrodynamics*, McGraw-Hill Book Co., Inc., New York, N.Y., 1966, pp. 505–507.
10. Kundzewicz, Z., "Elektrische Analogien zur Modellierung hydrologischer Systeme," submitted for publication in *Archiv für Elektrotechnik*.
11. Shen, J., "Use of Analog Models in the Analysis of Flood Runoff," *U.S. Geological Survey Professional Paper 506-A*, U.S. Geological Survey, 1965.

Ocean Outfall Dilution: Effects of Currents[a]

Discussion by Henry H. C. Lin,[2] A. M. ASCE

The author's paper presented a new aspect on the deepwater ocean outfall design, including the dynamic effect of prevailing currents for diffuser design. This concept was utilized in the design of an ocean outfall system for the city and county of San Francisco, California.

The San Francisco Ocean outfall system, currently being designed to have a peak capacity of 670 mgd (2.55×10^9 L/day), will include three separate outfalls. The dry weather pipe will discharge all flows up to a capacity of 190 mgd (722×10^6 L/day), a distance of approx 4 miles (6.4 km) offshore, at a depth of 80 ft (24.4 m). Two wet weather pipes will discharge all flows in excess of 190 mgd (722×10^6 L/day) up to their capacity of 480 mgd (1.82×10^9 L/day), a distance of approx 2-1/2 miles (4 km) at a depth of 50 ft (15.24 m).

---

[a]May, 1980, by Philip J. W. Roberts (Proc. Paper 15429).
[2]Project Engr., CH2M Hill, Inc., 450 Sansome St., San Francisco, Calif. 94111.

The dry weather outfall has a nominal diffuser length of 3,060 ft (930 m) and is intended to produce an average initial dilution of 100:1 at more than 80% of the time. Each wet weather outfall has a nominal diffuser length of 1,440 ft (439 m), and is intended to produce an average initial dilution of 25:1.

Two mathematical models were used in the San Francisco ocean outfall system design to determine diffuser length and location. The first model, "finite line plume" (5), as developed by the author, considers the discharge to be a finite

TABLE 1.—Dilution Comparison of Plume Model Test Results with Math Models Predictions

Test series (1)	Flow million gallons per day (2)	Density profile (3)	Current, in knots (4)	Measured		Koh's Model		Roberts Model	
				Minimum (5)	Average (6)	Average initial dilution (7)	Error, as a percentage[b] (8)	Average initial dilution (9)	Error, as a percentage (10)
WW-1	240	January 21, 1981 1,300 h	0	32	34	27	15.5	31	3.0
WW-2	240	January 21, 1978 1,300 h	0.25	41	60	—	—	40	2.5
DW-1	107	July	0	103	105	75	27.0	96	7.0
DW-2	107	Uniform	0	192	220	210	−9.5	183	4.5
DW-3	107	July	0.25	280	300	—	—	126	55.0
DW-4	107	Uniform	0.25	400	[a]	—	—	417	−4.0
DW-5	190	July	0	68	80	64	6.0	84	−23.5
DW-5	190	July	0	83	90	64	23.0	84	−1.0
DW-6	190	Uniform	0	139	170	156	−12.0	125	10.0

[a] Data insufficient to determine average dilution.

[b] % = (measured minimum dilution − predicted average initial dilution)/measured minimum dilution × 100%.

Note: The initial dilution predicted by Roberts' model is not as sensitive as Koh's model for a change of the port configuration in a fixed diffuser length.

line source of buoyant flux only. This model incorporates the effects of the ocean current in both speed and direction, but ignores the momentum of the discharge and individuality of the multiple ports. It is equivalent to using the simple plume formula (3) at no current condition, which does not take into account the angle of discharge, jet momentum, and merging of plumes. The second model "round buoyant jet" (8) predicts the plume behavior issuing from a diffuser in stagnant, density-stratified surroundings. This model considers the effect of interference from the multiple ports, as well as the effect of the effluent field's finite thickness. The ambient ocean is assumed motionless during the buoyant rise of the discharge.

During the project design, a physical model to study plume behavior was conducted at the California Institute of Technology (1,6). This model study was used to investigate the near-field dilution, height of rise, and other plume behavior expected from alternative diffuser designs under various flow and ocean conditions, and to verify and to calibrate the mathematical models.

The physical model tests determined the initial dilution to be expected in

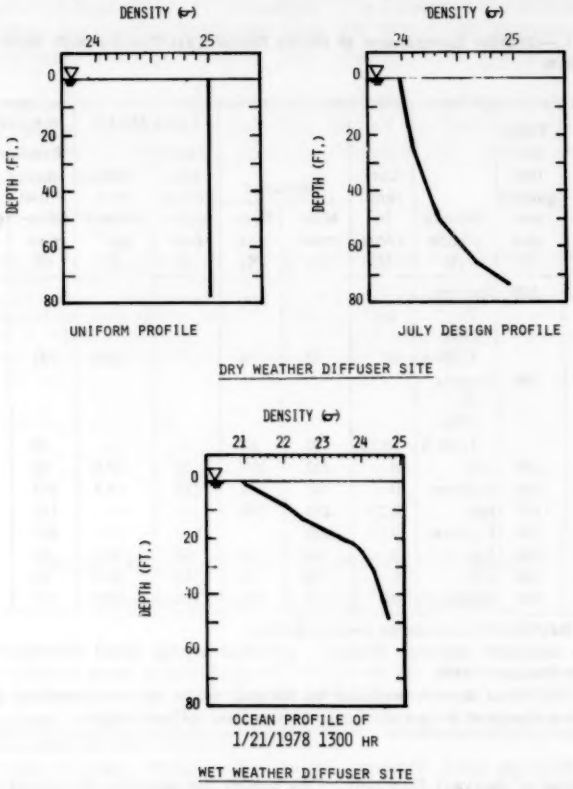

FIG. 14.—Density Profiles Simulated in Laboratory Tests

the horizontally spreading portions of the effluent plumes from the diffuser designs under various ambient ocean conditions and effluent discharge rates. The ocean conditions included typical and worst density-stratified cases as measured at the proposed outfall diffuser sites during the design period. Ambient ocean cross currents of 0 knots (0 m/sec) and 0.25 knots (0.12 m/s) were modeled. The wet weather diffuser was tested at its design peak rate of 240

mgd (912×10^6 L/day). The dry weather diffuser was tested at its average discharge rate of 107 mgd (350×10^6 L/day) and peak discharge rate of 190 mgd (722×10^6 L/day).

The test results of the physical model compared favorably with the predictions of the mathematical model developed by Koh (7,8) for the case of no current. This writer further utilized the test results to compare with the predictions of initial dilution by using the author's "finite line plume" model.

Table 1 shows the comparison of the physical model test results with the

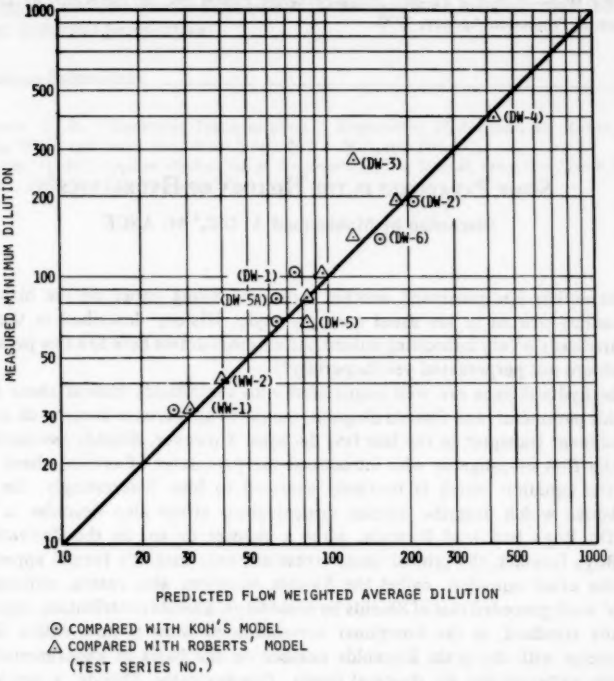

FIG. 15.—Comparison of Test Results with Math Models' Predictions

mathematical model's predictions. The test results clearly indicate that the effect of ocean currents is to increase dilution. Fig. 14 shows the selected density profiles to be simulated in the tests. The comparison between the flow-weighted average dilution predicted by Koh's model and the author's model and the minimum dilution measured in the laboratory (minimum in the vertical profile, temporally and laterally averaged) is shown on Fig. 15. The comparisons indicate that both Koh's model and the author's model are conservative, and are useful design tools for estimating the dilution for other ocean conditions at the proposed San Francisco ocean outfall site.

APPENDIX.—REFERENCES

6. Isaacson, M. S., Koh, R. C. Y., and Brooks, N. H., "Sectional Hydraulic Modeling Study of Plume Behavior: San Francisco Southwest Ocean Outfall Project, Final Report," *Technical Memorandum 79-4,* W. M. Keck Laboratory of Hydraulics and Water Resources, California Institute of Technology, Pasadena, Calif., Oct., 1979.
7. Koh, R. C. Y., "Buoyancy-Driven Gravitational Spreading," *Proceedings of the 15th Coastal Engineering Conference,* Vol. IV, July, 1976.
8. Koh, R. C. Y., and Fan, L. N., "Mathematical Models for the Prediction of Temperature Distribution Resulting from the Discharge of Heated Water into Large Bodies of Water," *EPA Water Pollution Control Research Series Report No. 16130DW010/70,* Environmental Protection Agency, 1970.

SOME PARADOXES IN THE HISTORY OF HYDRAULICS[a]

Discussion by Mohammad A. Gill,[2] M. ASCE

The author has presented another most interesting paper on the history of hydraulics written in his usual masterly style. History described in the form of paradoxes is very interesting indeed. Attention is drawn here to a few paradoxes which are not perpetuated yet (hopefully?).

The hydraulicians are well acquainted with the Shields cirtical shear stress, Shields parameter, and Shields diagram, thanks to an increase in research activity in sediment transport in the last few decades. However, Shields assuredly was not the first investigator who introduced the parameter of critical shear stress nor the equation which is routinely ascribed to him. Interestingly, the same textbooks which describe Shields critical shear stress also describe in detail the Du Boys bed load formula, after a chapter or so. In the derivation of Du Boys formula, the critical shear stress not only makes a formal appearance but the exact equation, called the Shields equation, also enters, although Du Boys' work preceded that of Shields by some 60 yr. Shields contribution, important by any standard, is the functional correlation of what is now called Shields parameter with the grain Reynolds number on the basis of experimental data Shields collected for his doctoral thesis. Paradoxically, Shields, a mechanical engineer, did not realize the importance of his contribution (unwittingly?).

The story was told by the author of how Ippen's name came to be associated with the equation of suspended sediment in one-dimensional, steady, uniform, open channel flow, although the work had been developed independently and published by the author. On the other hand, Ippen never published his work. Fortunately, this paradox appears to have been laid to rest.

What of the Einstein-Brown (or the other way round) and Kalinske-Brown sediment transport formulas? The writer had the occasion to use these formulas in some of his publications and the formulas were described, as in the foregoing,

[a]June, 1980, by Hunter Rouse (Proc. Paper 15475).

[2]Prof. of Hydr. Engrg., Civ. Engrg. Dept., Ahmadu Bello Univ., Zaria, Nigeria.

following the trend of earlier publications. Several years later, the acknowledgment note appearing at the end of the chapter on "Sediment Transportation" in Ref. 1 came to the writer's attention. Although the chapter is credited to C. Brown, the sections in which the previously mentioned formulas were given for the first time were written by no other person than the author of the original paper. As far as the writer is concerned, the paradox had been born and probably perpetuated. Just before writing this discussion, it was discovered that at least one book (2), if not more, described the foregoing formulas as Rouse-Einstein and Rouse-Kalinske formulas, respectively. The author has the right and the privilege to provide the background information to at least set the facts in correct historical perspective.

Appendix.—References

1. Brown, C. B., "Sediment Transportation," *Engineering Hydraulics*, H. Rouse, ed., John Wiley and Sons, Inc., New York, N.Y., 1950, pp. 769–857.
2. Morris, H. M., *Applied Hydraulics in Engineering*, The Ronald Press Co., New York, N.Y., 1963, pp. 328, 330, and 353.

Technical Papers

Original papers should be submitted in triplicate to the Manager of Technical and Professional Publications, ASCE, 345 East 47th Street, New York, N.Y. 10017. Authors must indicate the Technical Division or Council, Technical Committee, Subcommittee, and Task Committee (if any) to which the paper should be referred. Those who are planning to submit material will expedite the review and publication procedures by complying with the following basic requirements:

1. Titles must have a length not exceeding 50 characters and spaces.

2. The manuscript (an original ribbon copy and two duplicate copies) should be double-spaced on one side of 8-1/2-in. (220-mm) by 11-in. (280-mm) paper. Three copies of all figures and tables must be included.

3. Generally, the maximum length of a paper is 10,000 word-equivalents. As an *approximation*, each full manuscript page of text, tables or figures is the equivalent of 300 words. If a particular subject cannot be adequately presented within the 10,000-word limit, the paper should be accompanied by a rationale for the overlength. This will permit rapid review and approval by the Division or Council Publications and Executive Committees and the Society's Committee on Publications. Valuable contributions to the Society's publications are not intended to be discouraged by this procedure.

4. The author's full name, Society membership grade, and a footnote stating present employment must appear on the first page of the paper. Authors need not be Society members.

5. All mathematics must be typewritten and special symbols must be identified properly. The letter symbols used should be defined where they first appear, in figures, tables, or text, and arranged alphabetically in an appendix at the end of the paper titled Appendix.—Notation.

6. Standard definitions and symbols should be used. Reference should be made to the lists published by the American National Standards Institute and to the *Authors' Guide to the Publications of ASCE*.

7. Figures should be drawn in black ink, at a size that, with a 50% reduction, would have a published width in the *Journals* of from 3 in. (76 mm) to 4-1/2 in. (110 mm). The lettering must be legible at the reduced size. Photographs should be submitted as glossy prints. Explanations and descriptions must be placed in text rather than within the figure.

8. Tables should be typed (an original ribbon copy and two duplicates) on one side of 8-1/2-in. (220-mm) by 11-in. (280-mm) paper. An explanation of each table must appear in the text.

9. References cited in text should be arranged in alphabetical order in an appendix at the end of the paper, or preceding the Appendix.—Notation, as an Appendix.—References.

10. A list of key words and an information retrieval abstract of 175 words should be provided with each paper.

11. A summary of approximately 40 words must accompany the paper.

12. A set of conclusions must end the paper.

13. Dual units, i.e., U.S. Customary followed by SI (International System) units in parentheses, should be used throughout the paper.

14. A practical applications section should be included also, if appropriate.